

**Assessing the influence of the Pacific Decadal Oscillation and the
Atlantic Multidecadal Oscillation on discharge variability in
western North America**

by

Duane D. Noel

A Thesis

in the Department

of

Geography, Planning and Environment

Presented in partial fulfillment of the Requirements

For the Degree of Master of Science

(Geography, Urban and Environmental Studies) at

Concordia University

Montréal, Québec, Canada

June 2021

© Duane D. Noel, 2021

CONCORDIA UNIVERSITY

School of Graduate Studies

This is to certify that the thesis prepared

By: Duane D. Noel

Entitled: Assessing the influence of the Pacific Decadal Oscillation and the
Atlantic Multidecadal Oscillation on discharge variability in
western North America

and submitted in partial fulfillment of the requirements for the degree of

Master of Science (Geography, Urban and Environmental Studies)

complies with the regulations of the University and meets the accepted standards with respect to
originality and quality.

Signed by the final Examining Committee:

_____ Chair
Dr. Angela Kross

_____ External Examiner
Dr. Stephen Déry

_____ Examiner
Dr. Pascale Biron

_____ Supervisor
Dr. Jeannine-Marie St-Jacques

Approved by _____
Dr. Craig Townsend Chair of Department

_____ 2021 _____
Dr. Pascale Sicotte Dean of the Faculty of Arts and Science

ABSTRACT

Assessing the influence of the Pacific Decadal Oscillation and the Atlantic Multidecadal Oscillation on discharge variability in western North America

Duane D. Noel

The frequency of natural hazards in North America presents a significant challenge for governments due to the damages they cause to the environment. Floods are severe hydrological events caused by spring snowmelt and intense rain events. Flood frequency analysis studies assume that annual peak flood events occur independently of each other, regardless of previous flood events (the independent and identically distributed (*i.i.d.*) assumption); however, annual peak flood records do not necessarily appear to conform to these assumptions. First, a review of the literature on the effects of climate oscillations on extreme flood frequencies in North America was conducted. Then, the *i.i.d.* flood event assumption was tested by analyzing the effects of the Pacific Decadal Oscillation (PDO) and Atlantic Multidecadal Oscillation (AMO) on 250 naturally flowing annual peak flood records across the entire western North American margin. Using permutation tests on quantile-quantile (Q-Q) plots, I found that the PDO has a greater impact on the magnitude of annual peak floods than the AMO. Twenty-six percent of the gauges have higher magnitude annual floods depending on the PDO phase ($p < 0.1$). Next, I examined the interacting effects of the PDO and AMO on the frequencies of lower and upper quartile annual peak floods, and found reinforcing, cancelling, and dominating effects. Since these two climate oscillations have significant effects on the magnitudes of annual peak floods, the *i.i.d.* assumption does not hold. Hence, I advocate for the need to re-assess baseline flood analysis in western North America to improve flood management strategies.

ACKNOWLEDGEMENTS

I would like to thank my supervisor, Dr. Jeannine-Marie St-Jacques for her guidance, mentorship, and support throughout the development of this project. The entire master's thesis process was a great learning experience that challenged me to become a more critical researcher and writer of scientific work. I am grateful for the opportunity to work in the Climatology, Hydrology and Paleo-Environmental Laboratory over the course of three years and complete an honours project and master's thesis. Thank you to all my lab colleagues for their encouragement throughout the project. I would also like to thank Dr. Pascale Biron and Dr. Pedro Peres-Neto for their council and expertise in hydrology and statistics in this project. Their commentaries throughout the project were valuable in the preparation of the manuscript.

I would like to thank Concordia University for the opportunity to conduct this research in this academic establishment and for awarding me an entrance graduate scholarship to financially support this project. I am appreciative of the time I have spent in the Department of Geography, Planning and Environment and the positive research environment that its members have fostered.

Thank you to the Natural Sciences and Engineering Research Council of Canada for awarding me multiple Undergraduate Student Research Awards to gain exposure in environmental science research and more specifically, in hydrological research during my undergraduate studies at Concordia University. Thank you for the generous master's scholarship that provided the financial stability to pursue this research. Thank you to the *Fonds de recherche du Québec – Nature et technologies* and *Hydro-Québec* for the wonderful scholarships awarded to me for this project. I am grateful for your support. Lastly, I would like to thank my parents and my loved ones who have given their moral and emotional support throughout the entire process. Thank you for your prayers and kindness that you have bestowed upon me.

CONTRIBUTION OF AUTHORS

Chapter IV

Co-authors:

Jeannine-Marie St-Jacques and Dr. Sunil Gurrapu, National Institute of Hydrology, India (the production of the R code for the permutation tests on quantile-quantile (Q-Q) plots)

TABLE OF CONTENTS

List of Figures	viii
List of Tables	xiii
CHAPTER 1: Introduction	1
CHAPTER 2: Literature Review	5
Climate Oscillations in North America.....	5
<i>El Niño Southern Oscillation (ENSO)</i>	5
<i>Pacific Decadal Oscillation (PDO)</i>	7
<i>Atlantic Multidecadal Oscillation (AMO)</i>	10
Hydroclimatic studies of the Pacific Decadal Oscillation and El Niño Southern Oscillation ..	13
<i>Western Canada</i>	14
<i>Western United States</i>	15
<i>Australia</i>	17
Hydroclimatic studies of the Atlantic Multidecadal Oscillation ..	18
<i>Eastern Canada</i>	19
<i>United States</i>	20
<i>Mexico</i>	23
Hydroclimatic research of climate oscillations and floods in Western North America.....	24
CHAPTER 3: Research Question	25
CHAPTER 4: Manuscript	26
Abstract.....	27
Introduction.....	28
Data and Study Area Description.....	33
Methods.....	35
<i>Influence of the climate oscillations on the North American climate</i>	35
<i>Hydrological regimes of western North America</i>	35
<i>Relationships between annual peak floods and climate oscillations assessed by permutations on quantile-quantile plots</i>	36
<i>Relationships between annual peak floods and climate oscillations assessed by Spearman's ρ</i>	37
<i>Interacting effects of the PDO and AMO phases on frequencies of annual peak flood quartiles</i>	37

<i>Detection of shifts in mean dates of seasonal minima and maxima</i>	38
Results	39
<i>Correlations between climate and the PDO and AMO in western North America</i>	39
<i>Hydrological regimes along the western North American margin</i>	40
<i>Relationships between annual peak floods and climate oscillations assessed by permutations on quantile-quantile plots</i>	42
<i>Relationships between annual peak floods and climate oscillations assessed by Spearman's ρ</i>	44
<i>Interacting effects of the PDO and AMO phases on frequencies of annual peak flood quartiles</i>	45
<i>Detection of shifts in mean dates of seasonal minima and maxima</i>	50
Discussion	55
Conclusion.....	65
Data Availability	67
Additional Information.....	67
Acknowledgements	67
Manuscript Tables	68
CHAPTER 5: General Conclusions	71
References	73
Supplementary Figures	90
Supplementary Tables	116

List of Figures

Figure 1.1 1996 Willamette River Flood in Oregon, United States.....	1
Figure 1.2 The Okanogan River Flood in Omak, Washington, United States.....	2
Figure 2.1 The El Niño Southern Oscillation (ENSO) phases in the tropical Pacific Ocean. Figure courtesy of the <i>Joint Institute for the Study of the Atmosphere and Ocean (JISAO)</i>	6
Figure 2.2 (A) winter (November-March) averaged PDO and (B) annually (January-December) averaged AMO indices (1900-2017).	8
Figure 2.3 The Pacific Decadal Oscillation phases in the North Pacific Ocean basin. Figure courtesy of the <i>Joint Institute for the Study of the Atmosphere and Ocean (JISAO)</i>	9
Figure 2.4 The average annual Atlantic Multidecadal Oscillation (AMO) index variability spatial pattern. Spatial patterns were formed using the regression coefficients between the reconstructed time series and sea-surface temperature (SST) anomalies. Figure courtesy of Wang <i>et al.</i> (2008).	11
Figure 4.1 Locations of the 250 naturally flowing streamflow records across the western North American margin used in this study.....	34
Figure 4.2 Mixed nival-pluvial seasonal hydrographs of USGS station 12451000, Stehekin River at Stehekin, Washington, USA.	42
Figure 4.3 Significant permutation tests on quantile-quantile (Q-Q) plots of the annual peak flood records along the western North American margin stratified according to the A) winter (November-March) averaged PDO phase and B) annually-averaged AMO phase ($p \leq 0.1$).	44
Figure 4.4 Percentages of lower quartile floods for the four PDO and AMO combinations for the western North American margin: A) negative PDO and positive AMO, 1944-1963; B) negative PDO and negative AMO, 1964-1976; C) positive PDO and negative AMO, 1977-1994; and D) positive PDO and positive AMO, 1995-2008.....	48
Figure 4.5 Percentages of upper quartile floods for the four PDO and AMO combinations for the western North American margin: A) negative PDO and positive AMO, 1944-1963; B) negative PDO and negative AMO, 1964-1976; C) positive PDO and negative AMO, 1977-1994; and D) positive PDO and positive AMO, 1995-2008.....	49
Figure 4.6 Differences in the Julian dates of the seasonal streamflow extremes according to the PDO phase along the western North American margin for: A) fall maxima, B) winter maxima, C) spring maxima, and D) summer minima ($p \leq 0.1$).	52

Figure 4.7 Differences in the Julian dates of the seasonal streamflow extremes according to AMO phase along the western North American margin for: A) fall maxima, B) winter maxima, C) spring maxima, and D) summer minima ($p \leq 0.1$).....	54
Figure S1. Correlation plot between the winter-averaged (November-March) PDO and winter (November-March) precipitation for North America for 1949-2015.	90
Figure S2. Correlation plot between the annually-averaged (January-December) AMO and annual (January-December) precipitation for North America for 1949-2015.	90
Figure S3. Correlation plot between the winter-averaged (November-March) PDO and winter-averaged (November-March) temperature for North America for 1949-2015.....	91
Figure S4. Correlation plot between the annually-averaged AMO and annually-averaged temperature for North America for 1949-2015	91
Figure S5. Correlation plot between the spring-averaged (April-June) AMO and spring (April-June) precipitation for North America for 1949-2015.	92
Figure S6. Correlation plot between the spring-averaged (April-June) AMO and spring (April-June) temperature for North America for 1949-2015.	92
Figure S7. Locations of the 250 naturally flowing streamflow records, stratified according to their respective hydrological regimes (glacial, nival, pluvial and mixed) across the western North American margin.	93
Figure S8. Glacial regime seasonal hydrographs of WSC station 08LD001, Adams River near Squilax, British Columbia, Canada.....	93
Figure S9. Nival regime seasonal hydrographs of WSC station 08NJ013, Slocan River near Crescent Valley, British Columbia, Canada.	94
Figure S10. Pluvial regime seasonal hydrographs of USGS station 12025000, Newaukum River near Chehalis, Washington, USA.	94
Figure S11. Pluvial regime seasonal hydrographs of USGS station 10258000, Tahquitz Creek near Palm Springs, southern California, USA.	95
Figure S12. Significant Spearman’s rank correlations ρ between annual peak flood records and A) the winter (November-March) averaged PDO index, and B) the annually averaged AMO index ($p \leq 0.1$).....	95
Figure S13. Percentages of lower quartile floods for the four PDO and AMO combinations for the northern region: A) negative PDO and positive AMO, 1944-1963; B) negative PDO and negative AMO, 1964-1976; C) positive PDO and negative AMO, 1977-1994; and D) positive PDO and positive AMO, 1995-2008.	96

Figure S14. Percentages of lower quartile floods for the four PDO and AMO combinations for the Pacific Northwest: A) negative PDO and positive AMO, 1944-1963; B) negative PDO and negative AMO, 1964-1976; C) positive PDO and negative AMO, 1977-1994; and D) positive PDO and positive AMO, 1995-2008.	97
Figure S15. Percentages of lower quartile floods for the four PDO and AMO combinations for California: A) negative PDO and positive AMO, 1944-1963; B) negative PDO and negative AMO, 1964-1976; C) positive PDO and negative AMO, 1977-1994; and D) positive PDO and positive AMO, 1995-2008.	98
Figure S16. Percentages of upper quartile floods for the four PDO and AMO combinations for the northern region: A) negative PDO and positive AMO, 1944-1963; B) negative PDO and negative AMO, 1964-1976; C) positive PDO and negative AMO, 1977-1994; and D) positive PDO and positive AMO, 1995-2008.	99
Figure S17. Percentages of upper quartile floods for the four PDO and AMO combinations for the Pacific Northwest: A) negative PDO and positive AMO, 1944-1963; B) negative PDO and negative AMO, 1964-1976; C) positive PDO and negative AMO, 1977-1994; and D) positive PDO and positive AMO, 1995-2008.	100
Figure S18. Percentages of upper quartile floods for the four PDO and AMO combinations for California: A) negative PDO and positive AMO, 1944-1963; B) negative PDO and negative AMO, 1964-1976; C) positive PDO and negative AMO, 1977-1994; and D) positive PDO and positive AMO, 1995-2008.	101
Figure S19. Percentages of lower quartile floods for the two PDO phases for the western North American margin: A) positive PDO, 1977-2008; B) negative PDO, 1944-1976.	102
Figure S20. Percentages of lower quartile floods for the two PDO phases for the northern region: A) positive PDO, 1977-2008; B) negative PDO, 1944-1976.	102
Figure S21. Percentages of lower quartile floods for the two PDO phases for the Pacific Northwest: A) positive PDO, 1977-2008; B) negative PDO, 1944-1976.....	103
Figure S22. Percentages of lower quartile floods for the two PDO phases for California: A) positive PDO, 1977-2008; B) negative PDO, 1944-1976.....	103
Figure S23. Percentages of lower quartile floods for the two AMO phases for the western North American margin: A) positive AMO, 1944-1963, 1995-2008; B) negative AMO, 1964-1994.	104
Figure S24. Percentages of lower quartile floods for the two AMO phases for the northern region: A) positive AMO, 1944-1963, 1995-2008; B) negative AMO, 1964-1994.	104
Figure S25. Percentages of lower quartile floods for the two AMO phases for the Pacific Northwest: A) positive AMO, 1944-1963, 1995-2008; B) negative AMO, 1964-1994.....	105

Figure S26. Percentages of lower quartile floods for the two AMO phases for California: A) positive AMO, 1944-1963, 1995-2008; B) negative AMO, 1964-1994.....	105
Figure S27. Percentages of upper quartile floods for the two PDO phases for the western North American margin: A) positive PDO, 1977-2008; B) negative PDO, 1944-1976.	106
Figure S28. Percentages of upper quartile floods for the two PDO phases for the northern region: A) positive PDO, 1977-2008; B) negative PDO, 1944-1976.	106
Figure S29. Percentages of upper quartile floods for the two PDO phases for the Pacific Northwest: A) positive PDO, 1977-2008; B) negative PDO, 1944-1976.....	107
Figure S30. Percentages of upper quartile floods for the two PDO phases for California: A) positive PDO, 1977-2008; B) negative PDO, 1944-1976.....	107
Figure S31. Percentages of upper quartile floods for the two AMO phases for the North American margin: A) positive AMO, 1944-1963, 1995-2008; B) negative AMO, 1964-1994.	108
Figure S32. Percentages of upper quartile floods for the two AMO phases for the northern region: A) positive AMO, 1944-1963, 1995-2008; B) negative AMO, 1964-1994.	108
Figure S33. Percentages of upper quartile floods for the two AMO phases for the Pacific Northwest: A) positive AMO, 1944-1963, 1995-2008; B) negative AMO, 1964-1994.....	109
Figure S34. Percentages of upper quartile floods for the two AMO phases for California: A) positive AMO, 1944-1963, 1995-2008; B) negative AMO, 1964-1994.....	109
Figure S35. Differences in the Julian dates of the seasonal streamflow extremes according to the PDO phase in the northern region for: A) fall maxima, B) winter maxima, C) spring maxima, and D) summer minima ($p \leq 0.1$).	110
Figure S36. Differences in the Julian dates of the seasonal streamflow extremes according to AMO phase in the northern region for: A) fall maxima, B) winter maxima, C) spring maxima, and D) summer minima ($p \leq 0.1$).....	111
Figure S37. Differences in the dates of the seasonal streamflow extremes according to the PDO phase in the Pacific Northwest for: A) fall maxima, B) winter maxima, C) spring maxima, and D) summer minima ($p \leq 0.1$).	112
Figure S38. Differences in the dates of the seasonal streamflow extremes according to AMO phase in the Pacific Northwest for: A) fall maxima, B) winter maxima, C) spring maxima, and D) summer minima ($p \leq 0.1$).	113
Figure S39. Differences in the dates of the seasonal streamflow extremes according to PDO phase in California for: A) fall maxima, B) winter maxima, C) spring maxima, and D) summer minima ($p \leq 0.1$).	114

Figure S40. Differences in the Julian dates of the seasonal streamflow extremes according to AMO phase in California for: A) fall maxima, B) winter maxima, C) spring maxima, and D) summer minima ($p \leq 0.1$).....115

List of Tables

Table 1. Impacts of the PDO/AMO combinations on the frequencies of the lower and upper quartile floods (i.e., those $\leq Q_{0.25}$ and those $\geq Q_{0.75}$, respectively).	68
Table 2. Impacts of the individual PDO and AMO phases on the frequencies of the lower and upper quartile floods (i.e., those $\leq Q_{0.25}$ and those $\geq Q_{0.75}$, respectively).	69
Table 3. Permutation <i>t</i> -test results of shifts in the Julian dates of seasonal streamflow extremes during the different PDO and AMO phases.	70
Table S1. List of the 250 streamflow gauges from the U.S. Geological Survey and the Canadian Hydrometric Database (Water Survey of Canada) with their station number, location (AK = Alaska, BC = British Columbia, CA = California, OR = Oregon, WA = Washington, YT = Yukon), latitude ($^{\circ}$ N), longitude ($^{\circ}$ E), drainage area (km^2), number of years in record, and elevation from the stream gauge (m). Station records compiled from 1900-2017, inclusively...	116
Table S2. List of the significant streamflow gauges assessed by permutation tests on quantile-quantile (Q-Q) plots stratified according to the winter-averaged (November-March) PDO index with their station number, station name, location (AK = Alaska, BC = British Columbia, CA = California, OR = Oregon, WA = Washington, YT = Yukon), <i>p</i> -values ($p \leq 0.1$) and peak streamflow phase (negative and positive).	124
Table S3. List of the significant streamflow gauges assessed by permutation tests on quantile-quantile (Q-Q) plots stratified according to the annually-averaged (January-December) AMO index with their station number, station name, location (AK = Alaska, BC = British Columbia, CA = California, OR = Oregon, WA = Washington, YT = Yukon), <i>p</i> -values ($p \leq 0.1$) and peak streamflow phase (negative and positive).	126
Table S4. Significant streamflow gauges assessed by Spearman's rank correlation ρ stratified according to the winter-averaged (November-March) PDO index with their station number, station name, location (AK = Alaska, BC = British Columbia, CA = California, OR = Oregon, WA = Washington, YT = Yukon), ρ value and <i>p</i> -values ($p \leq 0.1$).....	127
Table S5. Significant streamflow gauges assessed by Spearman's rank correlation ρ stratified according to the annually-averaged (January-December) AMO index with their station number, station name, location (AK = Alaska, BC = British Columbia, CA = California, OR = Oregon, WA = Washington, YT = Yukon), ρ value and <i>p</i> -values ($p \leq 0.1$).....	129

CHAPTER 1: Introduction

The impacts of climate change on natural disasters have become a major concern for governments due to its devastating impact on society and the environment. Natural disasters such as floods and hurricanes have increased in intensity and/or frequency due to changes in the Earth's climate system, as a result of anthropogenic climate change (Mazouz *et al.*, 2012; Milly *et al.*, 2002). In addition, land-use changes near rivers (*e.g.* forest lands to urban areas) may also play an important role in the increased intensity and frequency of seasonal floods (Rogger *et al.*, 2017; Tollan, 2002). Flooding is a severe hydrological event caused by several factors such as snowmelt of winter snowpack (spring floods), intense rain events (flash floods), ice jams, storm surges and hurricanes (coastal floods), which continues to be a major concern for governments due to the economic losses it causes to society (Ashley & Ashley, 2008; Buttle *et al.*, 2016; Jonkman, 2005; Kundzewicz *et al.*, 2019a). These flood generating mechanisms may be influenced more heavily by large scale climate oscillations (Guimarães Nobre *et al.*, 2019).

Globally, floods represent approximately 43% of total natural disasters and 47% of all weather related natural disasters (Kundzewicz *et al.*, 2019a). An estimated average of 70 million people are affected by floods worldwide each year (Kundzewicz *et al.*, 2019a).



Figure 1.1. 1996 Willamette River Flood in Oregon, United States

Aerial photograph of the 1996 flood of the Willamette River in Oregon. Photograph courtesy of the National Weather Service Portland/U.S. Army Corps of Engineers (<https://www.wrh.noaa.gov/images/pqr/96flood.jpg>).

Floods have caused approximately \$10 billion US dollars in damages and over thousands of deaths each year around the world (Kundzewicz *et al.*, 2019a). Over a 29-year period (1985-2014), the U.S. government estimated that floods have cost over \$7.96 billion US dollars in property damages (Villarini & Slater, 2017). Globally in the last century, approximately 100,000 people were killed during flood events (Jonkman, 2005). Since 1900, in Canada alone, floods have taken the lives of at least 200 people and cost the federal government billions of dollars in damages to residential and commercial properties (Buttle *et al.*, 2016; Whitfield, 2012). Even more, in the last two decades, floods in Canadian urban areas have caused over \$20 billion dollars in damages as a result of sewer blockage (Thistlethwaite & Henstra, 2017).

Climate change due to anthropogenic activities continues to rapidly intensify the hydrological cycle, resulting in greater flood risk due to more frequent and intense rain and snow events (Milly *et al.*, 2002; Thistlethwaite & Henstra, 2017). Larger populations in areas that are prone to flooding also increase concerns of future flood damages (Corringham & Cayan, 2019). For instance, the Insurance Bureau of Canada projects that approximately 1.8 million households will be highly susceptible to flood damages to their homes in the future (Thistlethwaite & Henstra, 2017).



Figure 1.2. The Okanogan River Flood in Omak, Washington, United States
Photograph of the bank overflow of the Okanogan river in Omak, Washington. Photograph courtesy of the Northwest News Network (<https://www.opb.org/news/article/okanagan-river-valley-washington-canada-flooding-photos/>).

Floods are currently the most frequent naturally occurring hazard in North America (Buttle *et al.*, 2016; Nastev & Todorov, 2013; Villarini & Slater, 2017). Spring floods (due to snowmelt) and flash floods (due to intense rain events) in the summer are the two most common types of floods that occur in North America (Buttle *et al.*, 2016). There are three main factors that influence flood risk: flood hazards (peak and frequency of floods), exposure (proximity to the flood) and vulnerability (susceptibility to flood damages); these are all controlled by the climate system, the hydrological cycle and the socioeconomic system (Kundzewicz *et al.*, 2019a). Understanding the mechanisms of the frequent occurrence of floods in western North America is essential in developing preventative measures to reduce the damages these natural hazards cause to the environment and human societies. Therefore, accurate flood risk assessments are needed.

Due to the frequent flood events occurring in North America, hydrologists conduct flood risk assessments periodically in the form of flood frequency analysis (FFA) studies to assess the potential damages flooding may cause to the environment and human populations (Archer, 1998; England Jr. *et al.*, 2018). FFA studies on rivers are conducted to assess past flood events as well as to estimate the probability of future flood events occurring in a region (Archer, 1998; England Jr. *et al.*, 2018; Kidson & Richards, 2005). Flood risk assessments are essential during the design phase of new infrastructure such as culverts, bridges and dams (Archer, 1998; Kidson & Richards, 2005). Without these FFA studies, policy makers and urban planners will find it difficult to designate flood zones when planning out residential, commercial and agricultural zones (Archer, 1998). The series of annual flood maxima data are used to estimate the return period (the time interval between the re-occurrence of two flood events in a record) (Archer, 1998; England Jr. *et al.*, 2018; Kidson & Richards, 2005). Hydrologists conduct FFA studies to

design flood management plans that protect against the occurrence of a potential major flood event at various return periods (Archer, 1998; England Jr. *et al.*, 2018; Franks & Kuczera, 2002; Hodgkins *et al.*, 2017; Kidson & Richards, 2005). Although FFA studies provide important information on potential flood risk, this particular risk assessment makes a fundamental assumption. FFA studies assume that yearly peak flood events are independent of those of previous years (Archer, 1998; England Jr. *et al.*, 2018; Franks & Kuczera, 2002; Kidson & Richards, 2005). This independent flood event assumption, based on the independent and identically distributed (*i.i.d.*) principal is currently being investigated by many researchers in the literature (England Jr. *et al.*, 2018; Franks & Kuczera, 2002; Kwon *et al.*, 2008; Micevski *et al.*, 2006; Stedinger & Griffis, 2011; Tan & Gan, 2014). The effect of long-term climate variability on flood frequencies is also not considered in these calculations, thus, due to these two factors, FFA studies may be inaccurate in its projection of flood magnitudes at various return periods (Archer, 1998; Kidson & Richards, 2005). Therefore, analyzing the influence of atmospheric-ocean oscillations (quasi-periodic patterns in the atmosphere or sea surface temperatures) on annual flood maxima along the western North American margin is needed to determine whether floods are influenced by climate variability.

CHAPTER 2: Literature Review

Climate oscillations in North America

In this literature review, I will discuss previous studies of the effects of climate oscillations on flood frequencies and magnitudes in western Canada and North America. The literature review will be divided into two sections. The first section will explore the effects of the El Niño Southern Oscillation (ENSO), Pacific Decadal Oscillation (PDO), and the Atlantic Multidecadal Oscillation (AMO) on precipitation, streamflow and flood maxima in western Canada and North America. The second section will discuss the study and research objectives for this analysis.

El Niño Southern Oscillation (ENSO)

Along the western North American coast, there are at least three prominent climate oscillations that influence the climate and hydrology. The most dominant and well-known climate oscillation affecting the Pacific coast is the El Niño Southern Oscillation (ENSO), a large scale, climate oscillation pattern of sea-surface temperatures (SSTs) in the tropical Pacific Ocean (McPhaden, 1993; Philander, 1983; Rasmusson & Carpenter, 1982; Ropelewski & Halpert, 1987; Trenberth & Hoar, 1996; Wallace *et al.*, 1998). ENSO has been linked via its teleconnections to various changes in precipitation events and the strength of trade winds across North America and Asia, and the adjacent oceans, causing droughts in India, as well as intense winter weather conditions in North America (Dai & Wigley, 2000; Philander, 1983; Ropelewski & Halpert, 1987).

ENSO is a quasi-periodic oscillation that undergoes three phase changes (warm, neutral and cold) at interannual timescales (Figure 2.1) (Kundzewicz *et al.*, 2019b; Philander, 1983; Rasmusson *et al.*, 1990; Trenberth & Hoar, 1996). The warm and cold states of ENSO are

modulated by the positive Bjerknes feedback loop which controls the changes in trade wind intensity and differences in SSTs in the equatorial Pacific Ocean (Bjerknes, 1966, 1969; Cai *et al.*, 2015a; Cai *et al.*, 2015b; Neelin *et al.*, 1998). During a warm ENSO event, also known as the El Niño state, abnormally high SSTs in the western tropical Pacific Ocean start to form in the ocean basin (Cai *et al.*, 2015a; Philander, 1983; Piechota *et al.*, 1997; Trenberth & Hoar, 1996). The Bjerknes feedback loop activates when there is a reduction of the surface pressure gradient between the western Pacific Ocean and the eastern Pacific Ocean, causing a weakening of the trade winds (Bjerknes, 1966, 1969; Cai *et al.*, 2015a; Cai *et al.*, 2015b; Neelin *et al.*, 1998; Philander, 1983). The weakening of the trade winds enable warm water bodies to move towards the eastern tropical Pacific Ocean (Cai *et al.*, 2015a; Cai *et al.*, 2015b; Neelin *et al.*, 1998; Philander, 1983).

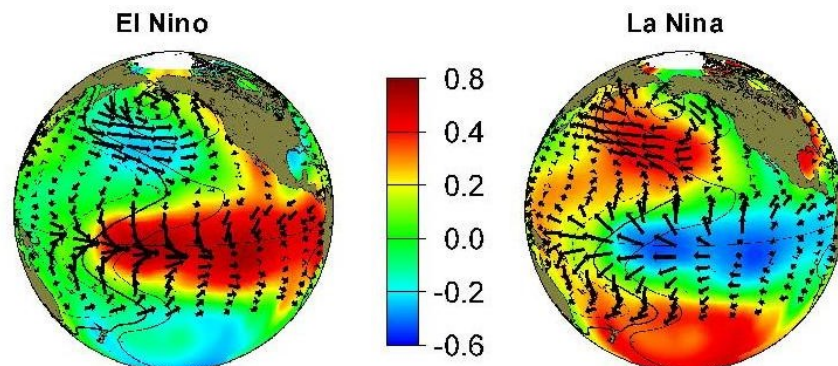


Figure 2.1. El Niño Southern Oscillation (ENSO) phases in the tropical Pacific Ocean. Warm and cold sea-surface temperatures (SSTs) depicted in red and blue, respectively, shown during El Niño (warm) and La Niña (cold) events. Surface wind patterns shown in black. Figure courtesy of the Joint Institute for the Study of the Atmosphere and Ocean (JISAO).

The movement of warm water along the eastern Pacific coast affects the existing cold water up-welling of the Humboldt current, causing temperatures to rise in the east (Neelin *et al.*, 1998; Philander, 1983). The warming temperatures along the western coast of the Americas have varying effects on precipitation, streamflow, and ocean fisheries (Andrews *et al.*, 2004; Grimm *et al.*, 2000; Philander, 1983; Ropelewski & Halpert, 1987). The El Niño state is typically

associated with higher precipitation in southern California, northern Mexico and southern South America (Grimm *et al.*, 2000; Magaña *et al.*, 2003; Penalba & Rivera, 2016; Ropelewski & Halpert, 1987; Wang *et al.*, 2014).

The end of an El Niño event is marked by the movement of a strong, cold current along the eastern Pacific coast that is driven by the strengthening of the surface pressure gradient from the Pacific Ocean basin (Bjerknes, 1966, 1969; Cai *et al.*, 2015a; Cai *et al.*, 2015b; Neelin *et al.*, 1998; Philander, 1983). The strengthening of the trade winds reinforces the feedback loop, causing warmer water bodies to move away from the eastern Pacific coast (Cai *et al.*, 2015a; Cai *et al.*, 2015b; Neelin *et al.*, 1998; Philander, 1983). Air temperatures along the eastern Pacific coast tend to cool while warm air temperatures move over to north Australia and Papua New Guinea, causing warmer SSTs in western tropical Pacific Ocean (Bjerknes, 1966, 1969; Cai *et al.*, 2015a; Neelin *et al.*, 1998; Philander, 1983). This cooling state of ENSO is known as the La Niña state. During the La Niña state, northern Canada and the Pacific Northwest receive higher precipitation (Ropelewski & Halpert, 1987). A neutral state also exists between the El Niño warm state and La Niña cold state where SSTs are less affected by surface pressure gradient changes (Kundzewicz *et al.*, 2019b). ENSO's teleconnections play a vital role in influencing temperature and precipitation patterns across various regions (Andrews *et al.*, 2004; Cai *et al.*, 2015a; Cai *et al.*, 2015b; Grimm *et al.*, 2000; Magaña *et al.*, 2003; Penalba & Rivera, 2016; Ropelewski & Halpert, 1987).

Pacific Decadal Oscillation (PDO)

The Pacific Decadal Oscillation (PDO) is another well-known climate oscillation pattern, closely related to ENSO, which affects the hydrology and climate in the northern Pacific Ocean basin (Mantua *et al.*, 1997; Mantua & Hare, 2002; Newman *et al.*, 2016). The PDO is a low

frequency, re-occurring pattern of north Pacific SSTs that alternates between its positive (warm) and its negative (cold) phases at a 20-30 year cycle (Figure 2.2A) (Mantua *et al.*, 1997; Mantua & Hare, 2002; Newman *et al.*, 2016; Whitfield *et al.*, 2010; Zhang *et al.*, 1997). The changes in SSTs in the PDO predominantly lie in the northern Pacific Ocean basin (Beebee & Manga, 2004; Mantua *et al.*, 1997; Mantua & Hare, 2002; Newman *et al.*, 2016). In the positive state, a strong Aleutian Low pressure system forms with increasing SSTs along the northwestern coast of North America (Beebee & Manga, 2004; Mantua *et al.*, 1997; Mantua & Hare, 2002; Newman *et al.*, 2016). In contrast, the Aleutian Low weakens during the cold PDO state, resulting in cooler SSTs along the north Pacific Ocean coast (Figure 2.3) (Beebee & Manga, 2004; Mantua *et al.*, 1997; Mantua & Hare, 2002; Newman *et al.*, 2016).

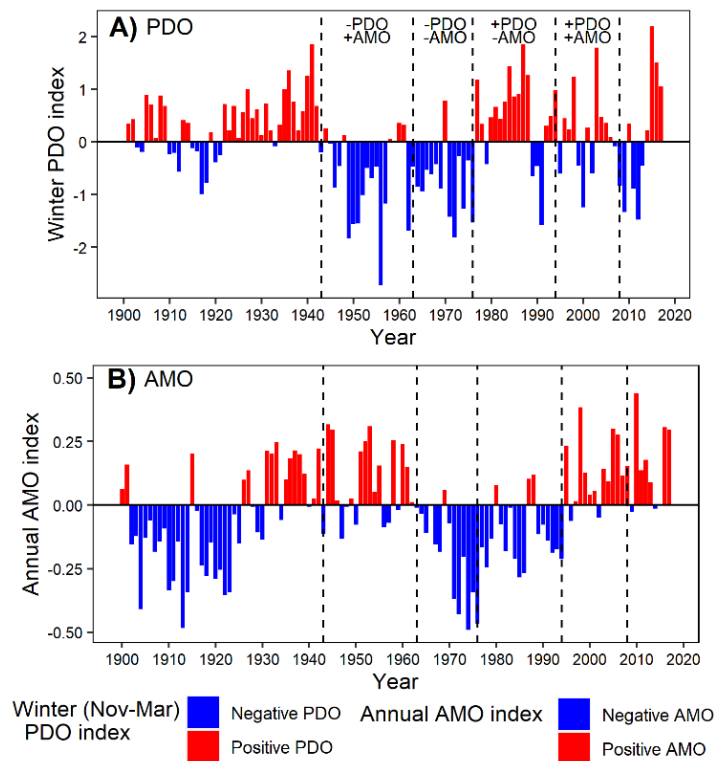


Figure 2.2. (A) winter (November-March) averaged PDO and (B) annually (January-December) averaged AMO indices (1900-2017). Negative PDO and AMO phases shown in blue, positive PDO and AMO phases shown in red. The dotted lines mark the PDO and AMO combinations: 1944-1963 – negative PDO and positive AMO, 1964-1976 – negative PDO and negative AMO, 1977-1994 – positive PDO and negative AMO, and 1995-2008 – positive PDO and positive AMO.

Several mechanisms have been proposed to account for the variability of the PDO (Alexander, 2013; Alexander & Deser, 1995; Barnett *et al.*, 1999; Latif & Barnett, 1996; Mantua *et al.*, 1997; Mantua & Hare, 2002; Miller *et al.*, 1994; Newman *et al.*, 2016). It has been proposed that a stochastic forcing via the passing of atmospheric storms affect SSTs in the mixed layer of the North Pacific Ocean, creating a negative air-sea feedback loop, which results in changes in the surface sensible and latent heat fluxes (Alexander, 2013; Alexander & Deser, 1995). The stochastic heat flux forcing causes strengthening or weakening of the SST anomalies. The combination of the stochastic heat flux forcing and fluctuations in the Aleutian Low results in the PDO's variability (Alexander, 2013; Alexander & Deser, 1995).

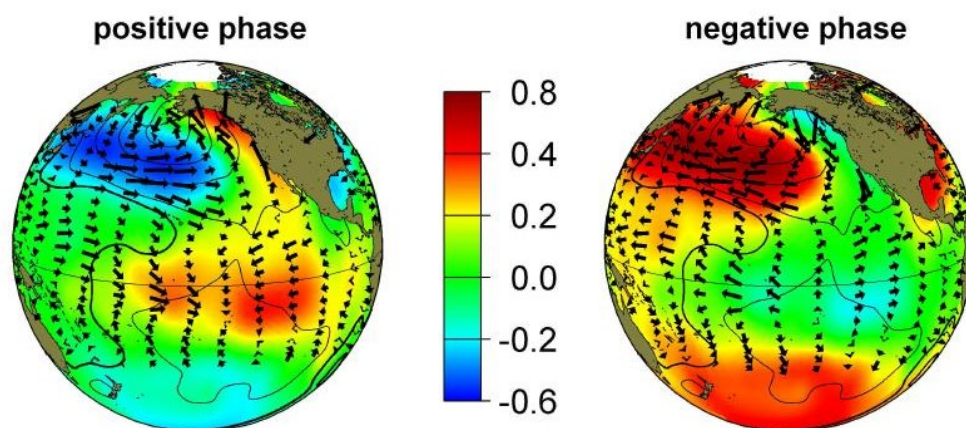


Figure 2.3. The Pacific Decadal Oscillation (PDO) phases in the North Pacific Ocean basin. Warm and cold SSTs shown as red and blue, respectively, during the positive PDO's positive (warm) and negative (cold) states. The surface wind patterns shown in black. Figure courtesy of the Joint Institute for the Study of the Atmosphere and Ocean (JISAO).

A second mechanism identifies the ENSO teleconnections in the tropical Pacific as influencing the PDO's variability via an "atmospheric bridge", whereby changes in surface air temperature, humidity and wind in the equatorial Pacific impact ocean currents, SSTs and salinities of the North Pacific (Alexander, 2013; Alexander *et al.*, 2002). Lastly, a re-emergence mechanism has been proposed to explain the variability of the PDO, whereupon seasonal temperature anomalies that are retained in the ocean mixed layer during the summer, resurface

during the following winter (Alexander, 2013; Alexander & Deser, 1995). The combination of all three proposed mechanisms, as well as the displacement of the North Pacific Ocean gyres, combined with Ekman transport of water are probably all factors in the PDO's variability (Alexander, 2013; Mantua & Hare, 2002; Miller *et al.*, 1994; Newman *et al.*, 2016).

Atlantic Multidecadal Oscillation (AMO)

The most prominent atmospheric-ocean oscillation influencing precipitation patterns in eastern North America is the Atlantic Multidecadal Oscillation (AMO); however, its effects are felt continent-wide, and even in Europe and Asia. The effects of the AMO have been studied to understand its influence on hurricanes in the Atlantic Ocean, as well as its impact on summer climate throughout North America and in Europe (Häkkinen *et al.*, 2011). There are multiple definitions of the AMO. For instance, Enfield *et al.* (2001) defined the AMO index as the 10-year running mean of linearly detrended averaged SSTs across the North Atlantic Ocean (from the equator to 70°N). Other researchers have used slightly different definitions to define the AMO index in the North Atlantic Ocean (Drinkwater *et al.*, 2014; Sutton & Hodson, 2005; Trenberth & Shea, 2006). Nevertheless, the most common definition of the AMO is the following. The AMO is characterized as a low frequency, re-occurring pattern of Atlantic SSTs in the North Atlantic Ocean (from the equator to 70°N) with a periodicity of 60-90 years (Dima & Lohmann, 2007; Enfield *et al.*, 2001; García-García & Ummenhofer, 2015; Kerr, 2000; Kundzewicz *et al.*, 2019b; Wang *et al.*, 2008). The AMO has two phases: a positive (or warm) phase where SST anomalies are above zero, and a negative (or cold) phase where SST anomalies are below zero (Figures 2.2B and 2.4).

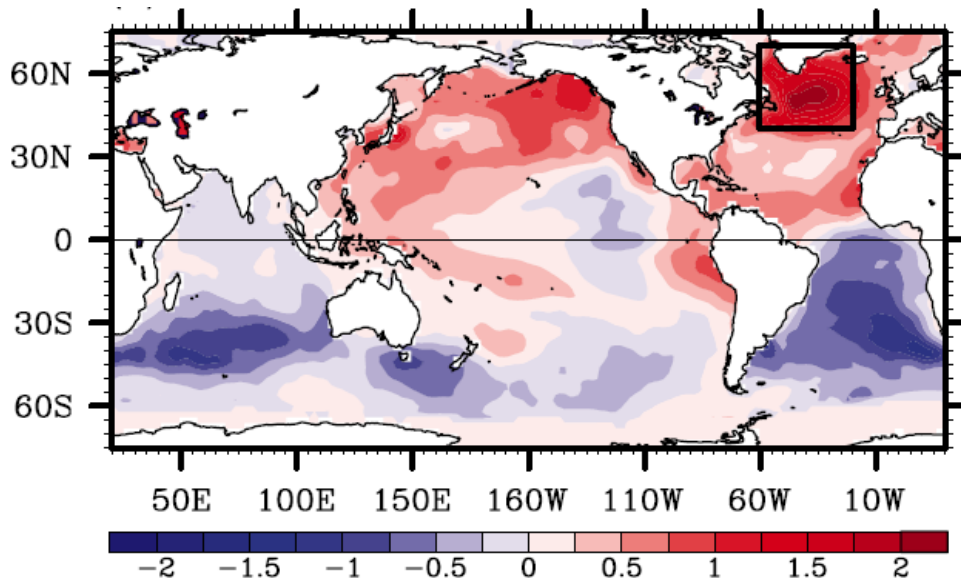


Figure 2.4. The average annual Atlantic Multidecadal Oscillation (AMO) index variability spatial pattern. Spatial patterns were formed using the regression coefficients between the reconstructed time series and sea-surface temperature (SST) anomalies. The black inset box represents the temporal variability of the North Atlantic region. Figure courtesy of Wang *et al.* (2008).

Instrumental records of the AMO begin in 1856 in its positive phase where SST anomalies are above zero (not shown). In 1901, the AMO switches from its positive phase to its negative phase where the SST anomalies in the North Atlantic Ocean were below zero (Figure 2.2B). During 1926-1962 period, significantly warmer SSTs were found in the North Atlantic Ocean. In 1963, the AMO switched again to its negative phase where colder SST anomalies were found in the North Atlantic Ocean (Figure 2.2B). In 1995 until present, the AMO changed to its positive phase (Figure 2.2B). The positive AMO phase is typically associated with more precipitation in western Europe, the Sahel, India, southeast Asia, and the United States' Pacific Northwest (Enfield *et al.*, 2001; García-García & Ummenhofer, 2015; Goswami *et al.*, 2006; Knight *et al.*, 2006; Sutton & Hodson, 2005). Conversely, the negative AMO phase is linked with more precipitation in the continental United States (Enfield *et al.*, 2001).

Several mechanisms have been proposed to generate the AMO. For instance, Häkkinen *et al.* (2011) proposed that atmospheric blocking (high-pressure systems that “block” westerly

winds in the mid- and high-latitudes) via changes in surface wind stress and wind stress curl influence ocean circulation patterns in the North Atlantic Ocean. They proposed that weakening of the wind stress curl contributes to weakening of the ocean gyre circulation which results in greater warming in the subpolar region of the Atlantic Ocean (Häkkinen *et al.*, 2011). During periods of atmospheric blocking in western Europe and Greenland, the AMO has its warmest SST anomalies (Häkkinen *et al.*, 2011). Conversely, the strengthening of the wind stress curl corresponds to strengthening of the ocean gyre circulation in the subpolar region, which results in cooling of the subpolar Atlantic Ocean (Häkkinen *et al.*, 2011). Stronger wind stress curl coincides with colder AMO SST anomalies (Häkkinen *et al.*, 2011). Other studies have proposed that the AMO phases covary with the strength of the Atlantic Meridional Overturning Circulation (AMOC), that is, the variation of the ocean thermohaline circulation (THC) in the North Atlantic Ocean (d'Orgeville & Peltier, 2007; Frajka-Williams *et al.*, 2017; García-García & Ummenhofer, 2015; Knight *et al.*, 2005). Warmer Atlantic SSTs are associated with a stronger AMOC, whereas colder Atlantic SSTs are associated with a weaker AMOC (Frajka-Williams *et al.*, 2017).

Dima & Lohmann (2007) proposed another mechanism for the AMO based on several atmospheric, ocean and sea ice interactions. In their proposed mechanism, the AMO undergoes a series of positive and negative feedback loops where the Atlantic SSTs have a positive feedback on the sea level pressure (SLP) in the Pacific Ocean via atmospheric teleconnections, and a negative feedback on the SLP in the Atlantic Ocean. The differences in SLP in the North Atlantic and North Pacific Ocean basins create a positive feedback on the SLP gradient which results in a positive feedback on wind stress in the North Atlantic Ocean (Dima & Lohmann, 2007). The positive feedback on wind stress results in more sea ice export from the North

Atlantic Ocean which causes a negative feedback on the THC due to influx of freshwater. The negative feedback on the THC occurs over a 10-20-year period, then the cycle is completed and the AMO switches to its opposite phase. They found that the sign of the AMO phase is lagged by the activity of the sea ice export. When sea ice export is at minimum activity, less sea ice is exported across the North Atlantic Ocean which results in less influx of cold freshwater, leading to a warmer THC and warmer SSTs in the Atlantic Ocean (positive AMO phase). Conversely, colder SSTs in the Atlantic Ocean are observed when sea ice export is at maximum activity (colder THC) (Dima & Lohmann, 2007).

Thus, there are multiple mechanisms proposed to describe the processes of the AMO. Atmospheric blocking via surface wind stress and wind stress curl, as well as the negative feedback on the THC due to sea ice transport all contribute to the mechanism of the AMO. A better understanding of the driving mechanism of the AMO will be useful in understanding of how the AMO influences North American climate.

Hydroclimatic studies of the El Niño Southern Oscillation and Pacific Decadal Oscillation

Numerous studies have explored the links between ENSO and the PDO on precipitation, streamflow and river discharge in western Canada, United States and Australia (Brabets & Walvoord, 2009; Burn *et al.*, 2004; Franks & Kuczera, 2002; Gurrapu *et al.*, 2016; Kiem *et al.*, 2003; Micevski *et al.*, 2006; Neal *et al.*, 2002; Praskievicz & Chang, 2009; Redmond & Koch, 1991; Whitfield *et al.*, 2010). In the following section, hydroclimatic studies conducted in western Canada will be presented first, followed by studies done in the United States, and lastly Australia.

Western Canada

Whitfield *et al.* (2010) surveyed the influence of the PDO on precipitation, temperature, streamflow, and snowpack in western Canada. They found that the PDO has a significant effect on spring temperature in northwestern North America, with warmer temperatures were observed during El Niño winters and the warm PDO phase in Alaska and British Columbia, and cooler temperatures observed during La Niña winters and the cold PDO phase. Similarly, the PDO has a varying impact on precipitation where seasonal precipitation varies depending on the PDO phase in Alaska, British Columbia, and the Yukon. Furthermore, they showed that the PDO influences snow accumulation, the timing of snowmelt and streamflow patterns in western Canada. During the positive PDO phase, snow accumulation decreases in southern British Columbia, resulting in earlier snowmelt, whereas, there is an increase in snow accumulation and later snowmelt in the negative PDO phase (Whitfield *et al.*, 2010). In southern British Columbia, earlier snowmelt leads to high winter streamflow, whereas later snowmelt in the negative PDO state leads to higher spring and summer streamflow.

Brabets & Walvoord (2009) studied the influence of the PDO on the monthly, seasonal, and annual discharge of 21 rivers from the Yukon River Basin from 1944 to 2005. They found that there is a strong relationship between streamflow and the PDO index where higher streamflow is observed during the positive PDO phase in December-February. They also found that lower streamflow occurs during the negative PDO phase (Brabets & Walvoord, 2009). As the PDO shifts from its negative state to its positive state, air temperature above the Yukon River Basin increases, causing permafrost to thaw more quickly, resulting in greater groundwater discharge. During July-September, higher streamflow is observed during the negative PDO phase, whereas lower streamflow is observed during the positive PDO phase.

Burn *et al.* (2004) analyzed the trends of several hydrological variables in the Liard River Basin in northern (Yukon, the Northwest Territories, and British Columbia) Canada and found that the PDO index correlates negatively with the annual maximum flood date and spring freshet date (defined as the date where streamflow is 1.5 times higher than the average flow from the last 16 days). During the positive PDO phase, snowmelt occurs earlier in the spring, whereas in the negative PDO phase, snowmelt occurs later in the summer (Burn *et al.*, 2004).

Gurrapu *et al.* (2016) examined the influence of the PDO on the flood frequencies of rivers in western Canada. They showed that annual peak flood records do not adhere to the independent and identically distributed (*i.i.d.*) assumption made in flood risk assessments as stations in British Columbia, Alberta and Saskatchewan recorded higher annual peak floods in the negative PDO phase; stations recorded lower peak annual floods when the PDO was in its positive state (Gurrapu *et al.*, 2016).

Although these above studies have shown that the PDO influences streamflow patterns, they did not consider the combined effects of multiple climate oscillations such as the PDO and AMO on historical annual peak flood records and the timing of seasonal maxima and seasonal minima.

Western United States

Redmond & Koch (1991) analyzed the correlation between the precipitation patterns of October and March, and the mean Southern Oscillation Index (SOI) (an ENSO metric) for the previous June through November months in coastal California to understand the changes of precipitation events during ENSO's El Niño and La Niña states. They concluded that California receives more precipitation during El Niño events and less precipitation during La Niña events (Redmond & Koch, 1991). Furthermore, Cayan *et al.* (1999) studied the relationship between the

SOI and the statistical frequency of daily precipitation events and the 50th and 90th percentiles of streamflow. They showed that daily precipitation events and streamflow were influenced by ENSO's El Niño state (Cayan *et al.*, 1999).

Andrews *et al.* (2004) studied the influence of ENSO on the frequency of floods along the Californian coast. They expanded the results of Schonher & Nicholson's (1989) study which found that winter precipitation in the coastal mountains is more sensitive to variations in ENSO than that in the interior regions. They concluded that southern California rainfall patterns are strongly influenced by ENSO patterns in comparison to those of central and northern California (Schonher & Nicholson, 1989). Andrews *et al.* (2004)'s study of ENSO's influence on flood frequency on the California coast showed that floods have greater magnitudes during the ENSO's El Niño state.

Praskievicz & Chang (2009) studied the separate and combined effects of ENSO and the PDO on winter precipitation intensity in Oregon's Willamette Valley. They showed that higher precipitation intensity is linked to ENSO's La Niña phase in November, whereas higher precipitation intensity is linked to ENSO's El Niño phase in April (Praskievicz & Chang, 2009). They concluded that there is greater precipitation during the negative PDO phase in Oregon.

Neal *et al.* (2002) studied the PDO's effect on streamflow discharge patterns in southern Alaska. They stratified streamflow records according the PDO's negative phase (1947-1976) and the PDO's positive phase (1977-1998) as reference points to mark the changes in Pacific SSTs (Neal *et al.*, 2002). They found that the winter monthly and seasonal river discharges were higher during the positive PDO phase. During the winter, precipitation in southeastern Alaska fell as rain in the positive PDO phase, whereas in the negative PDO phase, precipitation fell as snow. In

the negative PDO state, snowpack melted later in the season, causing a higher summer river discharge.

Beebee & Manga (2004) studied the influence of ENSO and the PDO on the annual average river discharge and snowmelt timing in eight watersheds in Oregon. They found that ENSO correlated with the variability of the annual average discharge, whereas the PDO correlated with the timing of spring snowmelt and annual peak floods. They found that the peak spring runoff occurs significantly earlier in the positive PDO and occurs later in the negative PDO phase (Beebee & Manga, 2004). These above studies have shown that ENSO and the PDO affect precipitation and streamflow patterns. However, these studies did not consider the individual and combined effects of other climate oscillations such as the AMO on annual peak flood records.

Australia

Kiem *et al.* (2003) analyzed the variability of flood risk across New South Wales, Australia, stratifying flood records according to the PDO and ENSO events. They concluded that higher flood risk occurs during La Niña events than El Niño events. In addition, flood risk elevates when the PDO is in its negative phase. They found that the PDO's modulation of ENSO is linked to rain-induced flooding in eastern Australia and flood risks are much greater when La Niña events coincides with the PDO's negative phase (Kiem *et al.*, 2003).

Franks & Kuczera (2002) analyzed annual maximum flood data in New South Wales, Australia to assess whether they adhere to the *i.i.d.* flood event assumption. They stratified records according to two periods: pre-1945 (when the Interdecadal Pacific Oscillation, a climate oscillation related to the PDO shifted from its positive to its negative phase) and post-1945 (the negative IPO phase) to determine the changes in flood frequencies (if any). They concluded that

a significant number of records had larger 20-year flood ratios (the distribution of floods in the negative and positive phases) after 1945 (during the negative IPO phase) in comparison to the pre-1945 period.

Micevski *et al.* (2006) tested the *i.i.d* flood event assumption by analyzing the effects of the IPO on annual maximum flood data in New South Wales and southern Queensland, Australia. Records were stratified according to the negative and positive IPO indices and their flood frequencies were calculated. They found that the IPO modulated flood risk in New South Wales and southern Queensland, where annual peak flood quantiles were 1.7 times higher during the negative IPO phase than the positive phase (Micevski *et al.*, 2006). They concluded that the change in flood frequencies were related to the shifts of SSTs and the movement of regional convergence zones. These above studies established that the *i.i.d* flood event assumption is untenable in Australia, a region whose hydroclimatology is strongly influenced by the two climate oscillations: ENSO and the IPO.

Hydroclimatic studies of the Atlantic Multidecadal Oscillation

Hydroclimatic studies of the AMO are predominantly focused on analyzing rain and mean annual or mean seasonal streamflow, rather than annual peak floods (Archfield *et al.*, 2016; Assani *et al.*, 2010a; Assani *et al.*, 2010b; Enfield *et al.*, 2001; Fortier *et al.*, 2011; Hodgkins *et al.*, 2017; Mallakpour & Villarini, 2017; Méndez & Magaña, 2010; Pascolini-Campbell *et al.*, 2017; Valdés-Manzanilla, 2016, 2018). These studies have been conducted on selective regions across eastern Canada, United States and Mexico. Studies in western Canada have largely focused on the effects of ENSO and the PDO on precipitation and streamflow patterns. However, very few studies have explored the effects of the AMO on precipitation,

streamflow, and river discharge in western Canada. Again, in this section, the hydroclimatic studies are organized according to their geographic location.

Eastern Canada

In southern Québec, Fortier *et al.* (2011) studied the temporal variability of large floods in the Matawin River, a sub-tributary of the St. Lawrence River. They compared the interannual variability of streamflow upstream and downstream to the Matawin dam. The streamflow gauge used upstream of the dam (Saint-Michel-Des-Saints) is part of the Canadian Reference Hydrometric Basin Network (RHBN) (station gauges that originate from protected watersheds which are not regulated or influenced by urbanization or reservoirs). They found that floods that were upstream to the Matawin dam correlated negatively to the AMO, whereas floods downstream to the dam correlated positively to the AMO (Fortier *et al.*, 2011).

Assani *et al.* (2010a) studied the temporal variability modes of annual maximum streamflow in the St. Lawrence watershed. They did a principal component analysis (PCA) to assess the temporal variability modes of floods in southern Québec. They used a correlation matrix to analyze the correlations among the streamflow gauges assessed in the St. Lawrence watershed. They found that the first three principal components explained 62% of the annual maximum streamflow variability (Assani *et al.*, 2010a). The first principal component (PC-I) corresponded with the north shore of the St. Lawrence River at 47°N, whereas PC-II and PC-III matched with the south shore of the river. The interannual variability analysis showed that the PC-I scores had a statistically significant positive trend (increase in maximum annual flow over time); this was detected using the Mann-Kendall test. Although PC-II and PC-III had negative trends in its interannual variability, they were not statistically significant. Furthermore, they showed that PC-I correlated negatively to the AMO. PC-II had a statistically significant positive

correlation to NINO3.4 and to the Southern Oscillation Index (SOI) (both metrics of ENSO). PC-III correlated positively to the Arctic Oscillation (AO); however, it was only significant at the 90% confidence level.

Moreover, a second Assani *et al.* (2010b) study was conducted in southern Québec examining the relationships between atmospheric-ocean oscillations and mean annual streamflow from 16 naturally flowing rivers in the St. Lawrence watershed. Similar to the first study, they conducted a PCA to determine the relationship between six climate indices and mean annual streamflow of the tributaries of the St. Lawrence River. Thirteen of sixteen streamflow gauges were common to both studies. They used a correlation matrix to analyze the correlations among the streamflow gauges analyzed in the study. Approximately 60% of the streamflow's variance was explained by the first three principal components. The first two principal components (PC-I and PC-II) were located near the south shore of the St. Lawrence River at 47°N, and the third principal component (PC-III) was located on the north shore of the river (Assani *et al.*, 2010b). They found that the AO and the AMO had negative correlations with PC-II and PC-III, respectively. Although the studies of Assani *et al.* (2010a, 2010b) have shown that there is a link between climate oscillations and streamflow patterns, their studies focused only on the lower St. Lawrence valley in southern Québec.

United States

Enfield *et al.* (2001) studied the impact of the AMO on precipitation and river flow across the continental United States. They discovered that there are significant correlations between precipitation and the negative AMO phase across the contiguous United States, except for Florida and the Pacific Northwest (significant positive correlations to precipitation). Furthermore, they found that summer rainfall is the most sensitive to changes in the AMO. In

addition, there is a significant positive correlation between winter rainfall and the positive AMO phase in Florida, whereas winter rainfall in the eastern Mississippi basin correlates with the negative AMO phase (Enfield *et al.*, 2001). The AMO's influence on rainfall variability also has a consequential effect on river flows; they found that streamflow increases during the positive AMO phase in Florida. They recommend that flood protection measures should be heightened when the AMO is in its positive phase. Furthermore, they found that the inflow of water in the negative AMO phase was two times lower than in the positive AMO phase in Florida.

Pascolini-Campbell *et al.* (2017) studied the influence of the AMO and PDO on monthly mean streamflow from naturally flowing rivers in the Upper Rio Grande Basin. They assessed the streamflow of 7 hydrometric gauges from New Mexico, United States. They found that the climate indices had stronger correlations with streamflow at decadal timescales. For instance, they found that decadal high streamflow from 1900-1920 and 1979-1995 were influenced by the AMO's negative phase and the PDO's positive (warm) phase. They found that decadal low streamflow from 1945-1975 and 1996-2014 were influenced by the AMO's positive phase and the PDO's negative (cold) phase. However, their study did not find that the PDO and AMO explain streamflow variability at annual timescales in the Upper Rio Grande Basin (Pascolini-Campbell *et al.*, 2017).

Archfield *et al.* (2016) studied the volume, frequency, magnitude, and duration of flood events across the United States using the peaks over threshold (POT) method (the selection of all extreme streamflow peaks above a streamflow threshold). Station gauges from only naturally flowing rivers were analyzed and their flood variables were correlated with the AMO, North Atlantic Oscillation (NAO), PDO and ENSO. They showed that only flood volume and flood duration correlated strongly to ENSO (25% of stations studied showed a significant effect).

Other climate indices such as the AMO, NAO and PDO did not correlate strongly with any of the streamflow gauges across different regions in the United States. Archfield *et al.* (2016) found that the New England region (eastern United States), the northern Great Plains and the Upper Mississippi Valley were the only regions to have significant changes in their flood properties. The New England region had increases in the frequency of flood events over the 1940-2013 period, despite having decreases in the magnitude, volume, and duration of these hydrological events. The northern Great Plains and Upper Mississippi Valley had different flood responses than the New England region. Although flood frequency decreased in these regions, flood volume, magnitude and duration were significantly higher during the 1940-2013 period. They concluded that there were no clear, distinct regional patterns which shows that climate oscillations are influencing floods across the United States (Archfield *et al.*, 2016). They do suggest, however, that examining flood properties at the catchment level may provide more information on the regional patterns that may exist in the United States.

Mallakpour & Villarini (2017) studied the seasonal and annual changes in frequency and magnitude of intense precipitation events across the contiguous United States. They utilized the POT method and the block maxima approach (extreme value theorem methods) to assess the frequency and magnitude of extreme precipitation events, respectively. They conducted a Mann-Kendall trend test to assess the trends of extreme precipitation events (Mallakpour & Villarini, 2017). Mallakpour & Villarini (2017) also used this test to analyze the positive and/or negative relationship between the magnitude of extreme precipitation events and several climate indices (*e.g.* AMO, NAO, PDO and ENSO). They found that climate variability has a prominent effect on the frequency of intense precipitation events across different regions in the United States. Most notably, the northeastern United States had the largest increase in intense precipitation

during the 1948-2012 period. In addition, they found that western United States coast have the most extreme precipitation events during the winter, whereas the highest occurrence of extreme precipitation events occurs in the summer in the eastern part of the southwestern United States region. Moreover, they found that the NAO and PDO had their most prominent impact on winter rainfall, whereas the AMO had its greatest impact on fall rainfall.

Hodgkins *et al.* (2017) analyzed the effects of the AMO and PDO on major flood patterns (the 100-year flood events) across North America and Europe using annual peak flow data from 1204 station gauges (Hodgkins *et al.*, 2017; Mantua *et al.*, 1997). A significant negative relationship was detected between flood events at the 25 and 50-year return periods and the AMO in large (greater than 1000 km²) catchments in North America (Hodgkins *et al.*, 2017). A positive temporal trend was detected for major flood events at the 50-year return period for medium sized catchments (100-1000 km²) in Europe.

Mexico

Valdés-Manzanilla (2016) studied historical flood events in Tabasco and Chiapas, Mexico, and found that most floods occurred during the positive phase of the AMO. They conducted an odds ratio test that showed it was approximately 1.9 times more likely for floods to occur in the positive AMO phase, than the negative AMO phase in southeastern Mexico (Valdés-Manzanilla, 2016). In a second study by Valdés-Manzanilla (2018), the effects of the AMO and the PDO on historical flood events in the Papaloapan River Basin in Mexico was studied. A wavelet coherence analysis was conducted and an in-phase relationship between the AMO and the PDO positive phases were found (Valdés-Manzanilla, 2018).

Méndez & Magaña (2010) studied the links between the AMO and PDO using drought indices (precipitation data) in Mexico. They showed that the combined effects of the AMO and

PDO phases play a role in the number of droughts that occur in Mexico (Méndez & Magaña, 2010). More specifically, droughts in northern Mexico occurred more frequently when the PDO was in its negative phase and the AMO is in its positive phase, whereas in southern Mexico, droughts were more frequent when the PDO is in its positive phase and the AMO is in its negative phase (Méndez & Magaña, 2010). Thus, the studies in Mexico and United States show that the occurrence of flood events in North America may be affected by the interactions between the AMO and PDO phases. However, these hydroclimatic studies have not yet assessed the impacts of climate oscillations on historical annual peak flood records across the entire western North American margin north of Mexico.

Hydroclimatic research of climate oscillations and floods in Western North America

Previous hydroclimate research indicates that atmosphere-climate oscillations (*e.g.* the PDO and AMO) influence precipitation and streamflow patterns in western Canada and the western United States. Although numerous studies have shown that these climate indices affect mean river discharges and extreme precipitation events in western North America, much less work has been done studying effects on peak annual floods. The individual and combined effects of the PDO and AMO on annual peak flood records have yet to be explored across the entire western North American margin, in a single study using the same metrics throughout. In the following chapters, the study's research question and objectives, and the manuscript containing the methods and results will be discussed in greater detail.

CHAPTER 3: Research Question

Along the western North American margin, there are still many questions that remain to be answered concerning the effects of the multiple climate oscillations that strongly affect this area, such as how they interact and combine. In addition, the identically and independently distributed (*i.i.d.*) flood event assumption, *i.e.*, that yearly peak flood events are independent of those of previous years, remains a fundamental hydrological concept, although it is under scrutiny. However, annual peak flood records in this area may not adhere to this *i.i.d.* assumption because of the influence of the multiple interacting climate oscillations. Therefore, the aim of this project is to answer the following research question: are annual peak floods in naturally flowing rivers along the western North American margin affected by the individual and combined effects of the Pacific Decadal Oscillation (PDO) and the Atlantic Multidecadal Oscillation (AMO)?

This study aims to address the following objectives: 1) to assess the individual effects of the PDO and AMO on annual peak flood magnitudes, 2) to quantify the individual and combined effects of the PDO and AMO on the frequencies of lower and upper quartile annual peak floods, and 3) to determine any shifts of the dates of seasonal maxima and seasonal minima during extreme PDO and AMO events.

CHAPTER 4: Manuscript

**ASSESSING THE INFLUENCE OF THE PACIFIC DECADAL OSCILLATION AND
THE ATLANTIC MULTIDECADAL OSCILLATION ON DISCHARGE VARIABILITY
IN WESTERN NORTH AMERICA**

Duane Darren Noel¹, Jeannine-Marie St-Jacques¹ and Sunil Gurrapu²

¹Department of Geography, Planning and Environment, Concordia University, Montréal,
Québec, Canada.

²National Institute of Hydrology, Jal Vigyan Bhawan, Roorkee – 247 667 (Uttarakhand), India.

Manuscript to be submitted to the *Journal of the American Water Resources Association*
(*JAWRA*)

ABSTRACT

Flood frequency analysis assumes that annual peak flood events occur independently of each other, regardless of previous flood events (the independent and identically distributed (*i.i.d.*) assumption); however, annual peak flood records do not necessarily appear to conform to these assumptions. We tested the *i.i.d.* assumption by analyzing the effects of the Pacific Decadal Oscillation (PDO) and Atlantic Multidecadal Oscillation (AMO) on 250 naturally flowing annual peak flood records across the entire western North American margin. Using permutation tests on quantile-quantile (Q-Q) plots, we found that the PDO has a greater impact on the magnitude of annual peak floods than the AMO. Twenty-six percent of the gauges have higher magnitude annual floods depending on the PDO phase ($p < 0.1$). Next, we examined the interacting effects of the PDO and AMO on the frequencies of lower and upper quartile annual peak floods, and found reinforcing, cancelling, and dominating effects. Lastly, we used permutation *t*-tests on the Julian dates of seasonal maximum and minimum streamflows to assess the impact of the PDO and AMO. We found that the PDO and AMO have substantial effects on the dates of winter maximum and summer minimum streamflow dates across the coastal margin. Since these two climate oscillations have significant effects on the magnitudes of annual peak floods, the *i.i.d.* assumption does not hold. Hence, we advocate for the need to re-assess baseline flood analysis in western North America to improve flood management strategies.

INTRODUCTION

Flooding is a severe hydrological event caused by several factors such as snowmelt of winter snowpack (spring floods), intense rain events (flash floods), ice jams, storm surges and hurricanes (coastal floods) (Buttle *et al.*, 2016; Kundzewicz *et al.*, 2019a). Globally, floods represent approximately 43% of total natural disasters and 47% of all weather related natural disasters (Kundzewicz *et al.*, 2019a). An estimated average of 70 million people worldwide are affected by floods each year (Kundzewicz *et al.*, 2019a). Furthermore, floods have caused approximately \$10 billion US dollars in damages and over thousands of deaths each year around the world (Kundzewicz *et al.*, 2019a). Climate change due to anthropogenic activities continues to rapidly intensify the hydrological cycle, resulting in greater flood risk due to more frequent and intense rain and snow events (Milly *et al.*, 2002). The growth of large populations in regions that are prone to flooding also presents additional challenges to mitigating flood risk in expanding industrial, commercial and residential areas in the future (Corringham & Cayan, 2019).

Flood frequency analysis (FFA) studies are conducted to assess regional flood risks (Archer, 1998; England Jr. *et al.*, 2018). FFA studies are conducted as part of flood management plans to protect against a potential 100-year peak flood (Archer, 1998; England Jr. *et al.*, 2018; Franks & Kuczera, 2002). However, FFA studies assume that yearly flood events are independent of those of previous years (the independent and identically distributed (*i.i.d.*) flood event assumption) (Archer, 1998; England Jr. *et al.*, 2018; Franks & Kuczera, 2002). The effect of long-term climate variability on flood frequencies is also not considered in these calculations, thus, due to these two factors, FFA studies may be inaccurate in their prediction of flood magnitudes at various return periods (Archer, 1998; Hamlet & Lettenmaier, 2007; Kidson &

Richards, 2005). Flood events may be influenced by atmosphere-ocean climate oscillations such as the Pacific Decadal Oscillation (PDO) and the Atlantic Multidecadal Oscillation (AMO).

The PDO is a low-frequency, re-occurring pattern of north Pacific sea-surface temperatures (SST) with phases that shift on multi-decadal timescales (Alexander, 2013; Mantua *et al.*, 1997; Mantua & Hare, 2002; Mochizuki *et al.*, 2010; Newman *et al.*, 2016; Zhang *et al.*, 1997). Defined by Latif and Barnett (1996) and Mantua *et al.* (1997) as an empirical orthogonal function (EOF) of North Pacific Ocean (20°-70°N) monthly average SST anomalies, the PDO oscillates between its negative (cold) phase and its positive (warm) phase. In contrast, the AMO is characterized as a low frequency, re-occurring pattern of SSTs in the North Atlantic Ocean (from the equator to 70°N) (Enfield *et al.*, 2001; García-García & Ummenhofer, 2015; Kundzewicz *et al.*, 2019b; Wang *et al.*, 2008). The AMO has a periodicity of approximately 60-90 years (Dima & Lohmann, 2007; Enfield *et al.*, 2001; García-García & Ummenhofer, 2015; Kerr, 2000; Kundzewicz *et al.*, 2019b). The positive (warm) AMO phase consists of SST anomalies greater than zero, whereas the negative (cold) AMO phase is comprised of SST anomalies below zero.

Recent hydroclimatic research has studied the influence of the PDO and AMO on mean annual streamflows, and begun the study of their influence on floods in North America (Gurrapu *et al.*, 2016; Hodgkins *et al.*, 2017; Kundzewicz *et al.*, 2019b; Neal *et al.*, 2002; Whitfield *et al.*, 2010). Gurrapu *et al.* (2016) analyzed the influence of the PDO on annual peak flows in western Canada and concluded that there are higher annual peak flows in the negative PDO phase than in the positive phase. Hodgkins *et al.* (2017) analyzed the influence of the PDO and the AMO on flood frequencies in North America and Europe and found a significant negative relationship between flood events at the 25 and 50-year return periods and the AMO in large (greater than

1000 km²) catchments in North America. They did not find significant relationships between major flood occurrences and the PDO at the continental scale. However, they proposed that analyzing the influence of the PDO and AMO on annual peak flood records across a smaller geographic region might identify more substantial relationships between PDO and AMO phases and flood occurrences (Hodgkins *et al.*, 2017).

Previous studies have primarily focused on the combined influence of the PDO and the related El Niño Southern Oscillation (ENSO) on streamflow hydrographs and flood risks in the western United States, and ignored the AMO (Beebee & Manga, 2004; Corringham & Cayan, 2019; Dai, 2013; Hamlet & Lettenmaier, 2007; Stewart *et al.*, 2005). Beebee & Manga (2004) examined the relationships between the PDO and ENSO, and snowmelt timing and the magnitude and timing of annual floods in Oregon. Stewart *et al.* (2005) focused on assessing the influence of the PDO and ENSO on snow-dominated gauge records across western North America. Their study focused on determining shifts of monthly and seasonal fractional flows, as well as changes in the flow dates of the annual flow centre of mass and the dates of spring snowmelt pulse onset (Stewart *et al.*, 2005). However, their study did not analyze the changes in annual peak flood magnitudes nor the dates of seasonal minima and maxima across the western North American margin. Hamlet & Lettenmaier (2007) utilized hydrological models to analyze large scale changes in flood risk, stratified according to the PDO and ENSO phases across the western United States. They found significant effects of the PDO and ENSO on floods, particularly when the climate oscillations were in phase and for southern California. However, their modelling study is dependent on the sensitivity of the hydrological model to accurately predict monthly changes in naturalized streamflow using daily temperature and precipitation records. Although their model has good fidelity at very large spatial scales (*i.e.* river basins with

drainage areas on the order of 10^4 - 10^5 km²), their analysis has biases on a smaller basin level scale due to the resolution limitations of their hydrological model (a $1/8^\circ$ resolution) (Hamlet & Lettenmaier, 2007). Dai (2013) demonstrated the influence of the Interdecadal Pacific Oscillation (IPO – closely related to the PDO) on the precipitation of continental United States using observational, reanalysis and modelled data. Although not based upon direct hydrological gauge data, Corringham and Cayan (2019) worked with the U.S. National Flood Insurance Program daily claims and losses to demonstrate their clear connections to ENSO state.

There has been a small amount of research on the combined effects of the AMO and PDO on streamflow and precipitation of the western North American margin. Much less research has been done on the effects of the AMO in this region compared to those of the PDO and ENSO, even though the AMO operates on a continental scale (Kundzewicz *et al.*, 2019b). Tootle & Piechota (2006) analyzed the impacts of both the PDO and AMO on streamflow patterns across the continental United States. However, their study utilized singular value decomposition to identify the relationships between the PDO and AMO and the annually-averaged streamflow variability, not annual peak floods (Tootle & Piechota, 2006). McCabe *et al.* (2004) analyzed the impacts of both the PDO and AMO on drought frequency for the entire continental United States. They calculated drought frequencies using mean annual precipitation and found that drought frequency increased during the positive AMO phase regardless of PDO phases (McCabe *et al.*, 2004).

Although these above studies analyzed the individual impacts of the PDO and AMO on flood risks, and the combined impacts of the PDO and AMO on annual streamflow discharge and precipitation variability, they did not assess the combined impacts of the PDO and AMO on the magnitude of observed annual peak floods. The climate oscillations' effects on mean annual

streamflow and precipitation are closely related to, but ultimately different from their effects on actual observed annual peak flows. This difference arises from floods being caused by not merely precipitation and total annual discharge (*i.e.* available water inputs), but by complex interactions among available water quantity, storm characteristics, catchment geometry, land surface characteristics and antecedent hydrological conditions (Hamlet & Lettenmaier, 2007). Due to these small-scale local factors, modelled data from studies across a broad geographical area will not be the same as actual observed gauge data (*e.g.* Hamlet & Lettenmaier, 2007). Furthermore, these analyses are usually focused on the western continental U.S., and not along the broader entire western North American margin which forms a distinct hydroclimatic region and which should therefore be analysed using consistent statistical methods. Lastly, none have analysed the individual effects of the PDO and AMO on the timing of seasonal hydrograph extremes throughout the year, other than the important spring snowmelt peaks (Beebee & Manga, 2004; Stewart *et al.*, 2005). For instance, the timing of summer minima is also important in this agricultural area and its water-stressed south reliant upon irrigation from surface water supplies.

In this study, we analyze the individual and combined effects of the PDO and AMO on annual peak floods along the western North American margin. We also analyse their individual effects on the timing of seasonal extremes throughout the year. We selected the western North American margin as our study region because of the control exerted upon its hydroclimatology by the North Pacific Ocean which is upstream in terms of regional air mass movements. We hypothesize that the *i.i.d.* flood event assumption is not tenable in this region that is subject to substantial impacts from these climate oscillations.

DATA AND STUDY AREA DESCRIPTION

We compiled annual peak flood magnitude data and seasonal extreme timing data from 250 naturally flowing rivers across the western North American margin (Figure 4.1 and Table S1). R version 4.0.3. (R Core Team, 2020) code was developed to analyze compiled streamflow records from the United States Geological Survey (USGS) (www.waterdata.usgs.gov/nwis) and Water Survey of Canada (WSC) (www.wateroffice.ec.gc.ca) databases. We selected station records with at least 40 years of annual and daily data (possibly discontinuous). Streamflow records were compiled up to 2017 inclusively. Annual peak floods were defined according to the water year (October 1st of the previous year to September 30th of the current year). Additionally, the Julian dates of the first occurrence of the absolute seasonal minima and maxima were identified for each year of each record. We defined the seasons according to the water year as follows: fall (October-December), winter (January-March), spring (April-June) and summer (July-September).

For North American monthly precipitation and monthly minimum and maximum temperatures, we used the Australian National University Spline (ANUSPLIN) 10 km-gridded climate data for 1949-2015 (McKenney *et al.*, 2011, Natural Resources Canada <https://cfs.nrcan.gc.ca/projects/3>). Monthly minimum and maximum temperatures were averaged to produce monthly mean temperatures.

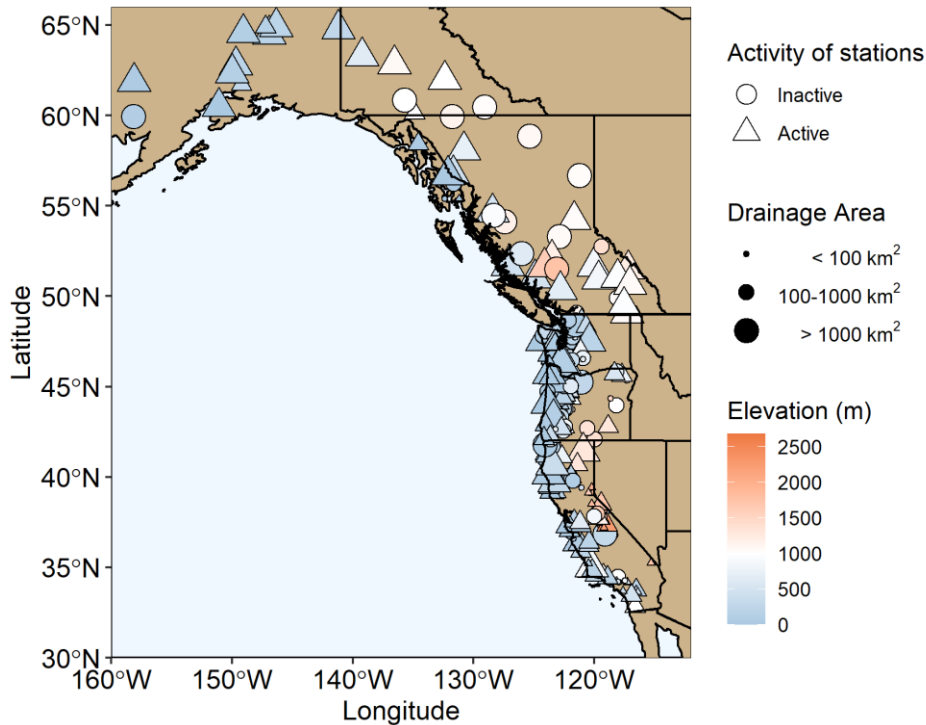


Figure 4.1. Locations of the 250 naturally flowing streamflow records across the western North American margin used in this study.

We used the PDO index from the Joint Institute for the Study of Atmosphere and Ocean (JISAO), University of Washington (<http://research.jisao.washington.edu/pdo/>) and the AMO index from the National Oceanic and Atmospheric Administration (NOAA) Physical Sciences Laboratory databases (<https://psl.noaa.gov/data/timeseries/AMO/>). In this analysis, we used the winter (November-March) averaged PDO index and the annually-averaged (January-December) AMO index. Negative phases of the PDO occurred during 1890-1924, 1947-1976, and 2009-2013; and positive phases occurred during 1925-1946, 1977-2008, and 2014-2017 (Figure 2.2A). Negative phases of the AMO occurred during 1901-1925 and 1963-1994; and positive phases occurred during 1856-1900, 1926-1962, and 1995-2017 (Figure 2.2B).

The study region of the western North American margin spans multiple climatic regions (Figure 4.1). According to the Köppen-Geiger classification of climate regions, our northernmost

region (Alaska, British Columbia, and the Yukon) is comprised primarily of a subarctic climate and a warm, humid continental climate (Peel *et al.*, 2007). The Pacific Northwest (Washington and Oregon) is composed mainly of a mild temperate, Mediterranean summer climate along the coast and an inland colder, summer continental climate (Chen & Chen, 2013; Peel *et al.*, 2007). Along coastal California, mild temperate Mediterranean conditions exist where temperature in the hottest month can exceed 22°C (Chen & Chen, 2013; Peel *et al.*, 2007). Dry and hot desert conditions exist in inland California where the mean annual temperature is above 18°C (Peel *et al.*, 2007).

METHODS

Influence of the climate oscillations on the North American climate

Correlation maps between ANUSPLIN precipitation and temperature and the PDO and AMO indices were made using Pearson's correlation to assess the effects of the climate oscillations on regional climates across North America following Mantua *et al.* (1997). Correlation maps between the winter-averaged (November-March) PDO and winter (November-March) precipitation and winter temperature were made; together with correlation maps between the annually-averaged (January-December) AMO index and annual precipitation and mean annual temperature. In addition, correlation maps were made between the spring-averaged (April-June) AMO index and spring precipitation and mean spring temperature.

Hydrological regimes of western North America

As background for examining the broad effects of the PDO and AMO on the western North American margin, annual hydrographs of daily streamflow were plotted for each station for each year to classify the hydrological regime of each river. Rivers were classified as glacial, nival, pluvial or mixed (a hybrid system of two classes, *e.g.* nival-glacial, pluvial-nival, *etc.*)

following the definitions of Burn & Whitfield (2017), Déry *et al.* (2009) and Schnorbus *et al.* (2014). As noted by Burn & Whitfield (2017), hydrological regimes are not natural constructs, but rather a continuum of patterns exhibited in a watershed. Rivers may change from one hydrological regime to another over time (Burn & Whitfield, 2017).

Relationships between annual peak floods and climate oscillations assessed by permutations on quantile-quantile plots

To assess the relationships between the annual peak flood magnitudes and the individual PDO and AMO indices, we conducted two-sided permutation tests on quantile-quantile (Q-Q) plots of ranked annual peak floods stratified according to climate oscillation phase (Gurrapu *et al.*, 2016; Helsel & Hirsch, 2002). Such non-parametric methods are suitable for this analysis due to the distribution and heterogeneity of variance of hydrological data (Wilks, 2011). For each station, the annual peak flood for the i^{th} ranked flood ($y_{(i)}$) of the negative PDO phase (y -axis) were plotted against the annual peak flood for the i^{th} ranked flood ($x_{(i)}$) of the positive PDO phase (x -axis). If the data lengths of the peak flow records were the same for both phases, the peak flows were directly plotted against each other. If the datasets were not of equal size, the quantiles were picked to correspond to the sorted values from the smaller dataset and then quantiles for the larger dataset were interpolated. The datasets can be assumed to be from the same population if the points fall along the 1:1 line. If the ratio $r_i = \left(\frac{y_i}{x_i}\right)$ of the i^{th} ranked floods is > 1 , then the i^{th} ranked flood of the negative PDO phase is higher than that of the positive PDO phase. In contrast, if the ratio $r_i = \left(\frac{y_i}{x_i}\right)$ of the i^{th} ranked floods is < 1 , then the i^{th} ranked flood in the positive PDO phase is higher than that in the negative PDO phase. If the PDO phase has no effect on a record, its mean \bar{r}_i ratio should be approximately 1. The Q-Q plots were permuted 10,000 times to assess their significance ($p \leq 0.1$). A similar analysis was done for the AMO.

Relationships between annual peak floods and climate oscillations assessed by Spearman's ρ

As further exploration, the relationships between the annual peak flood records and the PDO and AMO indices were analyzed for each station by computing Spearman's rank correlation ρ , a non-parametric statistical method between the records and indices.

Interacting effects of the PDO and AMO phases on frequencies of annual peak flood quartiles

Next, we explored the interacting combined effects of the PDO and AMO on annual peak floods (McCabe *et al.*, 2004). The annual time series of the PDO and AMO indices were used to identify combinations of positive and negative PDO and AMO phases (Figure 2.2). Four combinations were defined: negative PDO and positive AMO (1944-1963), negative PDO and negative AMO (1964-1976), positive PDO and negative AMO (1977-1994), and positive PDO and positive AMO (1995-2008). The 25th and 75th quartiles (lower quartile $Q_{0.25}$ and upper quartile $Q_{0.75}$, respectively) for each station's annual peak flood record were calculated using all available data. Then, for each station record and each PDO/AMO combination, lower quartile frequencies were determined by calculating the percentage of years with annual peak flow $\leq Q_{0.25}$. Since the normal frequency of occurrence of peak flows less than or equal to the lower quartile (lower quartile floods) is 25%, percentages $> 25\%$ represent a greater than normal probability of low annual peak flows, and values $< 25\%$ characterize less than normal chances of low peak flows. These excess or deficit lower quartile peak floods show the interacting effects of the PDO and AMO. Analogously, for each station record and each PDO/AMO combination, upper quartile frequencies were determined by calculating the percentage of years with annual peak flow $\geq Q_{0.75}$ (upper quartile floods). Here, percentages $> 25\%$ represent a greater than normal probability of high annual peak flows, and values $< 25\%$ characterize less than normal chances of high peak flows.

For comparison, for each station record and each individual PDO and AMO phase, lower quartile frequencies were also determined by calculating the percentage of years with annual peak flows $\leq Q_{0.25}$ and upper quartile frequencies were also determined by calculating the percentage of years with annual peak flow $\geq Q_{0.75}$. For this step, we used peak flood data from the negative PDO (1944-1976) and positive PDO (1977-2008) phases, and from the negative AMO (1964-1994) and positive AMO (1944-1963, 1995-2008) phases.

To assess the significance of the excess or deficit lower quartile and upper quartile floods in each PDO and AMO combination, permutation tests were done using 10,000 iterations of sampling without replacement ($p \leq 0.1$). For each record, if any of the four PDO/AMO combinations were missing $\geq 20\%$ of their data, that record was eliminated from the analysis. A similar process was done for the individual PDO and AMO phases to assess the significance of excess and deficit lower quartile and upper quartile floods.

Detection of shifts in mean dates of seasonal minima and maxima

At each station, to detect if the climate oscillations' phases affect the timing of the seasonal minima and maxima, permutation t -tests were conducted on the mean Julian dates of the seasonal minima and maxima, stratified according to extreme PDO and AMO events. We checked the records' distributions, and we did not assume equal variance. A winter-averaged (November-March) PDO index threshold of ± 0.25 and an annually-averaged (January-December) AMO index threshold of ± 0.10 were used to define extreme events. Minima and maxima dates were defined to be the Julian dates on which the minimum and maximum magnitude streamflow values occurred during the given analyzed period. The seasons were defined as follows: fall (October-December), winter (January-March), spring (April-June), and summer (July-September). We report the results for the maxima for the fall, winter, and spring,

and the first instance of the absolute minima for the summer since these were the four extremes showing substantial significant shifts according to climate oscillation phase. These four extremes are important for water management and flood mitigation in this region. To assess significance of the t -tests, 10,000 permutations were used ($p \leq 0.1$). If serial correlation is present in a record of dates of seasonal extremes, there may be an overestimation of the significance of the relationship between the mean dates and the PDO and AMO phases (Santer *et al.*, 2000). To determine whether serial correlation existed in each separate stratified record, its lag-1 autocorrelation was assessed using a Ljung-Box test. Records that have $p \leq 0.05$ for the Ljung-Box test were deemed to have statistically significant autocorrelation; therefore, their sample sizes were adjusted using the Santer *et al.* (2000) method to remove the effects of autocorrelation on t -tests. Records that had less than two years in either phase were eliminated from the analysis.

RESULTS

Correlations between climate and the PDO and AMO in western North America

The PDO and AMO influence precipitation and temperature across the western North American margin as shown by correlation plots between climate and the winter-averaged PDO, and annually-averaged and spring-averaged AMO (Figures S1-S6). During the negative PDO phase, winter precipitation increases across Alaska, British Columbia, the Yukon, Oregon, and Washington (Figure S1, following Mantua *et al.*, 1997). In contrast, winter precipitation increases during the positive PDO phase along the southern Alaskan coast and in southern California. Along the western North American margin, there is an alternating pattern of higher and lower annual precipitation according to the AMO phase (Figure S2). At northern latitudes, the Pacific Northwest and California, there is higher precipitation during the negative AMO phase (Figure S2). Along the entire western North American margin, there is a positive

correlation between winter-averaged temperature and the winter PDO index (Figure S3). A similar pattern is observed with the AMO, as higher annual temperatures are observed during the positive AMO phase (Figure S4).

The spring AMO and spring precipitation correlation map differed from the annual AMO and annual precipitation correlation map with spring precipitation increases in Alaska, the Pacific Northwest and California during the positive AMO phase (Figure S5). During the negative AMO phase, spring precipitation increases in the Yukon and coastal British Columbia. Along the entire continental margin, there is a positive correlation between spring temperatures and the spring-averaged AMO index (Figure S6).

Hydrological regimes along the western North American margin

As background for this study which covers a wide geographical area, the hydrological regimes of all 250 station records along the western North American margin were first identified (Figure S7). Naturally flowing rivers in the northern region (Alaska, Yukon and British Columbia) typically have glacial and nival hydrological regimes (Arp *et al.*, 2020; Déry *et al.*, 2009; Rood *et al.*, 2016; Schnorbus *et al.*, 2014). The glacial hydrological regime is characterized by a broad crest that occurs in the late spring, followed by a long, elongated falling limb of the hydrograph that occurs throughout the summer from melting glaciers (*e.g.* Figure S8 – Adams River near Squilax, British Columbia, Canada) (Schnorbus *et al.*, 2014). In contrast, the nival hydrological profile typically has a steep rising limb and a sharp spring crest from quick melting of snow and river ice, as well as rain (*e.g.* Figure S9 – Slocan River near Crescent Valley, British Columbia, Canada). After peak annual streamflow, these rivers have a steep falling limb. In nival regimes, annual peak streamflow typically occur during shorter temporal periods (Burn & Whitfield, 2017). In the northern region, 80% of the selected rivers have glacial

or nival hydrological regimes. There are also rivers in the northern region that exhibit a hybrid glacial-nival regime where discharge is heavily influenced by snowmelt (Eaton & Moore, 2010; Schnorbus *et al.*, 2014). These mixed glacial-nival regimes are typically seen along the northern coast of British Columbia (Eaton & Moore, 2010; Schnorbus *et al.*, 2014).

The pluvial hydrological regime is characterized by multiple, sharp peaks which indicate intense and frequent precipitation events. Peak streamflow in pluvial systems typically occur when excess rainfall is the highest in the year (Burn & Whitfield, 2017). Rivers with a pluvial hydrological regime are common in the Pacific Northwest and California. In the Pacific Northwest, rain events occur more frequently and with greater magnitude during the winter and spring seasons (*e.g.* Figure S10 – Newaukum River near Chehalis, Washington, USA). Roughly 94% of the selected naturally flowing rivers in the Pacific Northwest region exhibit a pluvial hydrological regime. In California, 91% of the selected rivers have a pluvial hydrological regime. However, there is a distinct difference between rivers in northern versus southern California. Northern Californian rivers have a similar hydrological regime profile to those in the Pacific Northwest where frequent, and high magnitude rain events occur during the fall and winter season (Berg & Hall, 2015; Lane *et al.*, 2017) (Figure S10). Southern Californian rivers tend to have much fewer rain events with low magnitudes (*e.g.* Figure S11 – Tahquitz Creek near Palm Springs, California, USA).

There are also rivers with mixed pluvial and nival regimes, *i.e.*, rivers with a definite spring peak from snowpack melt but which also have multiple, sharp peaks from intense and frequent precipitation events during the warm part of the year. An example of a river with such a hydrological regime is the Stehekin River near Stehekin, Washington, USA (Figure 4.2).

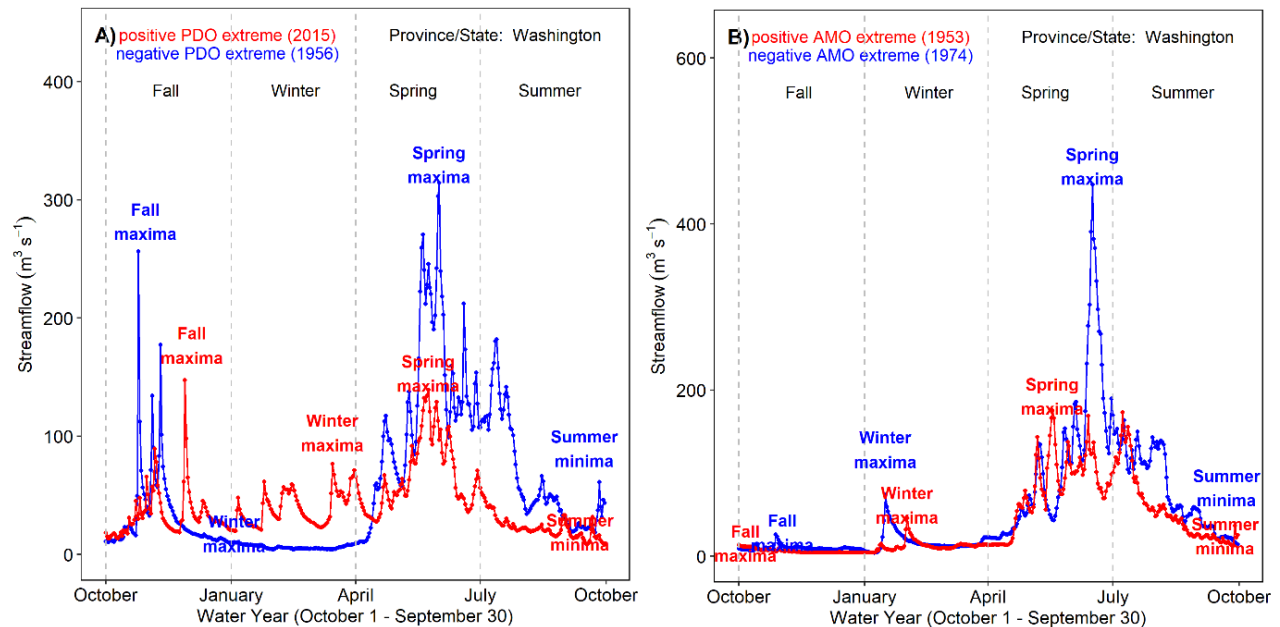


Figure 4.2. Mixed nival-pluvial seasonal hydrographs of USGS station 12451000, Stehekin River at Stehekin, Washington, USA. Separate hydrographs shown for extreme climate oscillation years: A) extreme positive and negative PDO years, 2015 and 1956, respectively; and B) extreme positive and negative AMO years, 1953 and 1974, respectively. Also shown are fall, winter and spring maxima and summer minima. Seasons defined as follows: winter (January-March), spring (April-June), summer (July-September) and fall (October-December).

Relationships between annual peak floods and climate oscillations assessed by quantile-quantile plots

The PDO has a clear impact on annual peak flood magnitudes across the western North American margin. Twenty-six percent of the 250 records have significantly different annual peak floods during the different PDO phases. Of these significant records, 80% have higher annual peak floods during the negative PDO phase (Figure 4.3A). There are distinct geographical patterns of response to the different PDO phases in this study's three subregions: the northern region (Alaska, the Yukon, and British Columbia), the Pacific Northwest (Washington and Oregon), and California.

In the northern region, 29% of the 51 records have significantly different annual peak flood magnitudes in the different PDO phases, with 93% of these significant records having

higher peak floods in the negative PDO phase (Figure 4.3A). In much of this region, winter precipitation is significantly higher in the negative PDO phase; however, coastal Alaska and the Yukon experience higher precipitation during the positive PDO phase (Figure S1).

In the Pacific Northwest, 27% of the 114 records have significantly different annual peak flood magnitudes in the different PDO phases, with 90% of these significant records having larger annual peak floods during the negative PDO phase. This pattern observed across the Pacific Northwest region is also broadly consistent with the pattern of the correlations between the winter PDO and winter precipitation (Figure S1).

In California, 24% of the 85 records have significantly higher annual peak flood magnitudes according to the PDO phase. Fifty-five percent of the 20 significant records, all located in northern California, have higher annual peak floods during the negative PDO phase. Stations in northern California behave similarly to stations in the Pacific Northwest as these stations experience similar weather conditions (Figures S1 and S3). The other significant stations are all located in southern California and have higher annual peak floods in the positive PDO phase. In southern California, the winter PDO correlates positively with the winter precipitation, thus supporting this geographical pattern (Figure S1).

In comparison to the PDO, annual peak flood magnitudes are less influenced by the AMO phase (Figure 4.3B). Only 12% of the 250 records have significantly different annual peak flood magnitudes during the different AMO phases. Of these significant stations, 50% of significant records have higher peak floods during the negative AMO phase. Less distinctive geographic patterns exist across the western North American margin in terms of flood differences according to AMO phase. However, the northern region and southern California tend

to have higher floods in the negative AMO phase, whereas British Columbia, the Pacific Northwest and northern California have higher floods in the positive AMO phase.

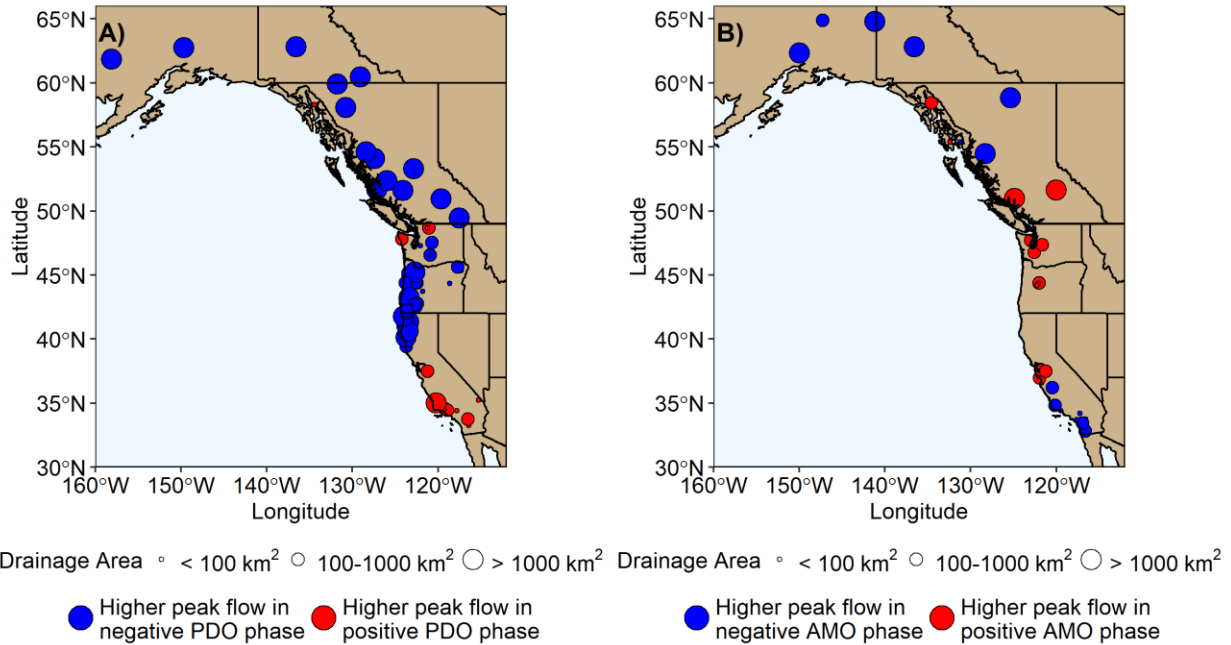


Figure 4.3. Significant permutation tests on quantile-quantile (Q-Q) plots of the annual peak flood records along the western North American margin stratified according to the A) winter (November-March) averaged PDO phase and B) annually-averaged AMO phase ($p \leq 0.1$).

Relationships between annual peak floods and climate oscillations assessed by Spearman's ρ

These results that the PDO has an influence on annual peak flood magnitudes along the western North American margin are confirmed by Spearman's rank correlations between the winter PDO and annual flood magnitudes (Figure S12). Significant relationships are shown by 29% of the 250 records, with 97% of these significant records having a negative relationship (Figure S12A). Most records with higher flows in the negative PDO phase are found in Oregon, Washington, and British Columbia. In contrast, Spearman's rank correlations between annual peak flood magnitudes and the annually-averaged AMO index are less significant as only 14% of the stations have a significant relationship; 59% of significant records have higher annual peak

floods during the negative AMO phase (Figure S12B). These are clustered in the Pacific Northwest.

Interacting effects of the PDO and AMO phases on frequencies of annual peak flood quartiles

The effects of the PDO and AMO phases on the frequencies of the annual peak flood quartiles interact: sometimes reinforcing each other, sometimes cancelling each other, and sometimes with one dominating over the other (Table 1 and Figures 4.4 and 4.5) (close-up figures for the northern regions, Pacific Northwest and California are shown in Supplementary Figures S13-S18). Unsurprisingly given the size of the study area, there are distinct geographic patterns to the effects of the interactions. Due to missing data, the number of records analyzed is sometimes less than the maximum possible 250 stations (51 for the northern region, 114 for the Pacific Northwest, 85 for California).

First, the impacts of the individual PDO and AMO phases on the frequencies of the lower quartile floods (*i.e.*, those $\leq Q_{0.25}$) and upper quartile floods (*i.e.*, those $\geq Q_{0.75}$) are presented (Table 2 and Figures S19-S34). Lower quartile floods are much less likely to occur in the negative PDO phase (1944-1976) across all of the North American margin, with 25% of the 232 records showing a significant deficit of such floods (Table 2 and Figures S19-S22). The results for the positive PDO phase (1977-2008) are weaker and more mixed. The northern region has a higher than expected frequency of lower quartile floods in the positive PDO phase (13% of its 48 records) (Figure S20). California clearly shows the PDO dipole in the positive PDO phase: northern California records have a higher than expected frequency of lower quartile floods (11% of its 79 records), while southern and central California have a lower than expected frequency of lower quartile floods (6% of the 79 stations) (Figure S22). The Pacific Northwest is mixed with 12% of its 105 stations

significantly showing an excess of lower quartile floods (mainly in Oregon), and 9% significantly showing deficits of lower quartile floods (mainly in Washington) (Figure S21).

Lower quartile floods are less likely to occur in the positive AMO phase (1944-1963, 1995-2008) across all of the North American margin, with 30% of the 248 stations showing a significant deficit of such floods (Table 2 and Figures S23-S26). The results for the negative AMO phase (1964-1994) are weaker and more mixed, with 13% of the 248 stations along the continental margin showing significantly less frequent lower quartile floods than expected, and 8% of the 248 stations showing significantly more frequent lower quartile floods. Alaska, the Yukon, the Puget Sound region, and southern California are locations showing significantly less frequent lower quartile floods than expected.

Given the higher winter precipitation of the negative PDO phase (Figure S1, Mantua *et al.*, 1997), the negative PDO results in a lower frequency of upper quartile floods than expected at 19% of the 232 stations (Table 2 and Figures S27-S30). This loss of extremes effect is prominent in the northern region (21% of the 48 records), Washington (33% of the 52 records) and California (22% of the 79 records). Contrarily, Oregon (26% of the 53 records) has a higher frequency of upper quartile floods than expected during the negative PDO (Figure S29). The positive PDO has a weaker and more mixed impact on the frequency of upper quartile floods that does not seem particularly notable, except for a reversal of the pattern in Washington and Oregon.

The positive AMO phase has a stronger and more geographically uniform impact on the frequency of upper quartile floods than the negative AMO phase does. Like the negative PDO, the positive AMO phase is characterized by stations with significantly less frequent upper quartile floods than expected (Table 2 and Figures S31-S34). This pattern holds for the entire continental margin (at 18% of the 248 records) (Figure S31), and especially for the northern region (37% of

the 51 records) (Figure S32) and California (18% of the 84 records) (Figure S34). The Pacific Northwest is more mixed. The negative AMO has a weaker and more mixed impact on the frequency of upper quartile floods that does not seem particularly notable (Figure S33).

Next, we present the effects of the four combinations of PDO and AMO phases on the frequencies of flood quartiles: negative PDO/positive AMO (1944-1963), negative PDO/negative AMO (1964-1976), positive PDO/negative AMO (1977-1994), and positive PDO/positive AMO (1995-2008) (Figure 2.2). The combinations of the positive PDO/negative AMO and negative PDO/positive AMO have the greatest effect on the frequencies of the lower quartile floods (Table 1 and Figures 4.4, S13-S15). In the positive PDO/negative AMO combination, the drying effect of the positive PDO is dominant over the weak mixed effect of the negative AMO, with the occurrences of lower quartile flows being more frequent than expected along the entire North American margin (23% of the 150 stations) (Figure 4.4). This effect is clear in all regions: the northern region (16% of the stations have significant increases of lower quartile flows), the Pacific Northwest (23%) and California (27%). In fact, the positive PDO/negative AMO combination produces more lower quartile flows than the positive PDO alone does.

The negative PDO/positive AMO phases act together with the effect of making the occurrences of lower quartile flows less frequent than expected along the entire North American margin (11% of 150 records – there are more incomplete records at this earlier time) (Figure 4.4). This effect is clearest in the northern region and the Pacific Northwest, with 24% and 11% of the stations, respectively, showing significant reinforcing effects (Figures S13-S15). In California, many stations show non-significant effects (Figure S15). This matches the results of the PDO and AMO phases considered individually.

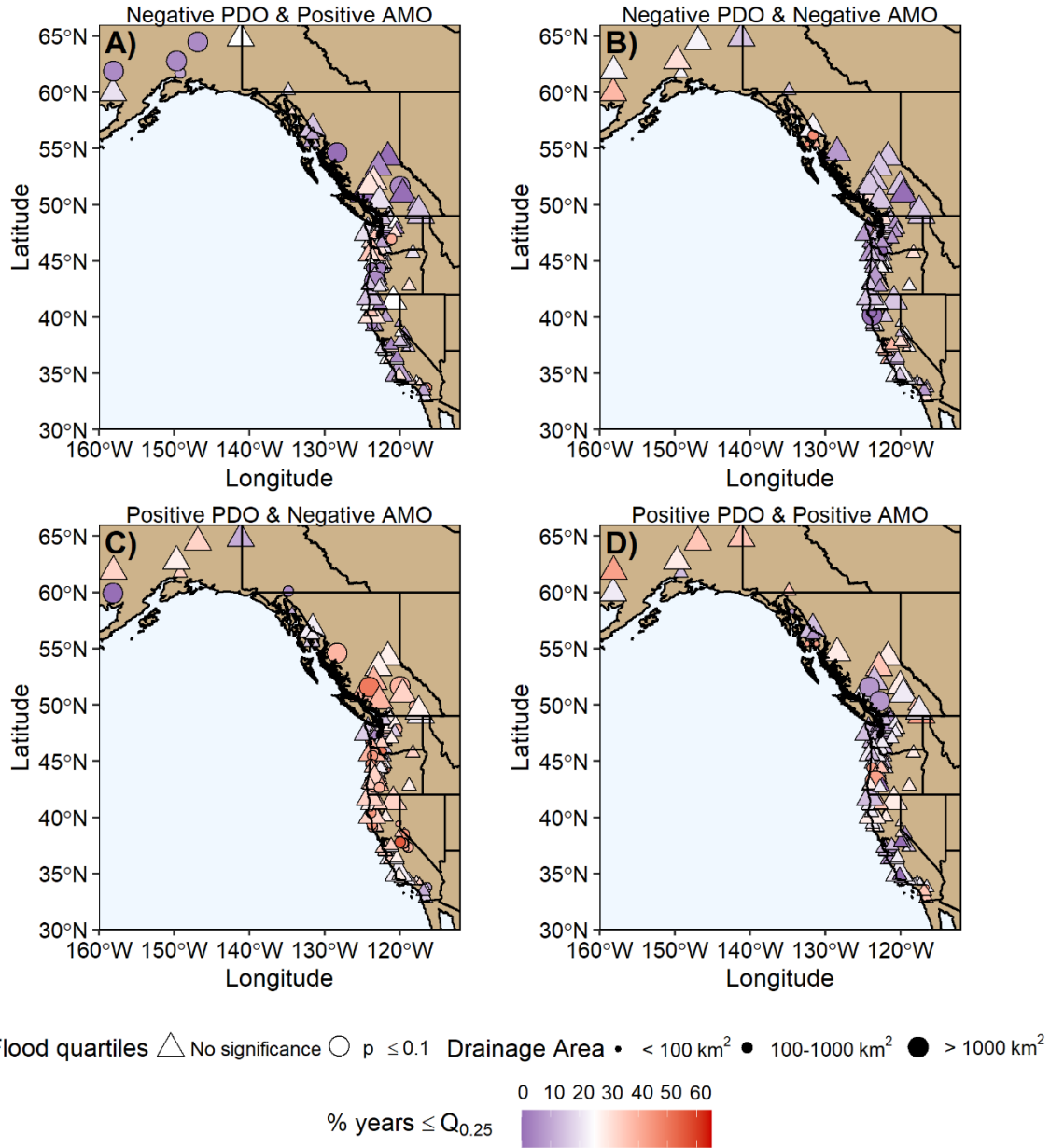


Figure 4.4. Percentages of lower quartile floods for the four PDO and AMO combinations for the western North American margin: A) negative PDO and positive AMO, 1944-1963; B) negative PDO and negative AMO, 1964-1976; C) positive PDO and negative AMO, 1977-1994; and D) positive PDO and positive AMO, 1995-2008. Significance assessed by permutation tests (10,000 iterations, $p \leq 0.1$).

The other two combinations, negative PDO/negative AMO and positive PDO/positive AMO interfere with each other and their individual effects on lower quartile flows cancel each other out (Figures 4.4, S13-S15). Neither produces any geographical patterns of either significantly

elevated numbers of lower quartile flows or significantly low numbers of lower quartile flows (Table 1).

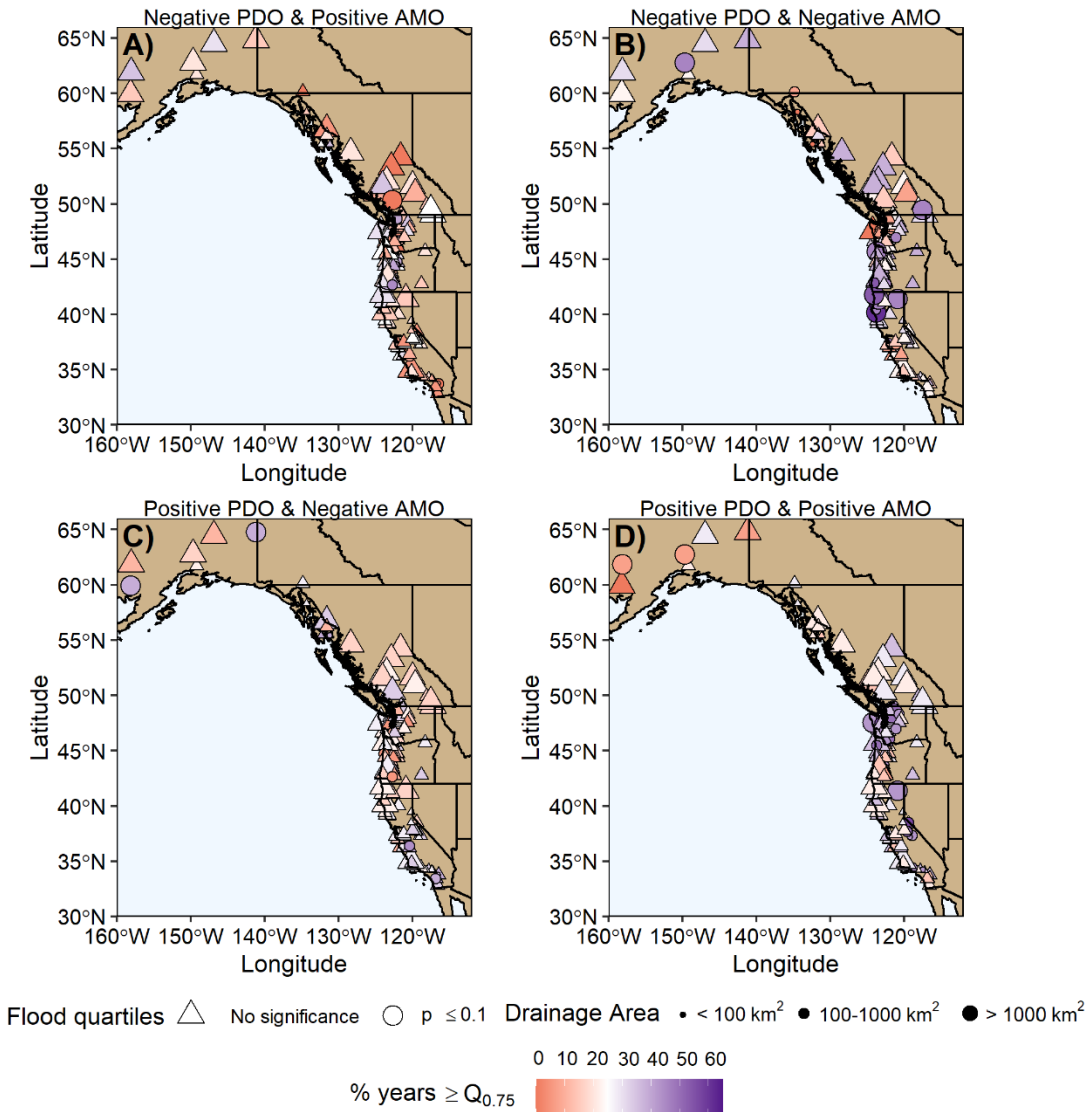


Figure 4.5. Percentages of upper quartile floods for the four PDO and AMO combinations for the western North American margin: A) negative PDO and positive AMO, 1944-1963; B) negative PDO and negative AMO, 1964-1976; C) positive PDO and negative AMO, 1977-1994; and D) positive PDO and positive AMO, 1995-2008. Significance assessed by permutation tests (10,000 iterations, $p \leq 0.1$).

In contrast to the above, the frequencies of the upper quartiles are most prominently affected by the negative PDO/negative AMO and positive PDO/positive AMO combinations (Table 1, Figures 4.5, S16-S18). In the negative PDO/negative AMO combination, the wetting

effect of the negative PDO is dominant over the weak drying effect of the negative AMO with 13% of the 150 stations showing significantly higher frequencies of upper quartile flows. The wetting effect of this combination is in the Pacific Northwest (10% of 70 stations) and California (18% of 55 stations), but not in the northern region. In the positive PDO/positive AMO combination, the wetting effect of the positive AMO is dominant over the drying effect of the positive PDO, with 20% of the 150 stations showing significantly higher frequencies of upper quartile flows. Again, the wetting effect of this combination is in the Pacific Northwest (29% of 70 records) and California (16% of 55 records), but not in the northern region.

Detection of shifts in mean dates of seasonal minima and maxima

The hydrograph plots of the different hydrological regimes of the western continental margin for years in which the PDO and AMO indices have extreme values suggest that the climate oscillations affect the timing and shape of the hydrograph in a way characteristic of each hydrological regime. For example, in the three selected northern and Pacific Northwest rivers, the winter (January-March) maxima occurred later in 2015 (Figures 4.2., S9 and S10), the most extreme positive PDO year than in 1956, the most extreme negative PDO year. In southern California (Tahquitz Creek), the summer (July-September) minimum occurred later in the negative PDO year (1956), than in the positive PDO year (2015) (Figure S11). In the two selected northern rivers, summer minima occurred later in the most negative AMO year (1974) than in the most positive AMO year (1953) (Figures S8 and S9). Conversely, in Tahquitz Creek, the summer minima occurred later in 1953 than in 1974. This study's earlier results show that the height of the main spring (April-June) snowmelt peak of the glacial and nival rivers varies depending on the climate oscillation phase (Figures 2.2 and 4.2).

Considered along the entire western North American margin, the dates of the fall, winter and spring maxima, and summer minima show significant shifts depending on the PDO and AMO phases (Figures 4.6 and 4.7). (Close-up figures for the northern regions, Pacific Northwest and California are shown in Supplementary Figures S35-S40). The dates of the fall and winter maxima generally occur later during the positive PDO phase, whereas the dates of the spring maxima and summer minima generally occur later during the negative PDO phase (Table 3 and Figure 4.6). The dates of the winter maxima and summer minima are the most sensitive to PDO phase changes in terms of number of records showing significant shifts. In the positive PDO phase, 26% of the 247 records had significantly later dates for the winter maxima. In the negative PDO phase, 24% of the 250 records had significantly later dates for the summer minima.

The dates of the fall maxima and summer minima generally occur later during the positive AMO phase along the western North American margin, while there are no overall patterns in the dates of the winter and spring maxima stratified according to AMO extreme events (Table 3 and Figure 4.7). The dates of the summer minima were the most sensitive to changes in the AMO oscillation. In the positive AMO phase, 18% of the 249 records had significantly later dates for the summer minima; in the negative AMO phase, only 5% of the records had later dates for the summer minima.

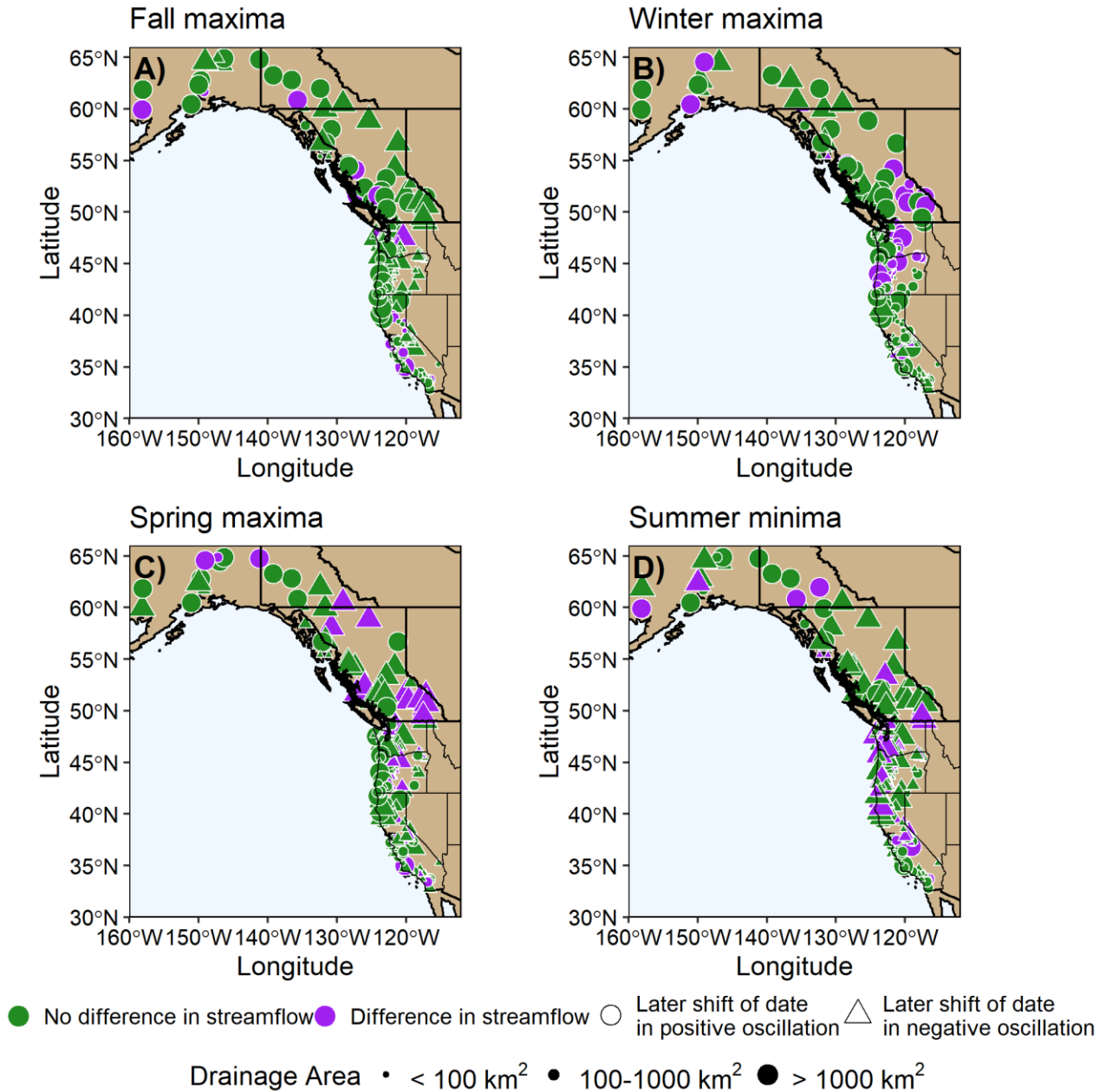


Figure 4.6. Differences in the Julian dates of the seasonal streamflow extremes according to the PDO phase along the western North American margin for: A) fall maxima, B) winter maxima, C) spring maxima, and D) summer minima ($p \leq 0.1$).

There are patterns of shifts in the timing of seasonal extremes according to PDO and AMO phases that appear at a finer geographic scale when examining separately the northern region, the Pacific Northwest, and California (Table 3, Figures 4.6-4.7, S35-S40). In the northern region, the PDO phase substantially influences the dates of the spring and winter maxima (Figures 4.6 and

S35). In the negative PDO phase, 25% of the 51 stations had significantly later dates for the spring maxima (in the positive PDO phase, only 6% had later dates for the spring maxima). In the positive PDO phase, 21% of the stations had significantly later dates for the winter maxima. In contrast, the dates of the summer minima are most sensitive to changes in the AMO phase, with 16% of the stations having significantly later dates during the negative AMO, which differs from the rest of the western North American margin (Figures 4.7 and S36).

Significant shifts in the dates of seasonal extremes according to PDO or AMO phase are most prevalent in the Pacific Northwest. The dates of the winter maxima and the summer minima are the most influenced by PDO phase (Figure S37). The dates of the winter maxima occur significantly later during the positive PDO in 46% of the 114 stations (with no significant later shifts during the negative PDO). The dates of the summer minima occur significantly later during the negative PDO in 35% of the 114 stations (with only one station significantly later during the positive PDO). Although the dates of the fall and spring maxima are less sensitive to the PDO phase, these dates often occur later in the negative PDO phase. The shift of dates of the fall maxima differs from the rest of the western North American margin. In contrast, the dates of the summer minima are the most sensitive to changes in the AMO phase in the Pacific Northwest, where 24% of the 114 stations have later dates during the positive AMO (with only one station significantly later during the negative AMO). This pattern of results is similar to that of the rest of the western North American margin, except for the northern region (Figure S38). The dates of the fall, winter, and spring maxima are less sensitive to the AMO phase.

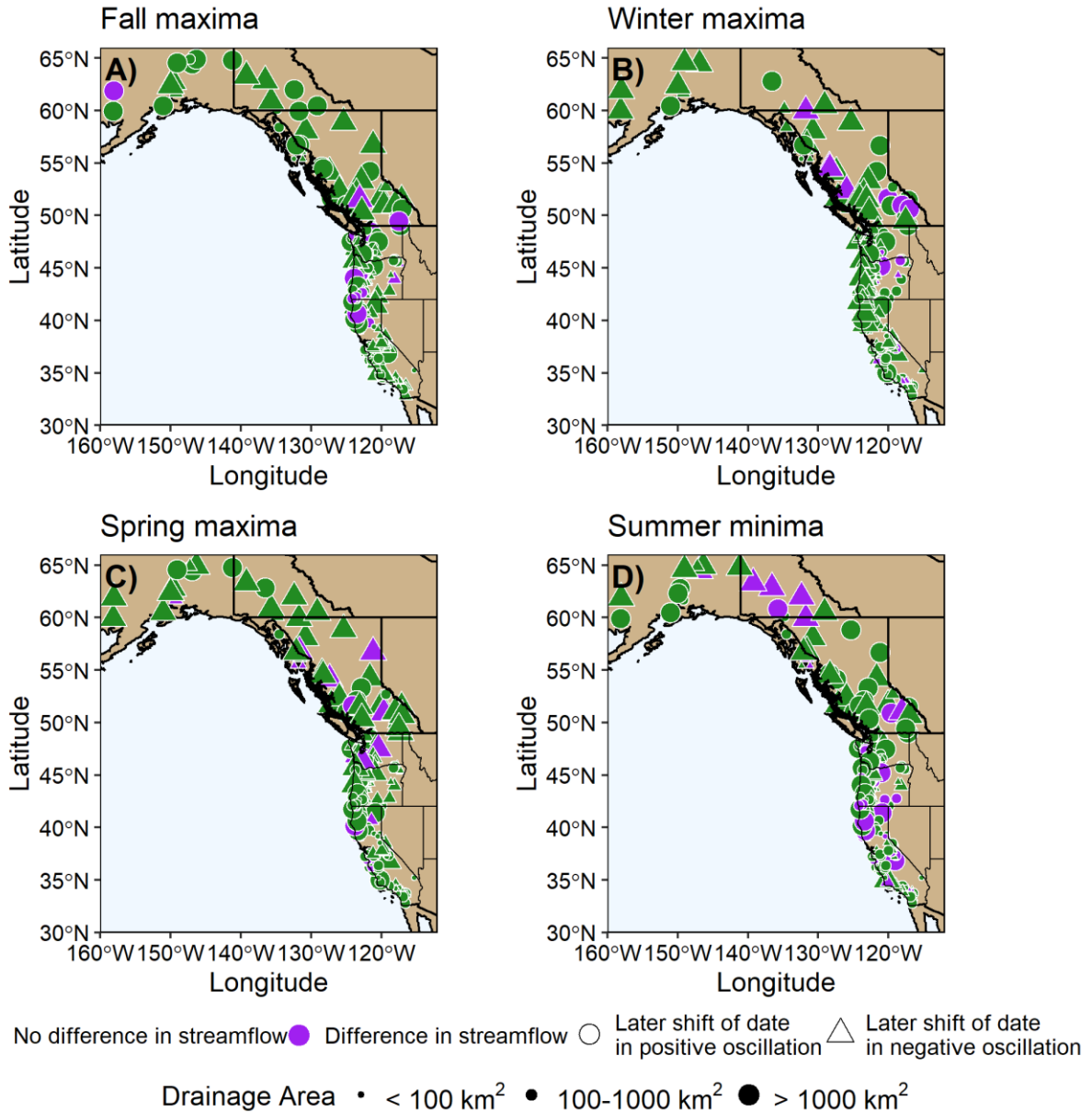


Figure 4.7. Differences in the Julian dates of the seasonal streamflow extremes according to AMO phase along the western North American margin for: A) fall maxima, B) winter maxima, C) spring maxima, and D) summer minima ($p \leq 0.1$).

In California, the PDO and AMO also significantly affect the dates of the seasonal extremes. The dates of the fall maxima are the most sensitive to the PDO phase, with 16% of 85 stations having the maxima occurring later in the positive PDO (Figure S39). The dates of the summer minima are also sensitive to the PDO phase. In northern California, 15% of the 85 stations have summer minima occurring later in the negative PDO, whereas in southern California, 7% of

the 85 stations have the minima occurring later in the positive PDO (Figure S39). The dates of the winter and spring maxima were less sensitive to the PDO phase. Likewise, in California, the dates of the summer minima are the most sensitive to the AMO phase with 20% of the 84 stations having later dates in the positive AMO (Figure S40), similar to the Pacific Northwest. The dates of the fall, winter and spring maxima are less influenced by the AMO. The dates of the fall and spring maxima are somewhat later during the positive AMO phase.

DISCUSSION

In summary, when considered individually, the PDO has a significant impact on the magnitudes of annual peak floods across the western North American margin, with higher flood magnitudes occurring in the negative PDO in the northern region, Pacific Northwest and northern California, and higher flood magnitudes in the positive PDO phase in southern California, as expected from the PDO and precipitation correlation plot (Figures 4.3, S1 and S12A) (Beebee & Manga, 2004; Gurrupu *et al.*, 2016; Mantua *et al.*, 1997; Mantua & Hare, 2002; Newman *et al.*, 2016; Stewart *et al.*, 2005; Zhang *et al.*, 1997). The number of lower quartile flows is less than expected (< 25%) during the wet negative PDO phase at many gauges along the North American margin (Table 2 and Figure S19). This deficit of lower quartile floods agrees with the Q-Q plot analysis and the increased winter precipitation at this time (Figures 4.3 and S1). However, the number of upper quartile flows is also less than expected (< 25%) during the negative PDO phase at many gauges along the North American margin (Table 2 and Figure S27). This does not agree with the general wetness of the negative PDO phase. Instead, it suggests that the negative PDO state ensures that lower quartile floods are much less likely to occur, but that the simply described broad geographical effect of the PDO phase is not sufficient to ensure an increased frequency of the upper quartile floods, and that local factors are also

necessary for these latter higher floods. This is unsurprising as floods are caused by complex interactions among available water quantity, storm characteristics, catchment geometry, land surface characteristics and antecedent hydrological conditions, and not purely by the amount of water input (Hamlet & Lettenmaier, 2007).

The dates of the seasonal extremes most affected by the PDO phase are the winter maxima which occur later in the season in the positive PDO phase in the northern region, particularly in British Columbia, and in the Pacific Northwest, and the summer minima which occur later in the season in the negative PDO phase along the entire North American margin (Table 3 and Figure 4.6). The later summer maxima in the negative PDO phase suggests that the greater amounts of water from enhanced winter snowpack and rainfall postpones the summer minima, together with less evapotranspiration due to the cooler winter temperatures associated with the negative PDO (Figure S3).

When considered individually, the AMO has a much more mixed effect in comparison to the PDO on the magnitude of annual peak floods across the western North American margin, having higher flows in its positive phase in coastal British Columbia, the coastal Pacific Northwest and northern California, but higher floods in its negative phase in Alaska, the Yukon, northern British Columbia, and southern California. This flood magnitude pattern matches the AMO correlation plot with spring precipitation for the Yukon, British Columbia, northern California, and the Pacific Northwest better than that with annual precipitation (Figures 4.3, S2, S6 and S12B). The flood magnitude pattern better matches the AMO correlation plot with annual precipitation for Alaska and southern California. Similar to the PDO case, the number of lower quartile flows is less than expected (< 25%) during the wet positive AMO phase at many gauges along the North American margin (Table 2 and Figure S23). This agrees with the generally

increased winter-spring precipitation at this time. However, the number of upper quartile flows is less than expected ($< 25\%$) during the positive AMO phase along the North American margin (Figure S31). This does not agree with the general wetness of the positive AMO phase. Instead, it again suggests that the positive AMO ensures that lower quartile floods are much less likely to occur and that the simply described AMO phase is not sufficient to ensure an increased frequency of the upper quartile floods, and that the occurrence of more complex, local factors are also necessary for these latter floods.

The dates of the seasonal extremes most affected by the AMO phase are the summer minima which occur later in the season in the positive AMO phase in the Pacific Northwest and California (Table 3 and Figure 4.7). The later summer maxima in the positive AMO suggests that the greater amounts of water from enhanced spring precipitation postpones the summer minima (Figure S6). A better understanding of the changes in the occurrence of summer minimum flows during the AMO and PDO phases is important in water management in the agricultural Pacific Northwest and California, the latter of which is additionally water-stressed.

When the PDO and AMO are considered together, their effects on the frequencies of the annual peak flood quantiles interact (Table 1 and Figures 4.4 and 4.5). With respect to the frequencies of the lower quartile floods, the PDO and AMO phases reinforce each other in a predictable fashion: the wet negative PDO and wet positive AMO combination results in fewer than expected ($< 25\%$) lower quartile floods at many gauges, and the dry positive PDO and dry negative AMO combination results in more than expected ($> 25\%$) lower quartile floods. The reinforced wetting combination of the negative PDO/positive AMO is seen most clearly in the northern region and Pacific Northwest and not in southern California. The reinforced drying combination of the positive PDO/negative AMO is seen everywhere except in Alaska and the

Yukon. The two remaining combinations, the negative PDO/negative AMO and positive PDO/positive AMO, interfere with each other and cancel each other out, which also makes sense.

What is unexpected is that with respect to the frequencies of the upper quartile floods, one climate oscillation dominates over the other (Table 1 and Figures 4.4 and 4.5). On the western continental U.S. margin, the wet negative PDO's effect is dominant over the dry negative AMO, resulting in higher than expected frequencies of upper quartile floods. Likewise, in the same region, the wet positive AMO's effect is dominant over the dry positive PDO, also resulting in higher-than-expected frequencies of upper quartile floods. There also is not any constructive reinforcement of the wet negative PDO/positive AMO and dry positive PDO/negative AMO combinations, *i.e.*, there are not higher or lower than expected numbers of upper quartile floods, respectively, in these combinations.

The winter surface air temperature along the western continental margin changes according to the PDO and AMO phases. During the positive PDO, the combination of warmer winter air temperatures and low precipitation results in smaller snowpack accumulation and drier winter conditions in northern Canada and the Pacific Northwest regions (Figures S3 and S4) (Enfield *et al.*, 2001; Mantua *et al.*, 1997; Mantua & Hare, 2002; Praskievicz & Chang, 2009; Whitfield *et al.*, 2010). As well, the increased winter air temperature causes an increase in snow sublimation (Mantua *et al.*, 1997; Mantua & Hare, 2002; McCabe & Dettinger, 2002; Whitfield *et al.*, 2010). During the negative AMO phase, a winter ridge-trough pattern strengthens across the Pacific Northwest, causing lower winter storm activity and less rainfall in the Pacific Northwest (Enfield *et al.*, 2001). When the PDO shifts to its negative phase and the AMO shifts to its positive phase, air temperatures start to cool, and winter snowpack starts to accumulate in

northern Canada and the Pacific Northwest regions (McCabe & Dettinger, 2002; Whitfield *et al.*, 2010). The winter ridge-trough pattern weakens across the Pacific Northwest, causing higher winter storm activity and rainfall in the Pacific Northwest (Enfield *et al.*, 2001; Mantua *et al.*, 1997; Mantua & Hare, 2002).

Our results confirm other researchers' examining the effects of the PDO on flood magnitudes and seasonal extreme timing. For instance, Burn *et al.* (2004) analyzed the relationships between the PDO and various hydrological variables (*i.e.*, magnitudes of the annual extremes and timings of peak floods, and spring freshet onset) in the Liard River Basin, a tributary basin of the Mackenzie River in northern Canada, and found that the PDO correlates negatively with the annual maximum flood date (from snowmelt) and spring freshet date. Their results are consistent with this study's results on the dates of the spring maxima in the northern region. Furthermore, they found that the PDO correlates positively with winter discharge and correlates negatively with summer discharge (Burn *et al.*, 2004). Beebee & Manga (2004) studied the influence of the PDO and ENSO on the timing and magnitude of stream discharge for eight watersheds in central and eastern Oregon and found, like our study, that the PDO correlates negatively with annual peak flood magnitude. They also found that peak spring runoff occurs significantly earlier in the positive PDO and occurs later in the negative PDO phase (Beebee & Manga, 2004). We found similar results for the spring maxima. Examining another feature of hydrograph changes according to the PDO phase, Stewart *et al.* (2005) found positive correlations between the PDO and the timing of the centre of mass of the annual flow throughout western North America.

Other researchers have studied the effect of the AMO on North American precipitation and streamflow. Enfield *et al.* (2001) studied the impact of the AMO on precipitation and found

that during the positive AMO, much of the continental U.S. experiences less than normal rainfall and that Mississippi River total discharge diminishes. However, the Pacific Northwest experiences greater than normal rainfall in the positive AMO, which accords with our flood magnitude results. Hodgkins *et al.* (2017) found a significant negative relationship between flood event magnitudes at the 25 and 50-year return periods and the AMO in large ($> 1000 \text{ km}^2$) catchments in North America, but they pooled their results and do not breakout their results for the western North American margin whose gauges form a very small subset of those analysed.

Pascolini-Campbell *et al.* (2017) studied the combined effects of the PDO and the AMO on monthly mean streamflow from naturally flowing rivers in the Upper Rio Grande Basin, U.S. and concluded that the decadal high streamflow from 1900-1920 and 1979-1995 were influenced by the positive PDO and the negative AMO phases. They also found that decadal low streamflow from 1945-1975 and 1996-2014 were influenced by the negative PDO and positive AMO phases. The Upper Rio Grande Basin is located in the continental interior, in Colorado and New Mexico, where Enfield *et al.* (2001) and our study report a negative relationship between precipitation and the AMO. Méndez and Magaña (2010) studied the links between the PDO and AMO using drought indices from precipitation data in Mexico. They found that droughts in northern Mexico occurred more frequently during the combined negative PDO/positive AMO phases (Méndez & Magaña, 2010). We found similar results in southern California where more frequent lower quartile floods occurred during the negative PDO/positive AMO combination.

Several mechanisms have been proposed to account for the variability of the PDO (Alexander, 2013; Alexander & Deser, 1995; Barnett *et al.*, 1999; Latif & Barnett, 1996; Mantua *et al.*, 1997; Mantua & Hare, 2002; Miller *et al.*, 1994; Newman *et al.*, 2016). It has been proposed that a stochastic forcing via the passing of atmospheric storms affect SSTs in the mixed

layer of the North Pacific Ocean, creating a negative air-sea feedback loop, which results in changes in the surface heat flux (Alexander, 2013; Alexander & Deser, 1995). The stochastic heat flux forcing causes strengthening or weakening of the SST anomalies. The combination of the stochastic heat flux forcing and fluctuations in the Aleutian Low results in the PDO's variability. Alexander (2013) and Alexander *et al.* (2002) propose a second mechanism in which ENSO teleconnections in the tropical Pacific influence the PDO's variability via an "atmospheric bridge", in which changes in surface air temperature, humidity and wind in the equatorial Pacific Ocean impact ocean currents, SSTs and salinities in the North Pacific Ocean. Lastly, Alexander (2013) and Alexander & Deser (1995) propose a re-emergence mechanism to explain the variability of the PDO, in which seasonal temperature anomalies, which are retained in the ocean mixed layer during the summer, resurface during the following winter. The combination of all three proposed mechanisms, as well as the displacement of the North Pacific Ocean gyres, and the Ekman transport of water are probably all factors in the PDO's variability (Alexander, 2013; Alexander *et al.*, 2002; Alexander & Deser, 1995; Mantua & Hare, 2002; Miller *et al.*, 1994; Newman *et al.*, 2016).

Several mechanisms have also been proposed to explain the generation of the AMO (Dima & Lohmann, 2007; Frajka-Williams *et al.*, 2017; García-García & Ummenhofer, 2015; Häkkinen *et al.*, 2011; Knight *et al.*, 2005). Häkkinen *et al.* (2011) proposed that atmospheric blocking (high-pressure systems that "block" westerly winds in the mid- and high latitudes) via changes in surface wind stress and wind stress curl influences ocean circulation patterns in the North Atlantic Ocean. They proposed that weakening of the wind stress curl contributes to the weakening of the ocean gyre circulation, which results in greater warming in the subpolar region of the Atlantic Ocean. During periods of atmospheric blocking in western Europe and Greenland,

the AMO has its warmest SST anomalies. Conversely, the strengthening of the wind stress curl corresponds to strengthening of the ocean gyre circulation in the subpolar region, which results in cooling of the subpolar Atlantic Ocean and colder AMO SST anomalies. Other studies have proposed that the AMO phases covary with the strength of the Atlantic Meridional Overturning Circulation (AMOC), *i.e.*, the variation of the thermohaline circulation (THC) in the North Atlantic Ocean (d'Orgeville & Peltier, 2007; Frajka-Williams *et al.*, 2017; García-García & Ummerhofer, 2015; Knight *et al.*, 2005). Warmer Atlantic SSTs are associated with a stronger AMOC, whereas colder Atlantic SSTs are associated with a weaker AMOC (Frajka-Williams *et al.*, 2017).

Dima and Lohmann (2007) proposed yet a third mechanism for the AMO based on several atmospheric, ocean and sea ice interactions. In their proposed mechanism, the AMO undergoes a series of positive and negative feedback loops where the Atlantic SSTs have a positive feedback on the sea level pressure (SLP) in the Pacific Ocean via atmospheric teleconnections, and a negative feedback on the SLP in the Atlantic Ocean. The differences in SLP in the North Atlantic and North Pacific Ocean basins create a positive feedback on the SLP gradient which results in a positive feedback on wind stress in the North Atlantic Ocean. The positive feedback on wind stress results in more sea ice export from the North Atlantic Ocean which causes a negative feedback on the THC due to influx of freshwater. The negative feedback on the THC occurs over a 10-20-year period, then the cycle is completed and the AMO switches to its opposite phase. They found that the sign of the AMO phase is lagged by the activity of the sea ice export. When sea ice export is at minimum activity, less sea ice is exported across the North Atlantic Ocean which results in less influx of cold freshwater, leading to a warmer THC and warmer SSTs in the Atlantic Ocean (*i.e.*, the positive AMO phase). Conversely, colder SSTs

in the Atlantic Ocean are observed when sea ice export is at maximum activity (colder THC). In conclusion, the PDO and AMO both have multiple plausible mechanisms, even if the relative importance of the various mechanisms are subjects of ongoing research.

There are statistical limitations in any study, such as ours, working with the daily flow records from streamflow gauges on the western continental margin. Unfortunately, the western North American margin has few stations with long, continuous records that exceeds 40 years of annual peak and daily streamflow data. The annual and seasonal extreme records are relatively short and frequently discontinuous, particularly prior to 1963. On average, each record had 66 years of annual peak flood data and started before the year 1936. However, key years were missing in the records, such as those during the negative PDO/positive AMO combination (1944-1963), needed to accurately assess the changes in the frequency of floods during the PDO/AMO combinations. Additionally, statistical power will be low for the PDO/AMO combination analysis since the number of years in these combinations are small: negative PDO/positive AMO (1944-1963) – 20 years, negative PDO/negative AMO (1964-1976) – 13 years, positive PDO/negative AMO (1977-1994) – 18 years, and positive PDO/positive AMO (1995-2008) – 14 years.

We did not perform any data infilling of the gaps of the records because our interest was to capture the annual and daily peak floods, which are potentially highly variable from day to day. In western Canada, most of the gauges are situated in the southern region, or near the coast, where there are larger human populations. Few station gauges are available that accurately represent the changes in annual and daily streamflow in the interior of the Yukon and northern British Columbia. Although there are more station records available in the United States, Alaska faces the same problems as northern Canada as there are fewer records that exceed the 40-year

threshold and are naturally flowing. Similarly, in the western United States, most of the gauges in the study are situated along the coastal margin, whereas few gauges are located inland. This irregular spatial distribution of the gauges may affect our ability to detect hydrological changes that occur during extreme climate oscillation events.

In addition, little information is easily accessible concerning the land-use changes near the gauged rivers that are not part of the Reference Hydrometric Basin Network (RHBN) and the National Network of Reference Watersheds (NNRW) databases. Gauges from the RHBN must meet the following requirements: a minimum of 20 years (may be discontinuous) with complete years of data, < 0.1% regulation (diversion, dams), less than 10% urbanization, 1-2 km/km² road density and 200-400 persons per km² (Pellerin & Nzokou Tanekou, 2020). Gauges from the NNRW were selected based on a disturbance criterion that selects negligible flow alternations, pollutant discharge and water withdrawals. Consequently, data availability and quality are two limiting factors that must be considered during the analysis of the study. However, this gauge data is all that is available.

The study region consists of a wide geographical margin along the coast of western North America with various sizes of individual drainage areas. The northern region consists of rivers with much larger drainage areas in comparison to the southern regions such as central and southern California. Due to human impacts on the environment, the number of pristine watersheds across this broad region is highly limited. Land use changes from forests to agricultural and urban areas have substantial effect on rivers (Roger *et al.*, 2017; Tollan, 2002; Wheeler & Evans, 2009). Rivers with medium to large size drainage area are most likely to be affected by these human impacts. For example, rivers in California with smaller drainage areas are less impacted by anthropogenic activity in comparison to rivers with larger drainage areas.

Therefore, there were more rivers with a similar profile that met our 40-year record length and undisturbed streamflow criteria. Although the effects of the size of drainage areas were not considered in the analysis, they are important factors that will affect the frequency of flooding across the western North American margin.

There also is the effect of drainage basin size on the ability of our analysis to detect a climate oscillation's effect on the basin. Rivers with smaller drainage areas are more susceptible to random processes such as flash flooding from small, warm-season convective storms due to their basin size, hence they might be less likely to record the effect of a climate oscillation. In contrast, rivers with large drainage areas may be so large that the effect of a climate oscillation changes sign over their drainage basin span, thus obscuring the oscillation's effect. These river characteristics must be considered when analyzing the magnitude and frequency of annual peak floods during these climate oscillation events. Regardless of the deficiencies of our records, our analysis does uncover significant effects of the PDO and AMO phases, and their interactions on floods along the western North American margin.

CONCLUSION

In this study, we show that the PDO and the AMO have substantial impacts on annual flood magnitudes, frequencies of upper and lower quartile annual peak floods, and timing of seasonal extremes on the North American west coast. The phases of the climate oscillations interact constructively, destructively and with one dominating over the other. The *i.i.d.* flood event assumption is untenable here.

Flood frequency analysis studies are dominated by numerous, complex mathematical models whose accuracy could be improved (Kidson & Richards, 2005). The stationary assumption is a key element in these mathematical models; however, it fails to consider the

effects of climate change which may result in non-stationary events occurring (Kidson & Richards, 2005; Milly *et al.*, 2008). Other alternatives have been proposed to address the issue of non-stationary to better predict return periods of extreme floods (Katz *et al.*, 2002; Kidson & Richards, 2005; Raff *et al.*, 2009; Rootzén & Katz, 2013; Salas & Obeysekera, 2014). Kidson and Richards (2005) have proposed the usage of self-similar (power law) models to be used to calculate the return periods of floods due to their simplicity and output of conservative results when using shorter records. Furthermore, the addition of paleoflood data to historical flood data may provide better baseline conditions due to the longer records (Kidson & Richards, 2005). Several studies have explored including paleoflood data together with instrumental records to generate more accurate calculations of the return periods of floods, particularly for the longer return intervals such as the 100-year flood (Baker, 1987; Kidson *et al.*, 2005; Lam *et al.*, 2017; Reinders & Muñoz, 2021; Salas *et al.*, 1994). These two examples illustrate two potential methods to compute more accurate return periods of floods without making the *i.i.d.* assumption that we show is untenable.

Due to the importance of flood frequency analysis studies in water management and infrastructure design, accurate predictions of annual peak floods are needed. Hence, understanding the influence of the atmospheric-ocean oscillations such as the PDO and AMO on peak annual floods is important. Future research can expand on this study by assessing the influence of other climate oscillations on flood risks in other regions around the world.

DATA AVAILABILITY

The observed daily flow records used in this analysis are publicly available at the United States Geological Survey (USGS) database, www.waterdata.usgs.gov/nwis and Water Survey of Canada (WSC) database, www.wateroffice.ec.gc.ca.

ADDITIONAL INFORMATION

All statistical tests were conducted using the R computing language, version 4.0.3 on Microsoft Windows 10. Additional supporting information are provided, containing higher resolution maps of the figures, with separate figures for the northern region, the Pacific Northwest and California for clarity. Also in the supporting information are the correlation plots between the climate oscillation indices and climate variables, and sample hydrographs from the different hydrological regimes along the western continental margin.

ACKNOWLEDGEMENTS

We would like to thank the Natural Sciences and Engineering Research Council (NSERC) Discovery Grant No. RGPIN/ 41795-2017 to J.M. St-Jacques for funding this project. We would also like to thank NSERC, the Fonds de recherche du Québec – Nature et technologies (FRQNT), Hydro Québec and Concordia University for scholarships to D.D. Noel.

MANUSCRIPT TABLES

Table 1. Impacts of the PDO/AMO combinations on the frequencies of the lower and upper quartile floods (i.e., those $\leq Q_{0.25}$ and those $\geq Q_{0.75}$, respectively). Upward and downward triangles signify the percentages of stations where there are significant percentages of floods above and below the expected 25% threshold, respectively ($p < 0.1$).

Region	Metric	Negative PDO/ Positive AMO (1944-1963)	Negative PDO/ Negative AMO (1964-1976)	Positive PDO/ Negative AMO (1977-1994)	Positive PDO/ Positive AMO (1995-2008)
Western North America (150 stations)	Q _{0.25}	▲2% ▼11%	▲4% ▼4%	▲23% ▼5%	▲5% ▼3%
	Q _{0.75}	▲5% ▼5%	▲13% ▼5%	▲7% ▼3%	▲20% ▼2%
Northern (25 stations)	Q _{0.25}	▲0% ▼24%	▲8% ▼4%	▲16% ▼8%	▲8% ▼12%
	Q _{0.75}	▲0% ▼4%	▲8% ▼12%	▲12% ▼0%	▲4% ▼8%
Pacific Northwest (70 stations)	Q _{0.25}	▲1% ▼11%	▲6% ▼1%	▲23% ▼0%	▲4% ▼1%
	Q _{0.75}	▲11% ▼4%	▲10% ▼3%	▲6% ▼6%	▲29% ▼1%
California (55 stations)	Q _{0.25}	▲4% ▼5%	▲0% ▼9%	▲27% ▼9%	▲4% ▼2%
	Q _{0.75}	▲0% ▼5%	▲18% ▼5%	▲7% ▼0%	▲16% ▼0%

Table 2. Impacts of the individual PDO and AMO phases on the frequencies of the lower and upper quartile floods (i.e., those $\leq Q_{0.25}$ and those $\geq Q_{0.75}$, respectively). The negative PDO phase spans 1944-1976 and the positive PDO spans 1977-2008; the negative AMO spans 1964-1994 and the positive AMO spans 1944-1963, 1995-2008. Upward and downward triangles signify the percentages of stations where there are significant percentages of floods above and below the expected 25% threshold, respectively ($p < 0.1$). In parentheses are numbers of records analyzed.

Region	Climate Index	Metric	Negative Phase	Positive Phase	
Western North America	PDO (232 stations)	Q _{0.25}	▲ 1% ▼ 25%	▲ 13% ▼ 7%	
		Q _{0.75}	▲ 8% ▼ 19%	▲ 12% ▼ 11%	
	AMO (248 stations)	Q _{0.25}	▲ 13% ▼ 8%	▲ 0% ▼ 30%	
		Q _{0.75}	▲ 6% ▼ 10%	▲ 3% ▼ 18%	
	Northern	PDO (48 stations)	Q _{0.25}	▲ 0% ▼ 33%	▲ 13% ▼ 4%
			Q _{0.75}	▲ 4% ▼ 21%	▲ 0% ▼ 15%
AMO (51 stations)		Q _{0.25}	▲ 12% ▼ 8%	▲ 0% ▼ 20%	
		Q _{0.75}	▲ 8% ▼ 10%	▲ 0% ▼ 37%	
Pacific Northwest		PDO (105 stations)	Q _{0.25}	▲ 1% ▼ 24%	▲ 13% ▼ 9%
			Q _{0.75}	▲ 13% ▼ 17%	▲ 14% ▼ 16%
	AMO (113 stations)	Q _{0.25}	▲ 10% ▼ 4%	▲ 0% ▼ 37%	
		Q _{0.75}	▲ 6% ▼ 10%	▲ 4% ▼ 14%	
	California	PDO (79 stations)	Q _{0.25}	▲ 1% ▼ 22%	▲ 11% ▼ 6%
			Q _{0.75}	▲ 4% ▼ 22%	▲ 16% ▼ 3%
AMO (84 stations)		Q _{0.25}	▲ 17% ▼ 15%	▲ 0% ▼ 27%	
		Q _{0.75}	▲ 8% ▼ 6%	▲ 1% ▼ 18%	

Table 3. Permutation *t*-test results of shifts in the Julian dates of seasonal streamflow extremes during the different PDO and AMO phases. For each region and climate oscillation phase, shown are the numbers of available records¹, and the percentages of significant shifts to later in the season. (+) x% denotes a significant shift to later in the season during the positive climate oscillation phase in x% of the records, (-) y% denotes a significant shift to later in the season during the positive climate oscillation phase in y% of the records. Bolding marks most important results.

Region	Climate Index	Fall Maxima	Winter Maxima	Spring Maxima	Summer Minima
Western North America margin	PDO	250	247	250	250
		(+) 9%	(+) 26%	(+) 5%	(+) 4%
		(-) 5%	(-) 2%	(-) 14%	(-) 24%
	AMO	249	242	249	249
(+) 8%		(+) 3%	(+) 4%	(+) 18%	
		(-) 1%	(-) 4%	(-) 5%	
Northern	PDO	51	48	51	51
		(+) 10%	(+) 21%	(+) 6%	(+) 2%
		(-) 2%	(-) 4%	(-) 25%	(-) 14%
	AMO	51	44	51	51
(+) 4%		(+) 7%	(+) 2%	(+) 4%	
		(-) 2%	(-) 11%	(-) 16%	
Pacific Northwest	PDO	114	114	114	114
		(+) 1%	(+) 46%	(+) 4%	(+) 1%
		(-) 11%	(-) 0%	(-) 13%	(-) 35%
	AMO	114	114	114	114
(+) 8%		(+) 4%	(+) 1%	(+) 24%	
		(-) 2%	(-) 4%	(-) 1%	
California	PDO	85	85	85	85
		(+) 16%	(+) 4%	(+) 7%	(+) 6%
		(-) 2%	(-) 2%	(-) 8%	(-) 15%
	AMO	84	84	84	84
(+) 11%		(+) 5%	(+) 11%	(+) 20%	
		(-) 0%	(-) 1%	(-) 4%	

¹Numbers of records analyzed change because of missing data and the requirement that there be at least 2 years in each climate oscillation phase.

CHAPTER 5: General Conclusions

In this study, the individual and combined effects of the PDO and AMO on annual peak flood magnitudes and the timing of seasonal extremes from 250 naturally flowing rivers were analyzed. Two non-parametric methods (permutated Q-Q plots and Spearman's correlation ρ) show that the PDO and AMO have substantial impacts on annual peak flood magnitudes. Most notably, the northern region (Alaska, the Yukon, and British Columbia), Pacific Northwest and northern California have substantially higher annual peak floods in the negative PDO phase. In contrast, historical annual peak flood magnitudes are significantly higher in southern California during the positive PDO phase. These particular methods show that the annual AMO index has a smaller influence on annual peak flood magnitudes in this region.

Furthermore, the individual and combined effects of the PDO and AMO phases have substantial effects on the frequencies of upper and lower quartile annual peak floods. The individual PDO and AMO phases impact the frequencies of annual peak floods in the lower quartile as lower annual peak floods occur less frequently than expected if there were no effect of the climate oscillations during the negative PDO and positive AMO phases along the western North American margin. When the PDO and AMO phases are combined, the phases of the climate oscillations may interact constructively, destructively, and with one dominating over the other. During the positive PDO and negative AMO phases, there is a clear drying effect in California with more low quartile floods than expected. In contrast, there are more upper quartile floods than expected in the Pacific Northwest when the PDO and AMO are in their positive phases. Such results show how additive, destructive and interference effects of the combined PDO and AMO phases play a role in the frequencies of extreme annual floods.

The timing of seasonal extremes along the western continental margin is substantially influenced by the individual effects of the PDO and AMO phases. At northern latitudes, the spring maxima dates are the most sensitive to changes in the winter PDO as peak streamflows occur much later during the negative PDO phase. In contrast, the occurrence of the winter maxima are substantially affected in the Pacific Northwest, with the peak winter streamflows occurring much later during the positive PDO phase. In California, the summer minima dates are sensitive to both the PDO and AMO phases. The summer minimum streamflow occurs much later during the negative PDO and positive AMO phases in this important agricultural region with large cities dependent on surface water availability for irrigation and urban water supplies.

Due to the importance of flood frequency analysis studies in water management and in the design of residential, commercial, and industrial infrastructure, accurate predictions of annual peak flood magnitudes are required to prepare adequate policies and designs. Additionally, results such as these in this thesis can provide better baseline conditions to improve hydrological models that will produce better flood forecasts across the western North American margin. These results have potential uses in agriculture and ocean fisheries due to the variations in annual peak streamflow magnitudes in rivers during PDO and AMO events. Hence, understanding the influence of the atmospheric-ocean oscillations such as the PDO and AMO is necessary in flood management plans to mitigate flood risk and reduce infrastructure damage near rivers. Future research can expand on this study through assessing the influence of other climate oscillations on flood risk in other regions around the world.

REFERENCES

- Alexander, M. (2013). Extratropical air-sea interaction, sea surface temperature variability, and the Pacific Decadal Oscillation. In *Climate Dynamics: Why Does Climate Vary?* (pp. 123–148). American Geophysical Union (AGU). <https://doi.org/10.1029/2008GM000794>
- Alexander, M. A., Bladé, I., Newman, M., Lanzante, J. R., Lau, N.-C., & Scott, J. D. (2002). The atmospheric bridge: The influence of ENSO teleconnections on air–sea interaction over the global oceans. *Journal of Climate*, *15*(16), 2205–2231. [https://doi.org/10.1175/1520-0442\(2002\)015<2205:TABTIO>2.0.CO;2](https://doi.org/10.1175/1520-0442(2002)015<2205:TABTIO>2.0.CO;2)
- Alexander, M. A., & Deser, C. (1995). A mechanism for the recurrence of wintertime midlatitude SST anomalies. *Journal of Physical Oceanography*, *25*(1), 122–137. [https://doi.org/10.1175/1520-0485\(1995\)025<0122:AMFTRO>2.0.CO;2](https://doi.org/10.1175/1520-0485(1995)025<0122:AMFTRO>2.0.CO;2)
- Andrews, E. D., Antweiler, R. C., Neiman, P. J., & Ralph, F. M. (2004). Influence of ENSO on flood frequency along the California coast. *Journal of Climate*, *17*(2), 337–348. [https://doi.org/10.1175/1520-0442\(2004\)017<0337:IOEOFF>2.0.CO;2](https://doi.org/10.1175/1520-0442(2004)017<0337:IOEOFF>2.0.CO;2)
- Archer, D. (1998). Flood frequency analysis. In *Encyclopedia of Hydrology and Lakes* (pp. 279–288). Springer Netherlands. https://doi.org/10.1007/1-4020-4497-6_86
- Archfield, S. A., Hirsch, R. M., Viglione, A., & Blöschl, G. (2016). Fragmented patterns of flood change across the United States. *Geophysical Research Letters*, *43*(19), 10,232–10,239. <https://doi.org/10.1002/2016GL070590>
- Arp, C. D., Whitman, M. S., Kemnitz, R., & Stuefer, S. L. (2020). Evidence of hydrological intensification and regime change from northern Alaskan watershed runoff. *Geophysical Research Letters*, *47*(17), e2020GL089186. <https://doi.org/10.1029/2020GL089186>

- Ashley, S. T., & Ashley, W. S. (2008). Flood fatalities in the United States. *Journal of Applied Meteorology and Climatology*, 47(3), 805–818.
<https://doi.org/10.1175/2007JAMC1611.1>
- Assani, A. A., Charron, S., Matteau, M., Mesfioui, M., & Quessy, J.-F. (2010a). Temporal variability modes of floods for catchments in the St. Lawrence watershed (Quebec, Canada). *Journal of Hydrology*, 385(1), 292–299.
<https://doi.org/10.1016/j.jhydrol.2010.02.031>
- Assani, A. A., Landais, D., Mesfioui, M., & Matteau, M. (2010b). Relationship between the Atlantic Multidecadal Oscillation index and variability of mean annual flows for catchments in the St. Lawrence watershed (Quebec, Canada) during the past century. *Hydrology Research*, 41(2), 115–125. <https://doi.org/10.2166/nh.2010.055>
- Baker, V. R. (1987). Paleoflood hydrology and extraordinary flood events. *Journal of Hydrology*, 96(1), 79–99. [https://doi.org/10.1016/0022-1694\(87\)90145-4](https://doi.org/10.1016/0022-1694(87)90145-4)
- Barnett, T. P., Pierce, D. W., Saravanan, R., Schneider, N., Dommenges, D., & Latif, M. (1999). Origins of the midlatitude Pacific decadal variability. *Geophysical Research Letters*, 26(10), 1453–1456. <https://doi.org/10.1029/1999GL900278>
- Beebe, R. A., & Manga, M. (2004). Variation in the relationship between snowmelt runoff in Oregon and ENSO and PDO. *JAWRA Journal of the American Water Resources Association*, 40(4), 1011–1024. <https://doi.org/10.1111/j.1752-1688.2004.tb01063.x>
- Berg, N., & Hall, A. (2015). Increased interannual precipitation extremes over California under climate change. *Journal of Climate*, 28(16), 6324–6334. <https://doi.org/10.1175/JCLI-D-14-00624.1>

- Bjerknes, J. (1966). A possible response of the atmospheric Hadley circulation to equatorial anomalies of ocean temperature. *Tellus*, 18(4), 820–829.
<https://doi.org/10.3402/tellusa.v18i4.9712>
- Bjerknes, J. (1969). Atmospheric teleconnections from the equatorial Pacific. *Monthly Weather Review*, 97(3), 163–172. [https://doi.org/10.1175/1520-0493\(1969\)097<0163:ATFTEP>2.3.CO;2](https://doi.org/10.1175/1520-0493(1969)097<0163:ATFTEP>2.3.CO;2)
- Brabets, T. P., & Walvoord, M. A. (2009). Trends in streamflow in the Yukon River basin from 1944 to 2005 and the influence of the Pacific Decadal Oscillation. *Journal of Hydrology*, 371(1–4), 12. <https://doi.org/10.1016/j.jhydrol.2009.03.018>
- Burn, D. H., Cunderlik, J. M., & Pietroniro, A. (2004). Hydrological trends and variability in the Liard River basin / Tendances hydrologiques et variabilité dans le bassin de la rivière Liard. *Hydrological Sciences Journal*, 49(1), 53–67.
<https://doi.org/10.1623/hysj.49.1.53.53994>
- Burn, D. H., & Whitfield, P. H. (2017). Changes in cold region flood regimes inferred from long-record reference gauging stations. *Water Resources Research*, 53(4), 2643–2658.
<https://doi.org/10.1002/2016WR020108>
- Buttle, J. M., Allen, D. M., Caissie, D., Davison, B., Hayashi, M., Peters, D. L., Pomeroy, J. W., Simonovic, S., St-Hilaire, A., & Whitfield, P. H. (2016). Flood processes in Canada: Regional and special aspects. *Canadian Water Resources Journal / Revue Canadienne Des Ressources Hydriques*, 41(1–2), 7–30.
<https://doi.org/10.1080/07011784.2015.1131629>
- Cai, W., Santoso, A., Wang, G., Yeh, S.-W., An, S.-I., Cobb, K. M., Collins, M., Guilyardi, E., Jin, F.-F., Kug, J.-S., Lengaigne, M., McPhaden, M. J., Takahashi, K., Timmermann, A.,

- Vecchi, G., Watanabe, M., & Wu, L. (2015a). ENSO and greenhouse warming. *Nature Climate Change*, 5(9), 849–859. <https://doi.org/10.1038/nclimate2743>
- Cai, W., Wang, G., Santoso, A., McPhaden, M. J., Wu, L., Jin, F.-F., Timmermann, A., Collins, M., Vecchi, G., Lengaigne, M., England, M. H., Dommenges, D., Takahashi, K., & Guilyardi, E. (2015b). Increased frequency of extreme La Niña events under greenhouse warming. *Nature Climate Change*, 5(2), 132–137. <https://doi.org/10.1038/nclimate2492>
- Cayan, D. R., Redmond, K. T., & Riddle, L. G. (1999). ENSO and hydrologic extremes in the western United States. *Journal of Climate*, 12(9), 2881–2893. [https://doi.org/10.1175/1520-0442\(1999\)012<2881:EAHEIT>2.0.CO;2](https://doi.org/10.1175/1520-0442(1999)012<2881:EAHEIT>2.0.CO;2)
- Chen, D., & Chen, H. W. (2013). Using the Köppen classification to quantify climate variation and change: An example for 1901–2010. *Environmental Development*, 6, 69–79. <https://doi.org/10.1016/j.envdev.2013.03.007>
- Corringham, T. W., & Cayan, D. R. (2019). The Effect of El Niño on flood damages in the western United States. *Weather, Climate, and Society*, 11(3), 489–504. <https://doi.org/10.1175/WCAS-D-18-0071.1>
- d’Orgeville, M., & Peltier, W. R. (2007). On the Pacific Decadal Oscillation and the Atlantic Multidecadal Oscillation: Might they be related? *Geophysical Research Letters*, 34(23). <https://doi.org/10.1029/2007GL031584>
- Dai, A. (2013). The influence of the inter-decadal Pacific oscillation on US precipitation during 1923–2010. *Climate Dynamics*, 41(3–4), 633–646. <https://doi.org/10.1007/s00382-012-1446-5>
- Dai, A., & Wigley, T. M. L. (2000). Global patterns of ENSO-induced precipitation. *Geophysical Research Letters*, 27(9), 1283–1286. <https://doi.org/10.1029/1999GL011140>

- Déry, S. J., Stahl, K., Moore, R. D., Whitfield, P. H., Menounos, B., & Burford, J. E. (2009). Detection of runoff timing changes in pluvial, nival, and glacial rivers of western Canada. *Water Resources Research*, 45(4). <https://doi.org/10.1029/2008WR006975>
- Dima, M., & Lohmann, G. (2007). A hemispheric mechanism for the Atlantic Multidecadal Oscillation. *Journal of Climate*, 20(11), 2706–2719. <https://doi.org/10.1175/JCLI4174.1>
- Drinkwater, K. F., Miles, M., Medhaug, I., Otterå, O. H., Kristiansen, T., Sundby, S., & Gao, Y. (2014). The Atlantic Multidecadal Oscillation: Its manifestations and impacts with special emphasis on the Atlantic region north of 60°N. *Journal of Marine Systems*, 133, 117–130. <https://doi.org/10.1016/j.jmarsys.2013.11.001>
- Eaton, B., & Moore, R. (2010). Chapter 4—Regional Hydrology. *Compendium of Forest Hydrology and Geomorphology in British Columbia*.
- Enfield, D. B., Mestas-Nuñez, A. M., & Trimble, P. J. (2001). The Atlantic Multidecadal Oscillation and its relation to rainfall and river flows in the continental U.S. *Geophysical Research Letters*, 28(10), 2077–2080. <https://doi.org/10.1029/2000GL012745>
- England Jr., J. F., Cohn, T. A., Faber, B. A., Stedinger, J. R., Thomas Jr., W. O., Veilleux, A. G., Kiang, J. E., & Mason Jr., R. R. (2018). *Guidelines for determining flood flow frequency—Bulletin 17C* (Report No. 4-B5; Techniques and Methods, p. 168). USGS Publications Warehouse. <https://doi.org/10.3133/tm4B5>
- Fortier, C., Assani, A. A., Mesfioui, M., & Roy, A. G. (2011). Comparison of the interannual and interdecadal variability of heavy flood characteristics upstream and downstream from dams in inversed hydrologic regime: Case study of Matawin River (Québec, Canada). *River Research and Applications*, 27(10), 1277–1289. <https://doi.org/10.1002/rra.1423>

- Frajka-Williams, E., Beaulieu, C., & Duchez, A. (2017). Emerging negative Atlantic Multidecadal Oscillation index in spite of warm subtropics. *Scientific Reports*, 7(1), 1–8. <https://doi.org/10.1038/s41598-017-11046-x>
- Franks, S. W., & Kuczera, G. (2002). Flood frequency analysis: Evidence and implications of secular climate variability, New South Wales. *Water Resources Research*, 38(5), 20-1-20–27. <https://doi.org/10.1029/2001WR000232>
- García-García, D., & Ummenhofer, C. C. (2015). Multidecadal variability of the continental precipitation annual amplitude driven by AMO and ENSO. *Geophysical Research Letters*, 42(2), 526–535. <https://doi.org/10.1002/2014GL062451>
- Goswami, B. N., Madhusoodanan, M. S., Neema, C. P., & Sengupta, D. (2006). A physical mechanism for North Atlantic SST influence on the Indian summer monsoon. *Geophysical Research Letters*, 33(2). <https://doi.org/10.1029/2005GL024803>
- Grimm, A. M., Barros, V. R., & Doyle, M. E. (2000). Climate variability in southern South America associated with El Niño and La Niña events. *Journal of Climate*, 13(1), 35–58. [https://doi.org/10.1175/1520-0442\(2000\)013<0035:CVISSA>2.0.CO;2](https://doi.org/10.1175/1520-0442(2000)013<0035:CVISSA>2.0.CO;2)
- Guimarães Nobre, G., Muis, S., Veldkamp, T. I. E., & Ward, P. J. (2019). Achieving the reduction of disaster risk by better predicting impacts of El Niño and La Niña. *Progress in Disaster Science*, 2, 100022. <https://doi.org/10.1016/j.pdisas.2019.100022>
- Gurrapu, S., St-Jacques, J.-M., Sauchyn, D. J., & Hodder, K. R. (2016). The influence of the Pacific Decadal Oscillation on annual floods in the rivers of western Canada. *JAWRA Journal of the American Water Resources Association*, 52(5), 1031–1045. <https://doi.org/10.1111/1752-1688.12433>

- Häkkinen, S., Rhines, P. B., & Worthen, D. L. (2011). Atmospheric blocking and Atlantic Multidecadal Ocean variability. *Science*, 334(6056), 655–659.
<https://doi.org/10.1126/science.1205683>
- Hamlet, A. F., & Lettenmaier, D. P. (2007). Effects of 20th century warming and climate variability on flood risk in the western U.S. *Water Resources Research*, 43(6), W06427.
<https://doi.org/10.1029/2006WR005099>
- Helsel, D. R., & Hirsch, R. M. (2002). Statistical methods in water resources. In *Techniques of Water Resources Investigations*. U.S. Geological Survey.
<https://pubs.usgs.gov/twri/twri4a3/>
- Hodgkins, G. A., Whitfield, P. H., Burn, D. H., Hannaford, J., Renard, B., Stahl, K., Fleig, A. K., Madsen, H., Mediero, L., Korhonen, J., Murphy, C., & Wilson, D. (2017). Climate-driven variability in the occurrence of major floods across North America and Europe. *Journal of Hydrology*, 552, 704717. <https://doi.org/10.1016/j.jhydrol.2017.07.027>
- Jonkman, S. N. (2005). Global perspectives on loss of human life caused by floods. *Natural Hazards*, 34(2), 151–175. <https://doi.org/10.1007/s11069-004-8891-3>
- Katz, R. W., Parlange, M. B., & Naveau, P. (2002). Statistics of extremes in hydrology. *Advances in Water Resources*, 25(8), 1287–1304. [https://doi.org/10.1016/S0309-1708\(02\)00056-8](https://doi.org/10.1016/S0309-1708(02)00056-8)
- Kerr, R. A. (2000). A north Atlantic climate pacemaker for the centuries. *Science*, 288(5473), 1984–1985. <https://doi.org/10.1126/science.288.5473.1984>
- Kidson, R., & Richards, K. S. (2005). Flood frequency analysis: Assumptions and alternatives. *Progress in Physical Geography: Earth and Environment*, 29(3), 392–410.
<https://doi.org/10.1191/0309133305pp454ra>

- Kidson, R., Richards, K. S., & Carling, P. A. (2005). Reconstructing the ca. 100-year flood in northern Thailand. *Geomorphology*, *70*, 279–295.
<https://doi.org/10.1016/j.geomorph.2005.02.009>
- Kiem, A. S., Franks, S. W., & Kuczera, G. (2003). Multi-decadal variability of flood risk. *Geophysical Research Letters*, *30*(2). <https://doi.org/10.1029/2002GL015992>
- Knight, J. R., Allan, R. J., Folland, C. K., Vellinga, M., & Mann, M. E. (2005). A signature of persistent natural thermohaline circulation cycles in observed climate. *Geophysical Research Letters*, *32*(20). <https://doi.org/10.1029/2005GL024233>
- Knight, J. R., Folland, C. K., & Scaife, A. A. (2006). Climate impacts of the Atlantic Multidecadal Oscillation. *Geophysical Research Letters*, *33*(17).
<https://doi.org/10.1029/2006GL026242>
- Kundzewicz, Z. W., Su, B., Wang, Y., Wang, G., Wang, G., Huang, J., & Jiang, T. (2019a). Flood risk in a range of spatial perspectives – from global to local scales. *Natural Hazards and Earth System Sciences*, *19*(7), 1319–1328. <https://doi.org/10.5194/nhess-19-1319-2019>
- Kundzewicz, Z. W., Szwed, M., & Pińskwar, I. (2019b). Climate variability and floods—A global review. *Water*, *11*(7), 1399. <https://doi.org/10.3390/w11071399>
- Kwon, H.-H., Brown, C., & Lall, U. (2008). Climate informed flood frequency analysis and prediction in Montana using hierarchical Bayesian modeling. *Geophysical Research Letters*, *35*(5). <https://doi.org/10.1029/2007GL032220>
- Lam, D., Thompson, C., Croke, J., Sharma, A., & Macklin, M. (2017). Reducing uncertainty with flood frequency analysis: The contribution of paleoflood and historical flood

- information. *Water Resources Research*, 53(3), 2312–2327.
<https://doi.org/10.1002/2016WR019959>
- Lane, B. A., Dahlke, H. E., Pasternack, G. B., & Sandoval-Solis, S. (2017). Revealing the diversity of natural hydrologic regimes in California with relevance for environmental flows applications. *JAWRA Journal of the American Water Resources Association*, 53(2), 411–430. <https://doi.org/10.1111/1752-1688.12504>
- Latif, M., & Barnett, T. P. (1996). Decadal climate variability over the north Pacific and North America: Dynamics and Predictability. *Journal of Climate*, 9(10), 2407–2423.
[https://doi.org/10.1175/1520-0442\(1996\)009<2407:DCVOTN>2.0.CO;2](https://doi.org/10.1175/1520-0442(1996)009<2407:DCVOTN>2.0.CO;2)
- Magaña, V. O., Vázquez, J. L., Pérez, J. L., & Pérez, J. B. (2003). Impact of El Niño on precipitation in Mexico. *Geofísica Internacional*, 42(3), 313–330.
- Mallakpour, I., & Villarini, G. (2017). Analysis of changes in the magnitude, frequency, and seasonality of heavy precipitation over the contiguous USA. *Theoretical and Applied Climatology*, 130(1), 345–363. <https://doi.org/10.1007/s00704-016-1881-z>
- Mantua, N. J., & Hare, S. R. (2002). The Pacific Decadal Oscillation. *Journal of Oceanography*, 58(1), 35–44. <https://doi.org/10.1023/A:1015820616384>
- Mantua, N. J., Hare, S. R., Zhang, Y., Wallace, J. M., & Francis, R. C. (1997). A Pacific interdecadal climate oscillation with impacts on salmon production*. *Bulletin of the American Meteorological Society*, 78(6), 1069–1080. [https://doi.org/10.1175/1520-0477\(1997\)078<1069:APICOW>2.0.CO;2](https://doi.org/10.1175/1520-0477(1997)078<1069:APICOW>2.0.CO;2)
- Mazouz, R., Assani, A. A., Quessy, J.-F., & Légaré, G. (2012). Comparison of the interannual variability of spring heavy floods characteristics of tributaries of the St. Lawrence River

- in Quebec (Canada). *Advances in Water Resources*, 35, 110–120.
<https://doi.org/10.1016/j.advwatres.2011.10.006>
- McCabe, G. J., & Dettinger, M. D. (2002). Primary modes and predictability of year-to-year snowpack variations in the western United States from teleconnections with Pacific Ocean climate. *Journal of Hydrometeorology*, 3(1), 13–25. [https://doi.org/10.1175/1525-7541\(2002\)003<0013:PMAPOY>2.0.CO;2](https://doi.org/10.1175/1525-7541(2002)003<0013:PMAPOY>2.0.CO;2)
- McCabe, G. J., Palecki, M. A., & Betancourt, J. L. (2004). Pacific and Atlantic Ocean influences on multidecadal drought frequency in the United States. *Proceedings of the National Academy of Sciences*, 101(12), 4136–4141. <https://doi.org/10.1073/pnas.0306738101>
- McKenney, D. W., Hutchinson, M. F., Papadopol, P., Lawrence, K., Pedlar, J., Campbell, K., Milewska, E., Hopkinson, R. F., Price, D., & Owen, T. (2011). Customized spatial climate models for North America. *Bulletin of the American Meteorological Society*, 92(12), 1611–1622. <https://doi.org/10.1175/2011BAMS3132.1>
- McPhaden, M. J. (1993). TOGA-TAO and the 1991-93 El Niño-Southern Oscillation Event. *Oceanography*, 6(2), 36–44.
- Méndez, M., & Magaña, V. (2010). Regional aspects of prolonged meteorological droughts over Mexico and central America. *Journal of Climate*, 23(5), 1175–1188.
<https://doi.org/10.1175/2009JCLI3080.1>
- Micevski, T., Franks, S. W., & Kuczera, G. (2006). Multidecadal variability in coastal eastern Australian flood data. *Journal of Hydrology*, 327(1), 219–225.
<https://doi.org/10.1016/j.jhydrol.2005.11.017>
- Miller, A. J., Cayan, D. R., Barnett, T. P., Graham, N. E., & Oberhuber, J. M. (1994). Interdecadal variability of the Pacific Ocean: Model response to observed heat flux and

- wind stress anomalies. *Climate Dynamics*, 9(6), 287–302.
<https://doi.org/10.1007/BF00204744>
- Milly, P. C. D., Betancourt, J., Falkenmark, M., Hirsch, R. M., Kundzewicz, Z. W., Lettenmaier, D. P., & Stouffer, R. J. (2008). Stationarity is dead: Whither water management? *Science*, 319(5863), 573–574. <https://doi.org/10.1126/science.1151915>
- Milly, P. C. D., Wetherald, R. T., Dunne, K. A., & Delworth, T. L. (2002). Increasing risk of great floods in a changing climate. *Nature*, 415(6871), 514.
<https://doi.org/10.1038/415514a>
- Mochizuki, T., Ishii, M., Kimoto, M., Chikamoto, Y., Watanabe, M., Nozawa, T., Sakamoto, T. T., Shiogama, H., Awaji, T., Sugiura, N., Toyoda, T., Yasunaka, S., Tatebe, H., & Mori, M. (2010). Pacific Decadal Oscillation hindcasts relevant to near-term climate prediction. *Proceedings of the National Academy of Sciences*, 107(5), 1833–1837.
<https://doi.org/10.1073/pnas.0906531107>
- Nastev, M., & Todorov, N. (2013). Hazus: A standardized methodology for flood risk assessment in Canada. *Canadian Water Resources Journal / Revue Canadienne Des Ressources Hydriques*, 38(3), 223–231. <https://doi.org/10.1080/07011784.2013.801599>
- Neal, E. G., Todd Walter, M., & Coffeen, C. (2002). Linking the Pacific Decadal Oscillation to seasonal stream discharge patterns in Southeast Alaska. *Journal of Hydrology*, 263(1), 188–197. [https://doi.org/10.1016/S0022-1694\(02\)00058-6](https://doi.org/10.1016/S0022-1694(02)00058-6)
- Neelin, J. D., Battisti, D. S., Hirst, A. C., Jin, F.-F., Wakata, Y., Yamagata, T., & Zebiak, S. E. (1998). ENSO theory. *Journal of Geophysical Research: Oceans*, 103(C7), 14261–14290. <https://doi.org/10.1029/97JC03424>

- Newman, M., Alexander, M. A., Ault, T. R., Cobb, K. M., Deser, C., Di Lorenzo, E., Mantua, N. J., Miller, A. J., Minobe, S., Nakamura, H., Schneider, N., Vimont, D. J., Phillips, A. S., Scott, J. D., & Smith, C. A. (2016). The Pacific Decadal Oscillation, revisited. *Journal of Climate*, 29(12), 4399–4427. <https://doi.org/10.1175/JCLI-D-15-0508.1>
- Pascolini-Campbell, M., Seager, R., Pinson, A., & Cook, B. I. (2017). Covariability of climate and streamflow in the Upper Rio Grande from interannual to interdecadal timescales. *Journal of Hydrology: Regional Studies*, 13, 58–71. <https://doi.org/10.1016/j.ejrh.2017.07.007>
- Peel, M. C., Finlayson, B. L., & McMahon, T. A. (2007). Updated world map of the Köppen-Geiger climate classification. *Hydrology and Earth System Sciences*, 11(5), 1633–1644. <https://doi.org/10.5194/hess-11-1633-2007>
- Pellerin, J., & Nzokou Tanekou, F. (2020). Reference hydrometric basin network update. *Environment and Climate Change Canada*, 37.
- Penalba, O. C., & Rivera, J. A. (2016). Precipitation response to El Niño/La Niña events in southern South America – emphasis in regional drought occurrences. *Advances in Geosciences*, 42, 1–14. <https://doi.org/10.5194/adgeo-42-1-2016>
- Philander, S. G. H. (1983). El Niño Southern Oscillation phenomena. *Nature*, 302(5906), 295–301. <https://doi.org/10.1038/302295a0>
- Piechota, T. C., Dracup, J. A., & Fovell, R. G. (1997). Western US streamflow and atmospheric circulation patterns during El Niño-Southern Oscillation. *Journal of Hydrology*, 201(1), 249–271. [https://doi.org/10.1016/S0022-1694\(97\)00043-7](https://doi.org/10.1016/S0022-1694(97)00043-7)

- Praskievicz, S., & Chang, H. (2009). Winter precipitation intensity and ENSO/PDO variability in the Willamette Valley of Oregon. *International Journal of Climatology*, 29(13), 2033–2039. <https://doi.org/10.1002/joc.1838>
- R Core Team. (2020). R: A language and environment for statistical computing. *R Foundation for Statistical Computing, Vienna, Austria*. <https://www.R-project.org/>
- Raff, D. A., Pruitt, T., & Brekke, L. D. (2009). A framework for assessing flood frequency based on climate projection information. *Hydrology and Earth System Sciences*, 13(11), 2119–2136. <https://doi.org/10.5194/hess-13-2119-2009>
- Rasmusson, E. M., & Carpenter, T. H. (1982). Variations in tropical sea surface temperature and surface wind fields associated with the Southern Oscillation/El Niño. *Monthly Weather Review*, 110(5), 354–384. [https://doi.org/10.1175/1520-0493\(1982\)110<0354:VITSST>2.0.CO;2](https://doi.org/10.1175/1520-0493(1982)110<0354:VITSST>2.0.CO;2)
- Rasmusson, E. M., Wang, X., & Ropelewski, C. F. (1990). The biennial component of ENSO variability. *Journal of Marine Systems*, 1(1), 71–96. [https://doi.org/10.1016/0924-7963\(90\)90153-2](https://doi.org/10.1016/0924-7963(90)90153-2)
- Redmond, K. T., & Koch, R. W. (1991). Surface climate and streamflow variability in the western United States and their relationship to large-scale circulation indices. *Water Resources Research*, 27(9), 2381–2399. <https://doi.org/10.1029/91WR00690>
- Reinders, J. B., & Muñoz, S. E. (2021). Improvements to flood frequency analysis on alluvial rivers using paleoflood data. *Water Resources Research*, 57(4), e2020WR028631. <https://doi.org/10.1029/2020WR028631>
- Rogger, M., Agnoletti, M., Alaoui, A., Bathurst, J. C., Bodner, G., Borga, M., Chaplot, V., Gallart, F., Glatzel, G., Hall, J., Holden, J., Holko, L., Horn, R., Kiss, A., Kohnová, S.,

- Leitinger, G., Lennartz, B., Parajka, J., Perdigão, R., *et al.* (2017). Land use change impacts on floods at the catchment scale: Challenges and opportunities for future research. *Water Resources Research*, *53*(7), 5209–5219.
<https://doi.org/10.1002/2017WR020723>
- Rood, S. B., Foster, S. G., Hillman, E. J., Luek, A., & Zanewich, K. P. (2016). Flood moderation: Declining peak flows along some Rocky Mountain rivers and the underlying mechanism. *Journal of Hydrology*, *536*, 174–182.
<https://doi.org/10.1016/j.jhydrol.2016.02.043>
- Rootzén, H., & Katz, R. W. (2013). Design life level: Quantifying risk in a changing climate. *Water Resources Research*, *49*(9), 5964–5972. <https://doi.org/10.1002/wrcr.20425>
- Ropelewski, C. F., & Halpert, M. S. (1987). Global and regional scale precipitation patterns associated with the El Niño/Southern Oscillation. *Monthly Weather Review*, *115*(8), 1606–1626. [https://doi.org/10.1175/1520-0493\(1987\)115<1606:GARSPP>2.0.CO;2](https://doi.org/10.1175/1520-0493(1987)115<1606:GARSPP>2.0.CO;2)
- Salas, J. D., & Obeysekera, J. (2014). Revisiting the concepts of return period and risk for nonstationary hydrologic extreme events. *Journal of Hydrologic Engineering*, *19*(3), 554–568.
- Salas, J. D., Wohl, E. E., & Jarrett, R. D. (1994). Determination of flood characteristics using systematic, historical and paleoflood data. In G. Rossi, N. Harmancıoğlu, & V. Yevjevich (Eds.), *Coping with Floods* (pp. 111–134). Springer Netherlands.
https://doi.org/10.1007/978-94-011-1098-3_7
- Santer, B. D., Wigley, T. M. L., Boyle, J. S., Gaffen, D. J., Hnilo, J. J., Nychka, D., Parker, D. E., & Taylor, K. E. (2000). Statistical significance of trends and trend differences in

- layer-average atmospheric temperature time series. *Journal of Geophysical Research: Atmospheres*, 105(D6), 7337–7356. <https://doi.org/10.1029/1999JD901105>
- Schnorbus, M., Werner, A., & Bennett, K. (2014). Impacts of climate change in three hydrologic regimes in British Columbia, Canada. *Hydrological Processes*, 28(3), 1170–1189. <https://doi.org/10.1002/hyp.9661>
- Schonher, T., & Nicholson, S. E. (1989). The relationship between California rainfall and ENSO events. *Journal of Climate*, 2(11), 1258–1269. [https://doi.org/10.1175/1520-0442\(1989\)002<1258:TRBCRA>2.0.CO;2](https://doi.org/10.1175/1520-0442(1989)002<1258:TRBCRA>2.0.CO;2)
- Stedinger, J. R., & Griffis, V. W. (2011). Getting from here to where? Flood frequency analysis and climate. *JAWRA Journal of the American Water Resources Association*, 47(3), 506–513. <https://doi.org/10.1111/j.1752-1688.2011.00545.x>
- Stewart, I. T., Cayan, D. R., & Dettinger, M. D. (2005). Changes toward earlier streamflow timing across western North America. *Journal of Climate*, 18(8), 1136–1155. <https://doi.org/10.1175/JCLI3321.1>
- Sutton, R. T., & Hodson, D. L. R. (2005). Atlantic Ocean forcing of North American and European summer climate. *Science*, 309(5731), 115–118. <https://doi.org/10.1126/science.1109496>
- Tan, X., & Gan, T. Y. (2014). Nonstationary analysis of annual maximum streamflow of Canada. *Journal of Climate*, 28(5), 1788–1805. <https://doi.org/10.1175/JCLI-D-14-00538.1>
- Thistlethwaite, J., & Henstra, D. (2017). Municipal flood risk sharing in Canada: A policy instrument analysis. *Canadian Water Resources Journal / Revue Canadienne Des Ressources Hydriques*, 42(4), 349–363. <https://doi.org/10.1080/07011784.2017.1364144>

- Tollan, A. (2002). Land-use change and floods: What do we need most, research or management? *Water Science and Technology*, 45(8), 183–190.
<https://doi.org/10.2166/wst.2002.0176>
- Tootle, G. A., & Piechota, T. C. (2006). Relationships between Pacific and Atlantic ocean sea surface temperatures and U.S. streamflow variability. *Water Resources Research*, 42(7).
<https://doi.org/10.1029/2005WR004184>
- Trenberth, K. E., & Hoar, T. J. (1996). The 1990–1995 El Niño-Southern Oscillation event: Longest on record. *Geophysical Research Letters*, 23(1), 57–60.
<https://doi.org/10.1029/95GL03602>
- Trenberth, K. E., & Shea, D. J. (2006). Atlantic hurricanes and natural variability in 2005. *Geophysical Research Letters*, 33(12). <https://doi.org/10.1029/2006GL026894>
- Valdés-Manzanilla, A. (2016). Historical floods in Tabasco and Chiapas during sixteenth–twentieth centuries. *Natural Hazards*, 80(3), 1563–1577. <https://doi.org/10.1007/s11069-015-2039-5>
- Valdés-Manzanilla, A. (2018). Effect of climatic oscillations on flood occurrence on Papaloapan River, México, during the 1550–2000 period. *Natural Hazards*, 94(1), 167–180.
<https://doi.org/10.1007/s11069-018-3379-8>
- Villarini, G., & Slater, L. (2017). Climatology of flooding in the United States. *Oxford Research Encyclopedia of Natural Hazard Science*.
<https://doi.org/10.1093/acrefore/9780199389407.013.123>
- Wallace, J. M., Rasmusson, E. M., Mitchell, T. P., Kousky, V. E., Sarachik, E. S., & Storch, H. von. (1998). On the structure and evolution of ENSO-related climate variability in the

- tropical Pacific: Lessons from TOGA. *Journal of Geophysical Research: Oceans*, 103(C7), 14241–14259. <https://doi.org/10.1029/97JC02905>
- Wang, C., Lee, S.-K., & Enfield, D. B. (2008). Atlantic warm pool acting as a link between Atlantic Multidecadal Oscillation and Atlantic tropical cyclone activity. *Geochemistry, Geophysics, Geosystems*, 9(5). <https://doi.org/10.1029/2007GC001809>
- Wang, S., Huang, J., He, Y., & Guan, Y. (2014). Combined effects of the Pacific Decadal Oscillation and El Niño-Southern Oscillation on global land dry–wet changes. *Scientific Reports*, 4(1), 6651. <https://doi.org/10.1038/srep06651>
- Wheater, H., & Evans, E. (2009). Land use, water management and future flood risk. *Land Use Policy*, 26, S251–S264.
- Whitfield, P. H. (2012). Floods in future climates: A review. *Journal of Flood Risk Management*, 5(4), 336–365. Scopus. <https://doi.org/10.1111/j.1753-318X.2012.01150.x>
- Whitfield, P. H., Moore, R. D. (Dan), Fleming, S. W., & Zawadzki, A. (2010). Pacific Decadal Oscillation and the hydroclimatology of western Canada—Review and Prospects. *Canadian Water Resources Journal / Revue Canadienne Des Ressources Hydriques*, 35(1), 1–28. <https://doi.org/10.4296/cwrj3501001>
- Wilks, D. (2011). *Statistical Methods in the Atmospheric Sciences* (3rd ed., Vol. 100). Elsevier Academic Press.
- Zhang, Y., Wallace, J. M., & Battisti, D. S. (1997). ENSO-like interdecadal variability: 1900–93. *Journal of Climate*, 10(5), 1004–1020. [https://doi.org/10.1175/1520-0442\(1997\)010<1004:ELIV>2.0.CO;2](https://doi.org/10.1175/1520-0442(1997)010<1004:ELIV>2.0.CO;2)

SUPPLEMENTARY FIGURES

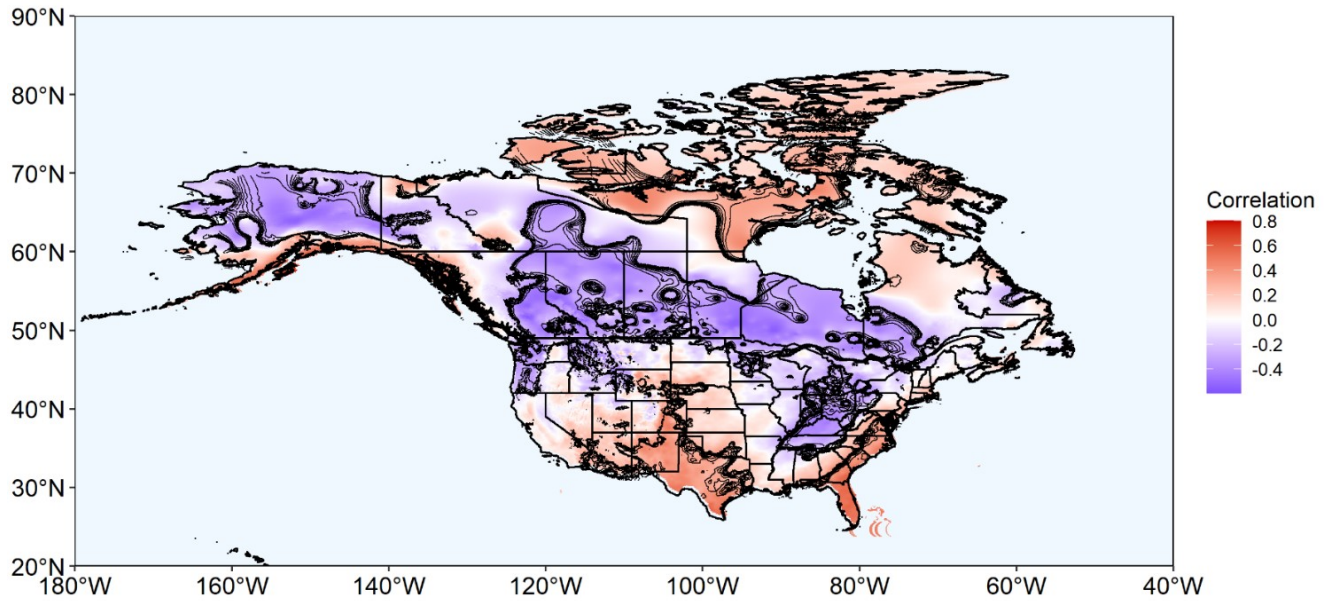


Figure S1. Correlation plot between the winter-averaged (November-March) PDO and winter (November-March) precipitation for North America for 1949-2015. Black lines represent significant correlation values between the PDO and precipitation at the 90% confidence level.

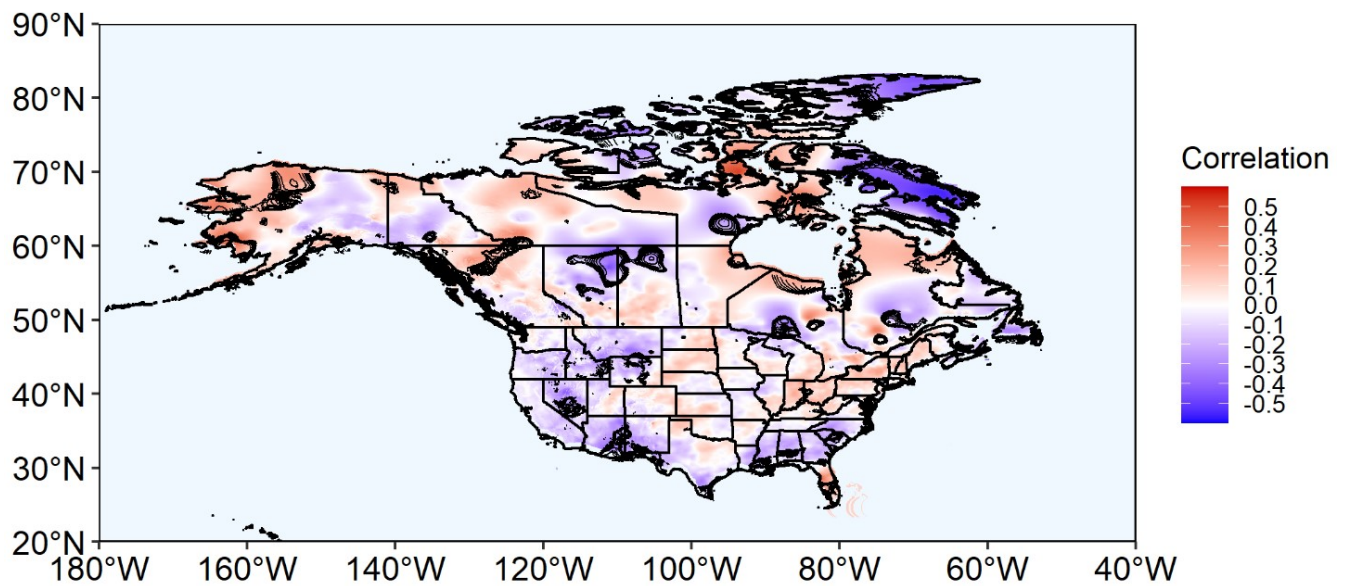


Figure S2. Correlation plot between the annually-averaged (January-December) AMO and annual (January-December) precipitation for North America for 1949-2015. Black lines represent significant correlation values between the AMO and precipitation at the 90% confidence level.

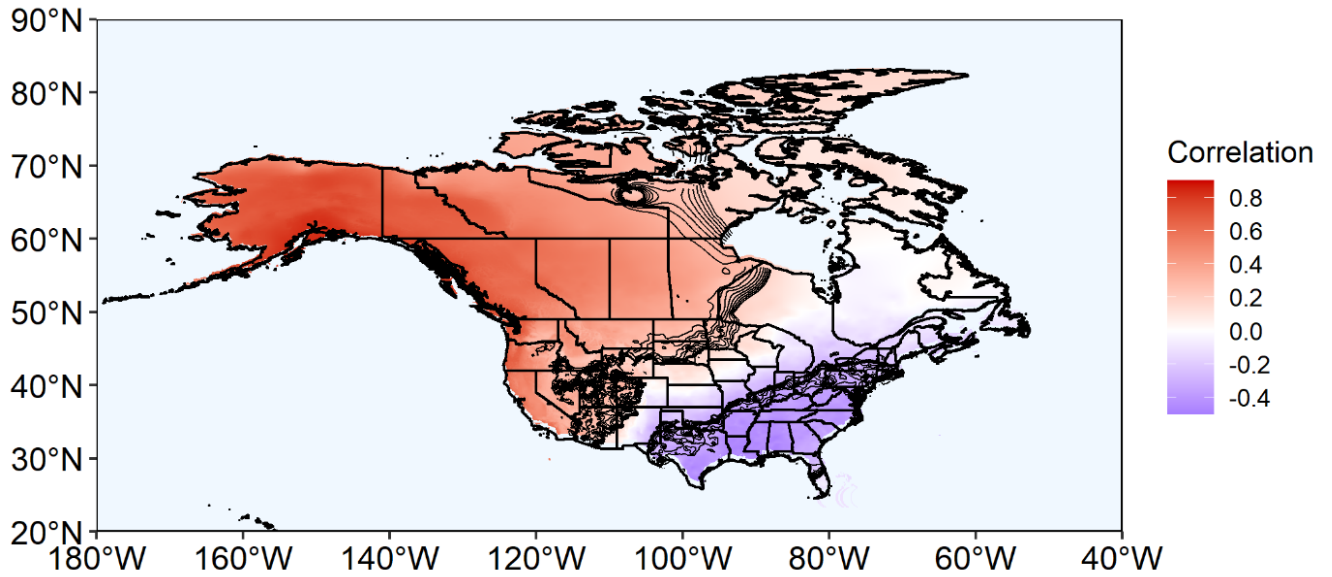


Figure S3. Correlation plot between the winter-averaged (November-March) PDO and winter-averaged (November-March) temperature for North America for 1949-2015. Black lines represent significant correlation values between the PDO and precipitation at the 90% confidence level.

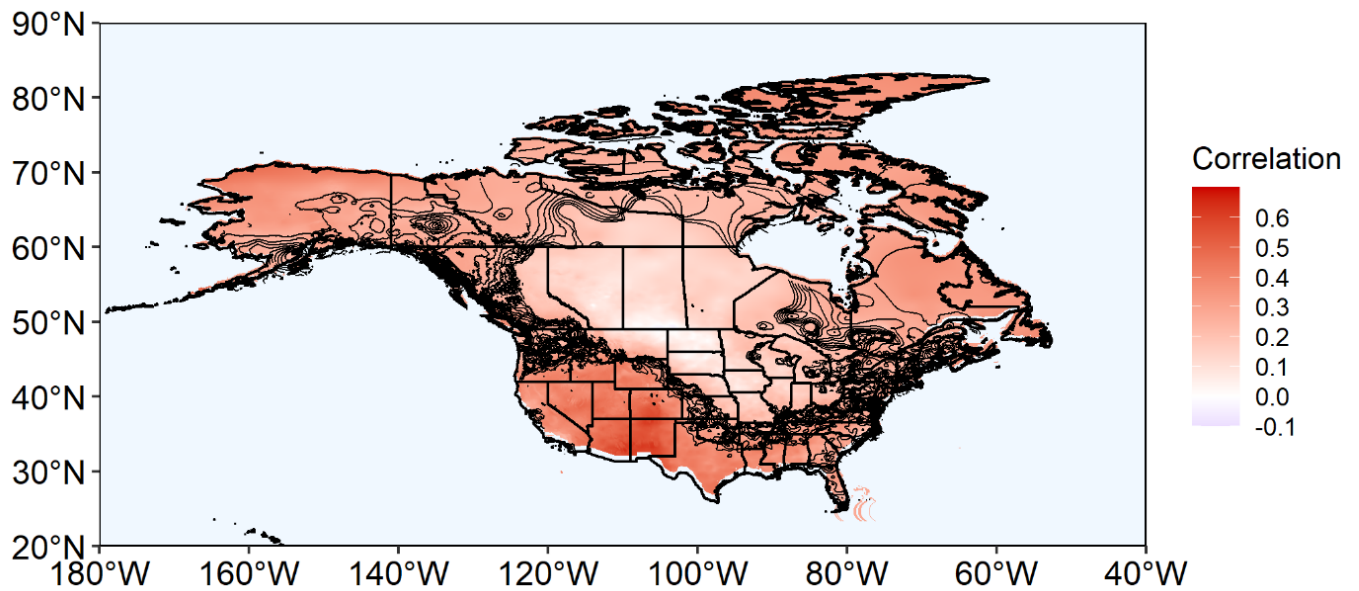


Figure S4. Correlation plot between the annually-averaged AMO and annually-averaged temperature for North America for 1949-2015. Black lines represent significant correlation values between the AMO and precipitation at the 90% confidence level.

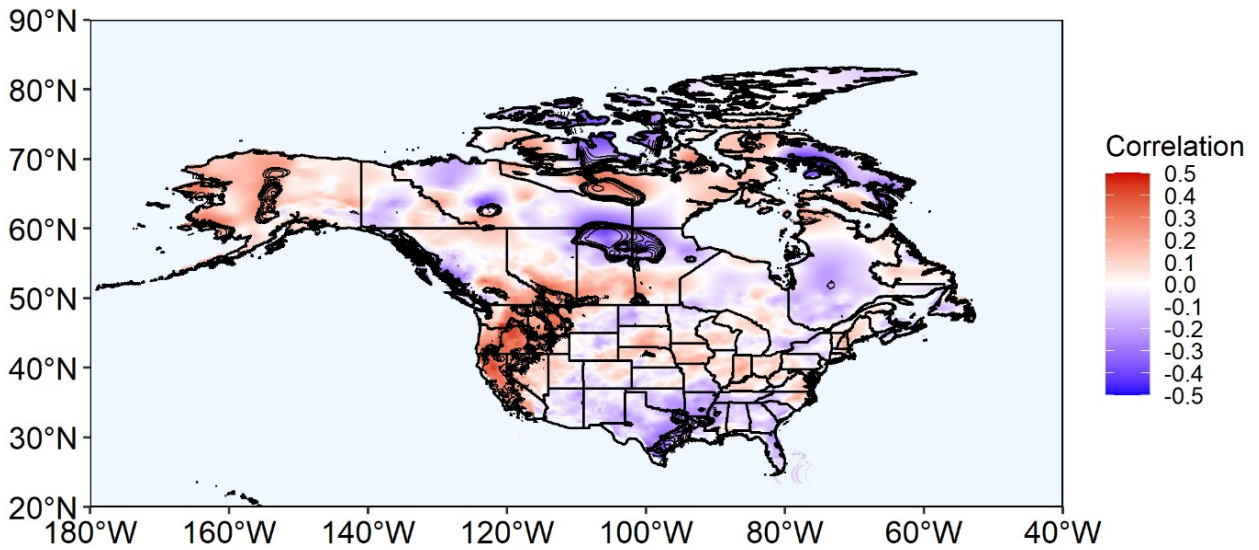


Figure S5. Correlation plot between the spring-averaged (April-June) AMO and spring (April-June) precipitation for North America for 1949-2015. Black lines represent significant correlation values between the AMO and precipitation at the 90% confidence level.

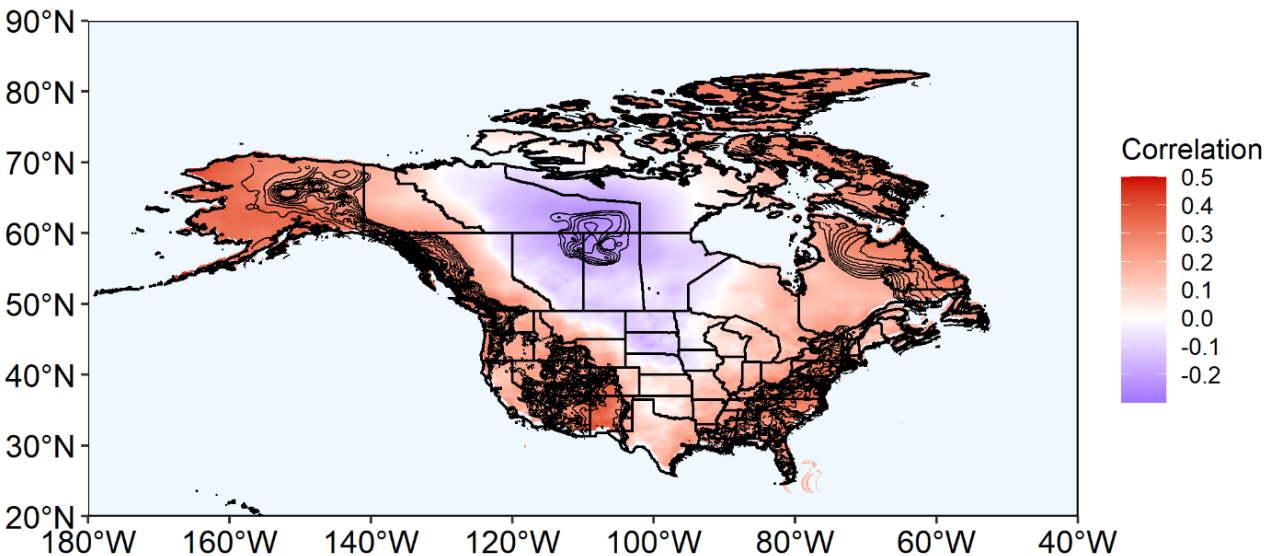


Figure S6. Correlation plot between the spring-averaged (April-June) AMO and spring (April-June) temperature for North America for 1949-2015. Black lines represent significant correlation values between the AMO and temperature at the 90% confidence level.

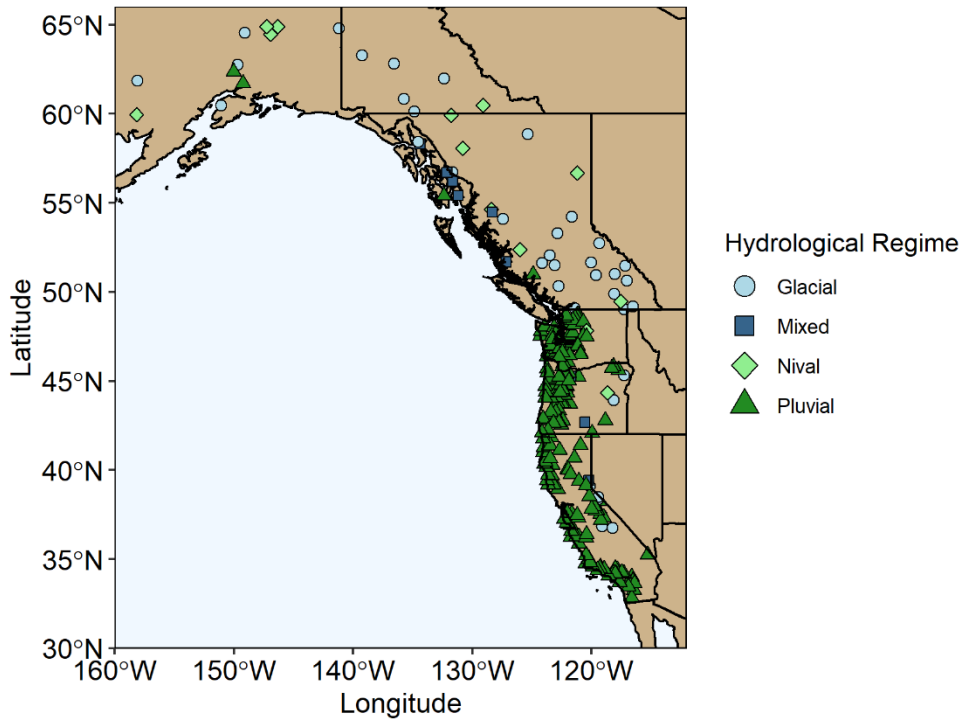


Figure S7. Locations of the 250 naturally flowing streamflow records, stratified according to their respective hydrological regimes (glacial, nival, pluvial and mixed) across the western North American margin.

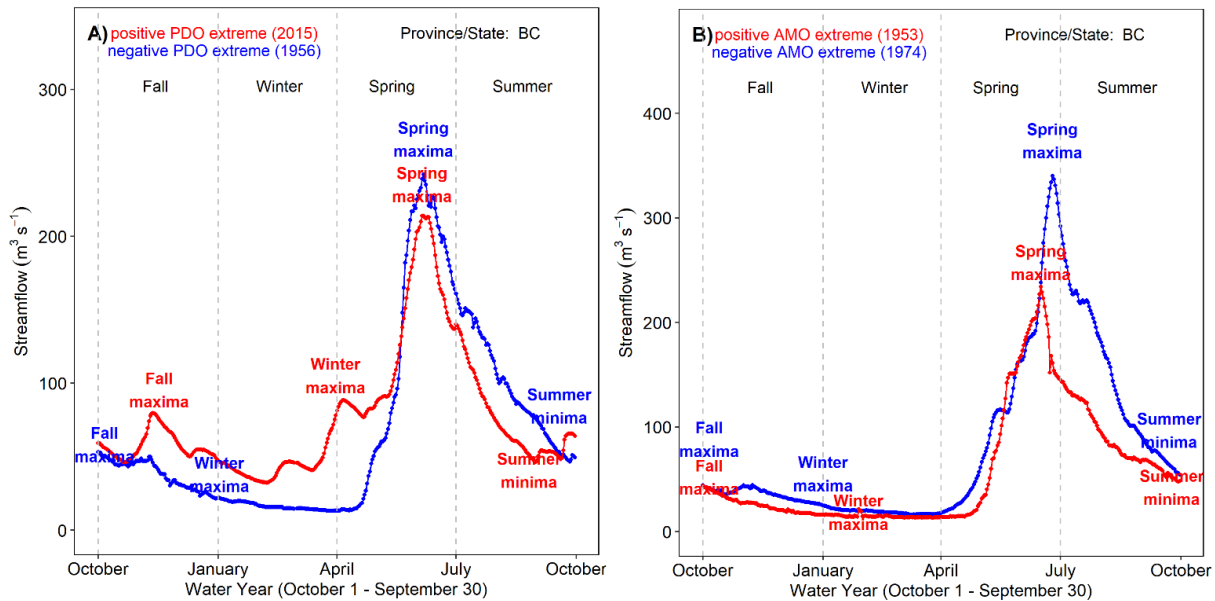


Figure S8. Glacial regime seasonal hydrographs of WSC station 08LD001, Adams River near Squilax, British Columbia, Canada. Separate hydrographs shown for extreme climate oscillation years: A) extreme positive and negative PDO years, 2015 and 1956, respectively; and B) extreme positive and negative AMO years, 1953 and 1974, respectively. Also shown are fall, winter and spring maxima and summer minima. Seasons defined as follows: winter (January-March), spring (April-June), summer (July-September) and fall (October-December).

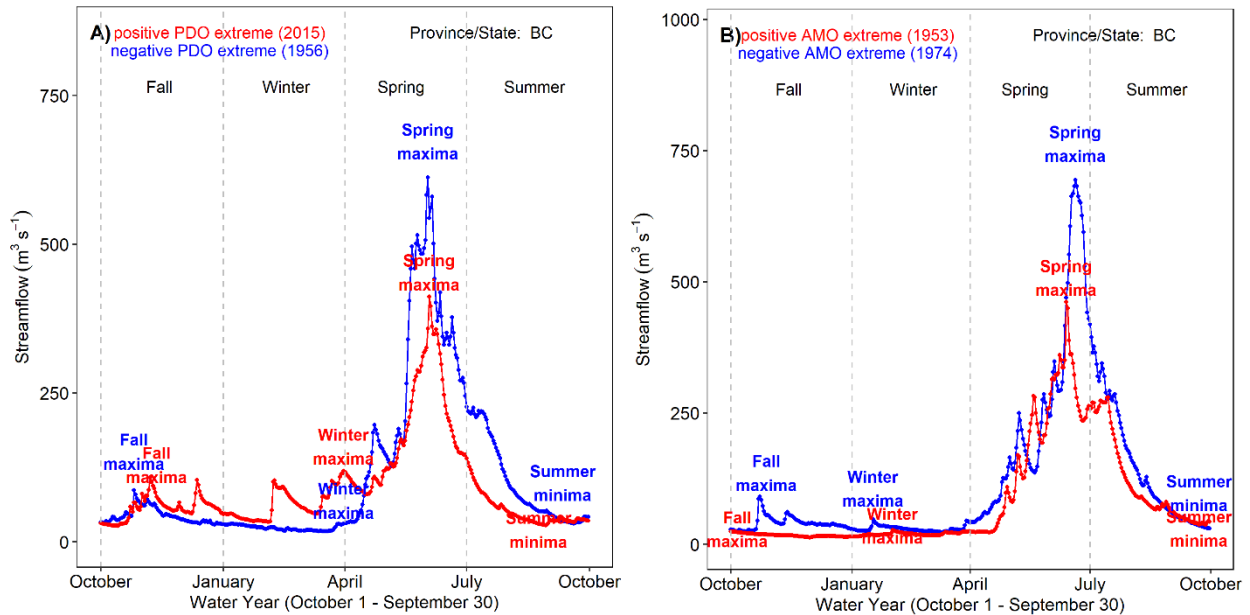


Figure S9. Nival regime seasonal hydrographs of WSC station 08NJ013, Slokan River near Crescent Valley, British Columbia, Canada. Separate hydrographs shown for extreme climate oscillation years: A) extreme positive and negative PDO years, 2015 and 1956, respectively; and B) extreme positive and negative AMO years, 1953 and 1974, respectively. Also shown are fall, winter and spring maxima and summer minima. Seasons defined as follows: winter (January-March), spring (April-June), summer (July-September) and fall (October-December).

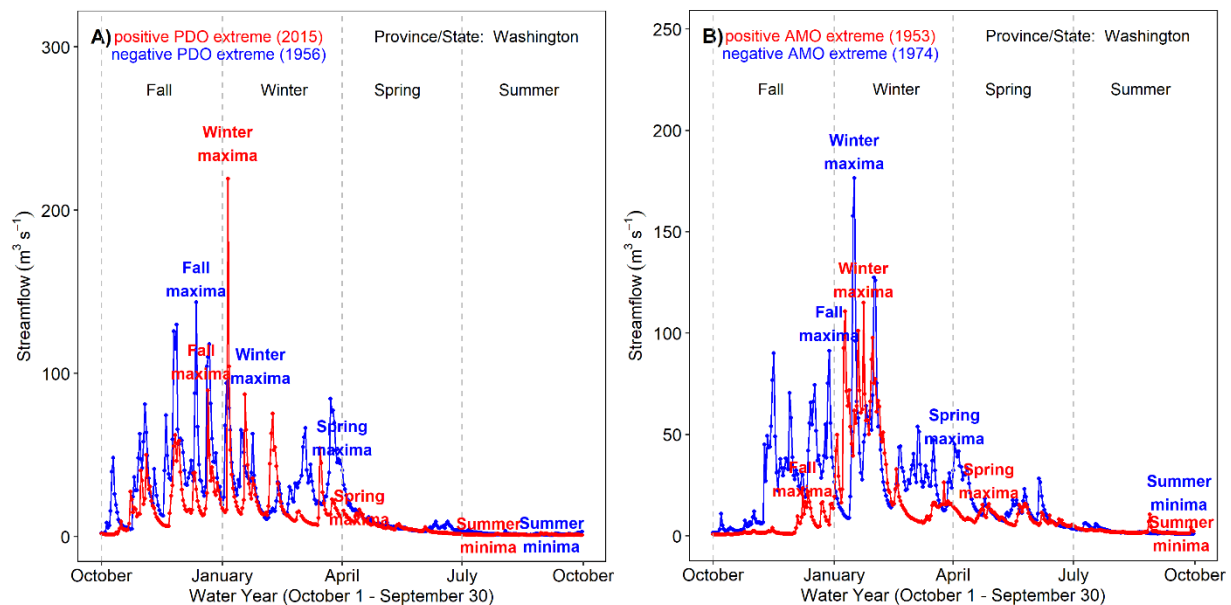


Figure S10. Pluvial regime seasonal hydrographs of USGS station 12025000, Newaukum River near Chehalis, Washington, USA. Separate hydrographs shown for extreme climate oscillation years: A) extreme positive and negative PDO years, 2015 and 1956, respectively; and B) extreme positive and negative AMO years, 1953 and 1974, respectively. Also shown are fall, winter and spring maxima and summer minima. Seasons defined as follows: winter (January-March), spring (April-June), summer (July-September) and fall (October-December).

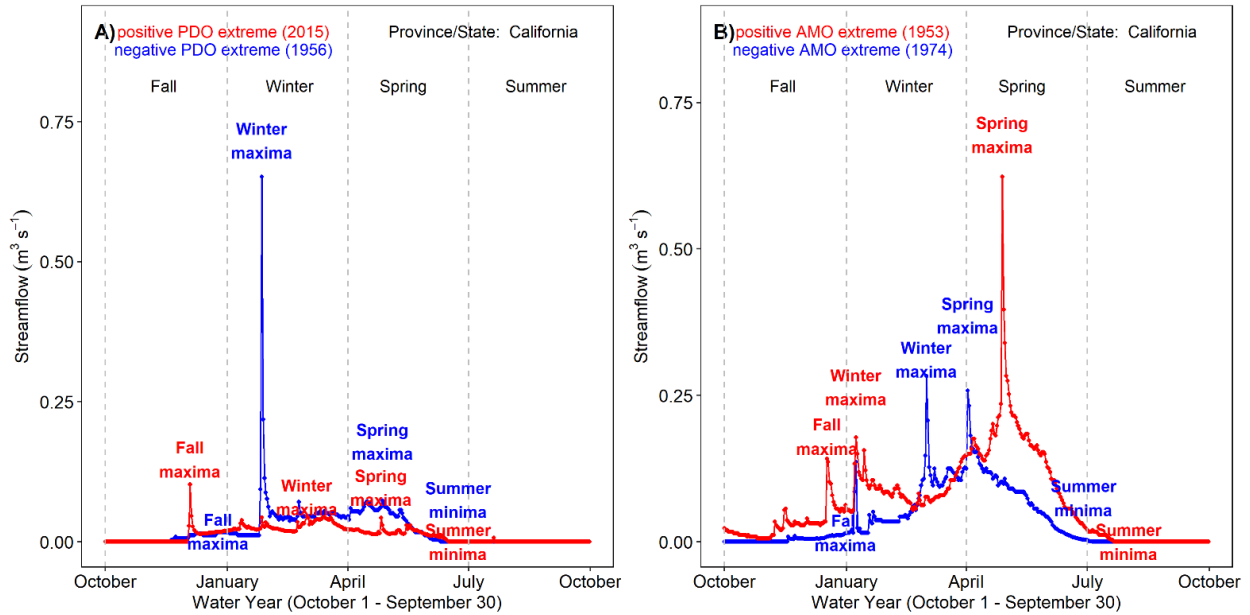


Figure S11. Pluvial regime seasonal hydrographs of USGS station 10258000, Tahquitz Creek near Palm Springs, southern California, USA. Separate hydrographs shown for extreme climate oscillation years: A) extreme positive and negative PDO years, 2015 and 1956, respectively; and B) extreme positive and negative AMO years, 1953 and 1974, respectively. Also shown are fall, winter and spring maxima and summer minima. Seasons defined as follows: winter (January-March), spring (April-June), summer (July-September) and fall (October-December).

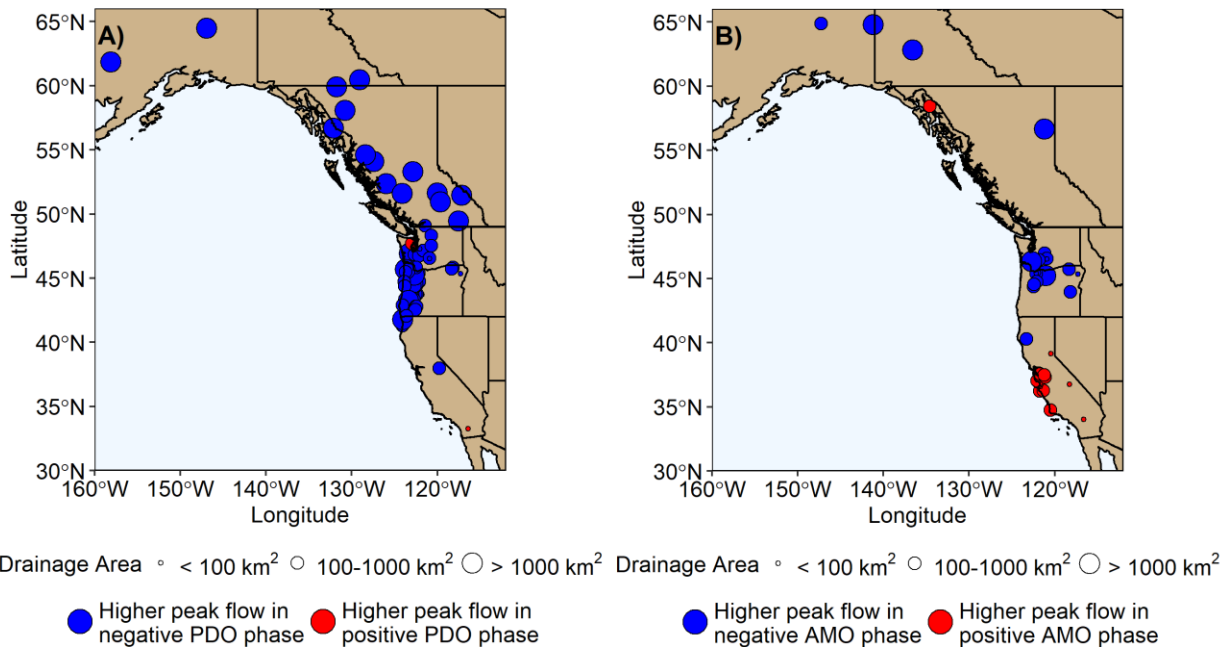
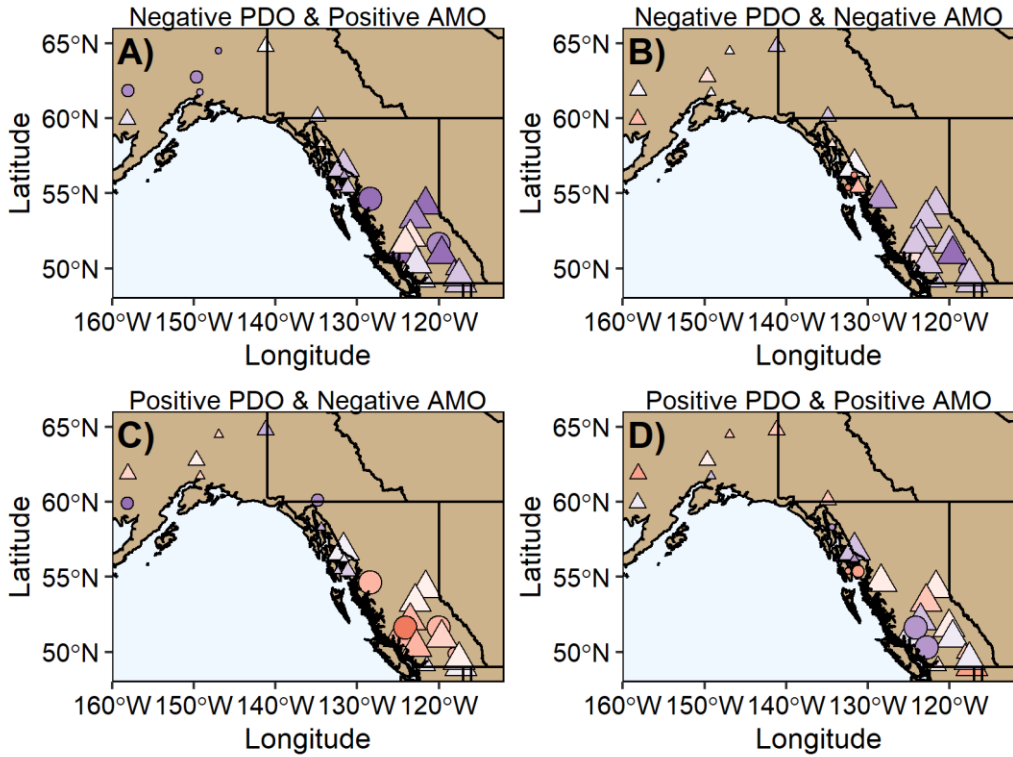


Figure S12. Significant Spearman's rank correlations ρ between annual peak flood records and A) the winter (November-March) averaged PDO index, and B) the annually averaged AMO index ($p \leq 0.1$).



Flood quartiles \triangle No significance \circ $p \leq 0.1$ Drainage Area \bullet $< 100 \text{ km}^2$ \bullet $100\text{-}1000 \text{ km}^2$ \bullet $> 1000 \text{ km}^2$

0 10 20 30 40 50 60
 % years $\leq Q_{0.25}$

Figure S13. Percentages of lower quartile floods for the four PDO and AMO combinations for the northern region: A) negative PDO and positive AMO, 1944-1963; B) negative PDO and negative AMO, 1964-1976; C) positive PDO and negative AMO, 1977-1994; and D) positive PDO and positive AMO, 1995-2008. Significance assessed by permutation tests (10,000 iterations, $p \leq 0.1$).

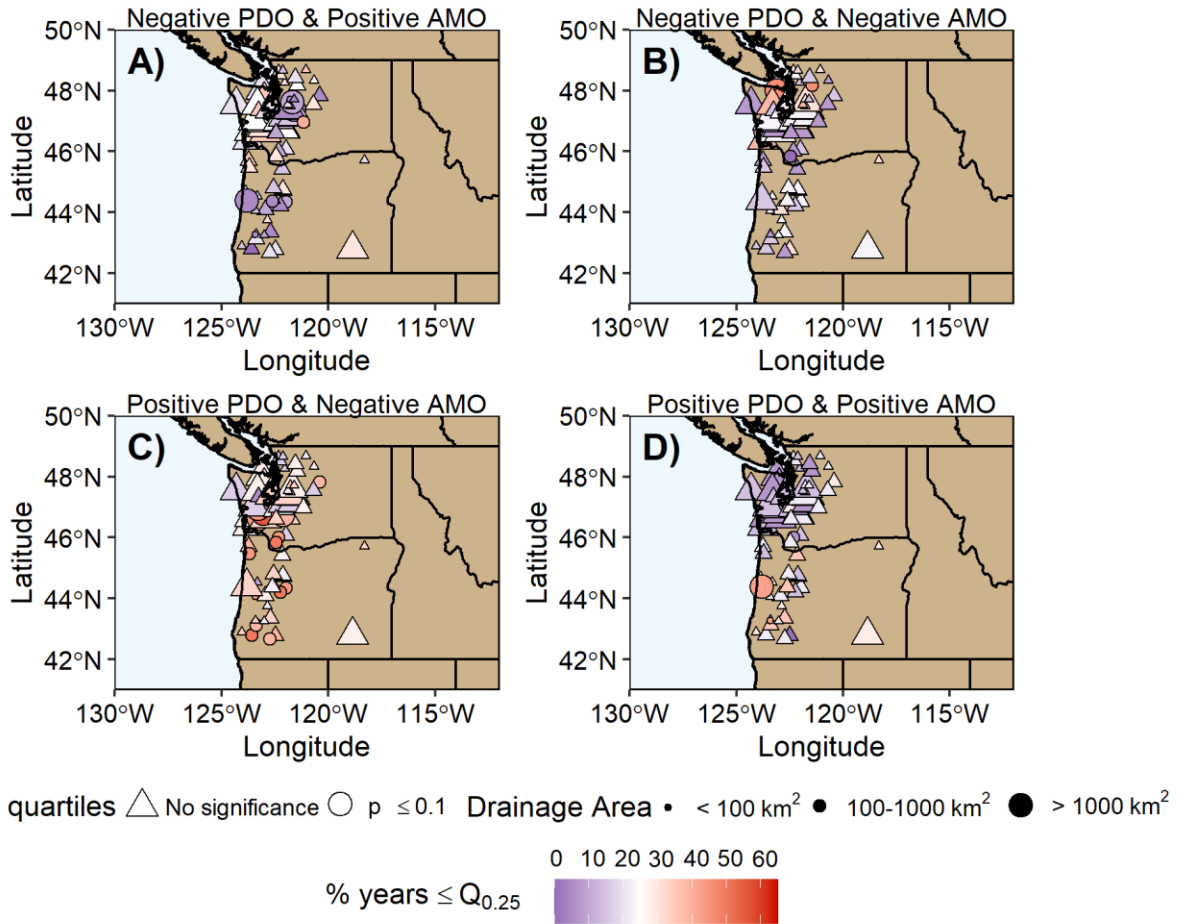


Figure S14. Percentages of lower quartile floods for the four PDO and AMO combinations for the Pacific Northwest: A) negative PDO and positive AMO, 1944-1963; B) negative PDO and negative AMO, 1964-1976; C) positive PDO and negative AMO, 1977-1994; and D) positive PDO and positive AMO, 1995-2008. Significance assessed by permutation tests (10,000 iterations, $p \leq 0.1$).

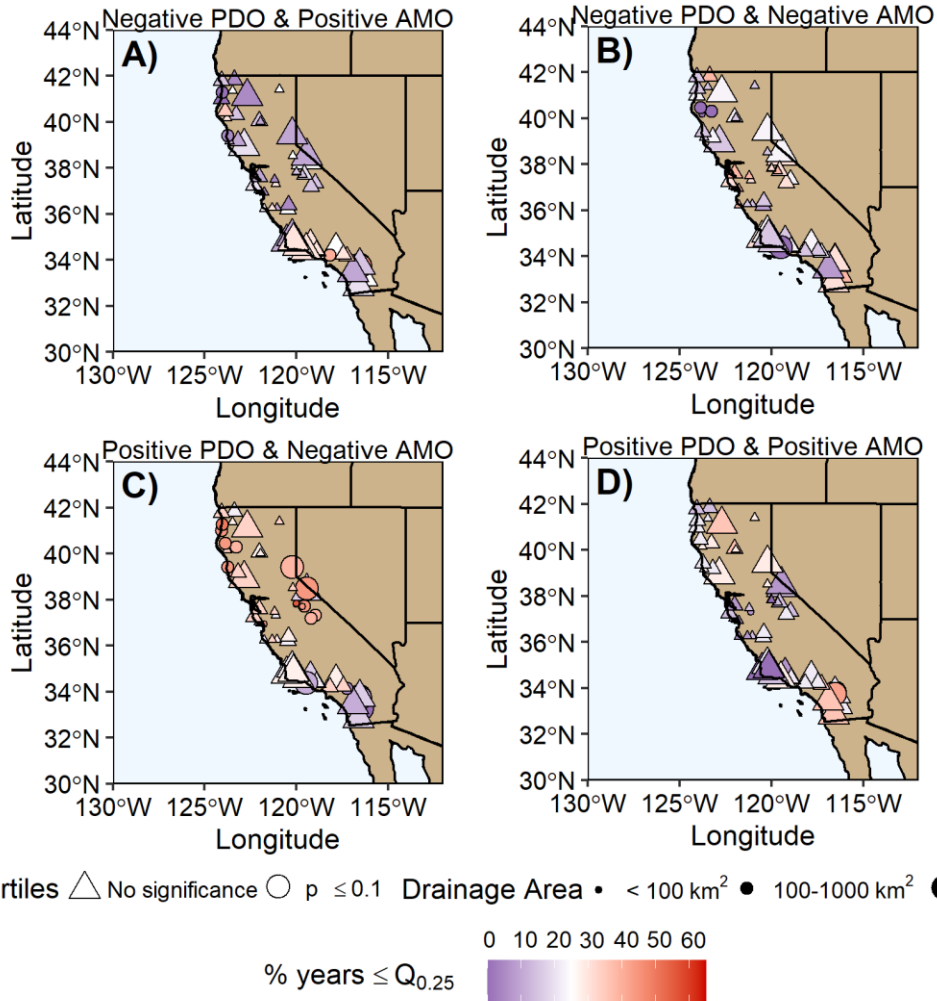


Figure S15. Percentages of lower quartile floods for the four PDO and AMO combinations for California: A) negative PDO and positive AMO, 1944-1963; B) negative PDO and negative AMO, 1964-1976; C) positive PDO and negative AMO, 1977-1994; and D) positive PDO and positive AMO, 1995-2008. Significance assessed by permutation tests (10,000 iterations, $p \leq 0.1$).

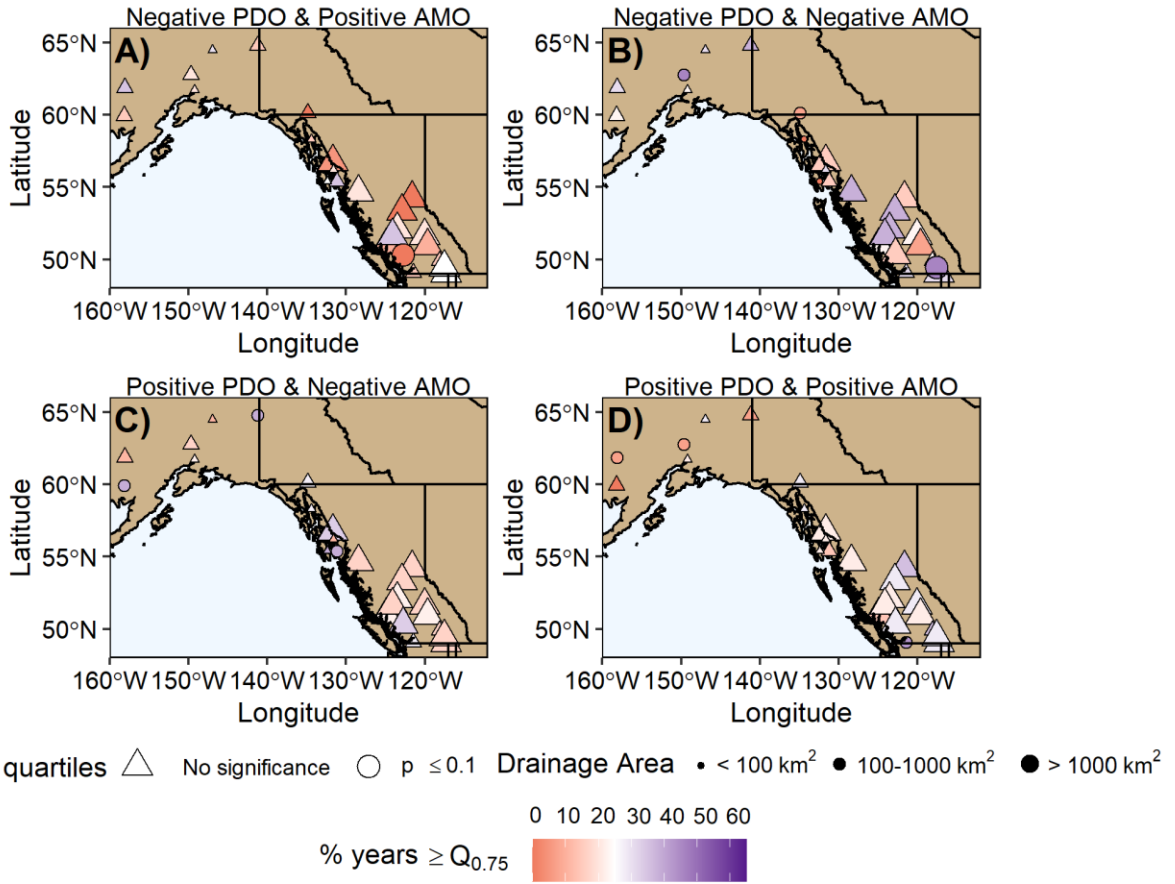


Figure S16. Percentages of upper quartile floods for the four PDO and AMO combinations for the northern region: A) negative PDO and positive AMO, 1944-1963; B) negative PDO and negative AMO, 1964-1976; C) positive PDO and negative AMO, 1977-1994; and D) positive PDO and positive AMO, 1995-2008. Significance assessed by permutation tests (10,000 iterations, $p \leq 0.1$).

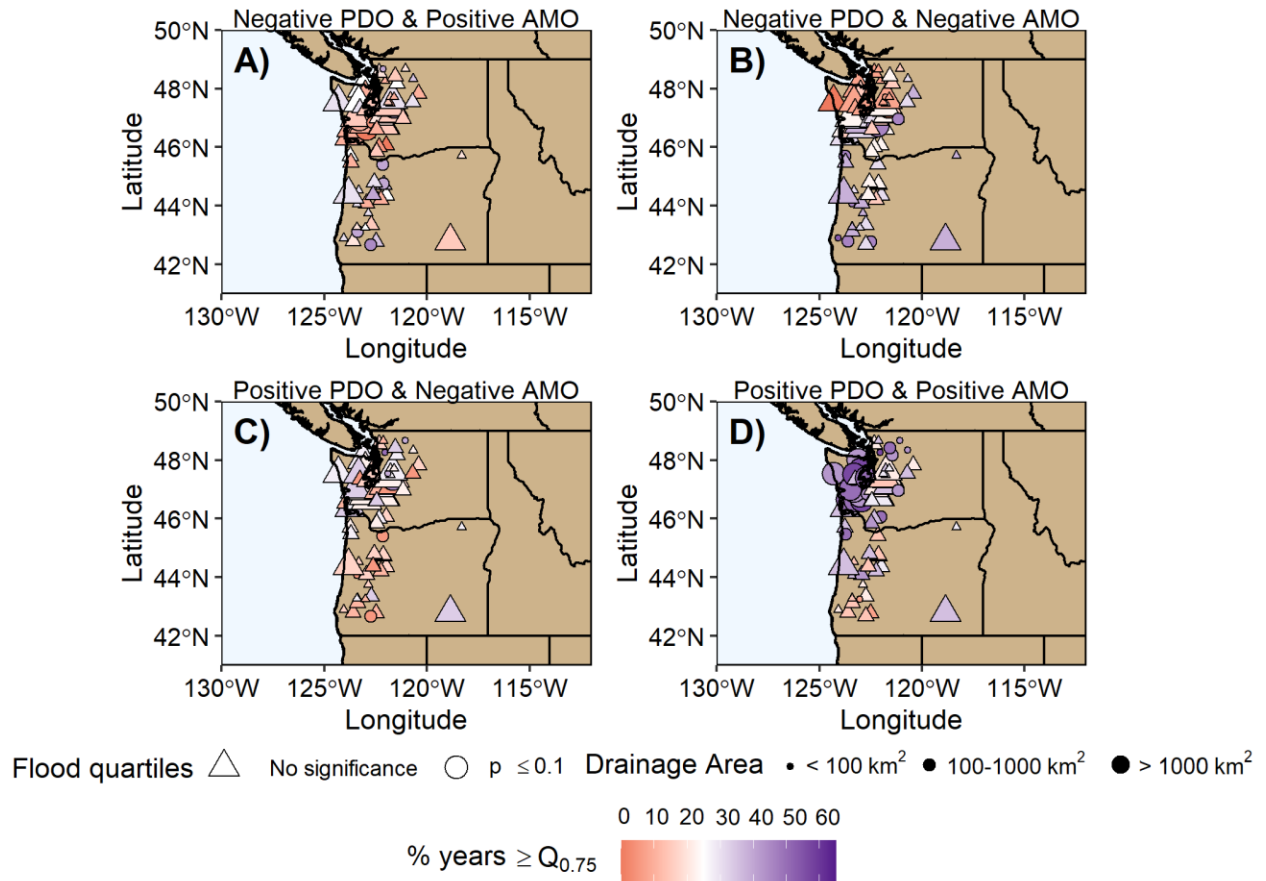


Figure S17. Percentages of upper quartile floods for the four PDO and AMO combinations for the Pacific Northwest: A) negative PDO and positive AMO, 1944-1963; B) negative PDO and negative AMO, 1964-1976; C) positive PDO and negative AMO, 1977-1994; and D) positive PDO and positive AMO, 1995-2008. Significance assessed by permutation tests (10,000 iterations, $p \leq 0.1$).

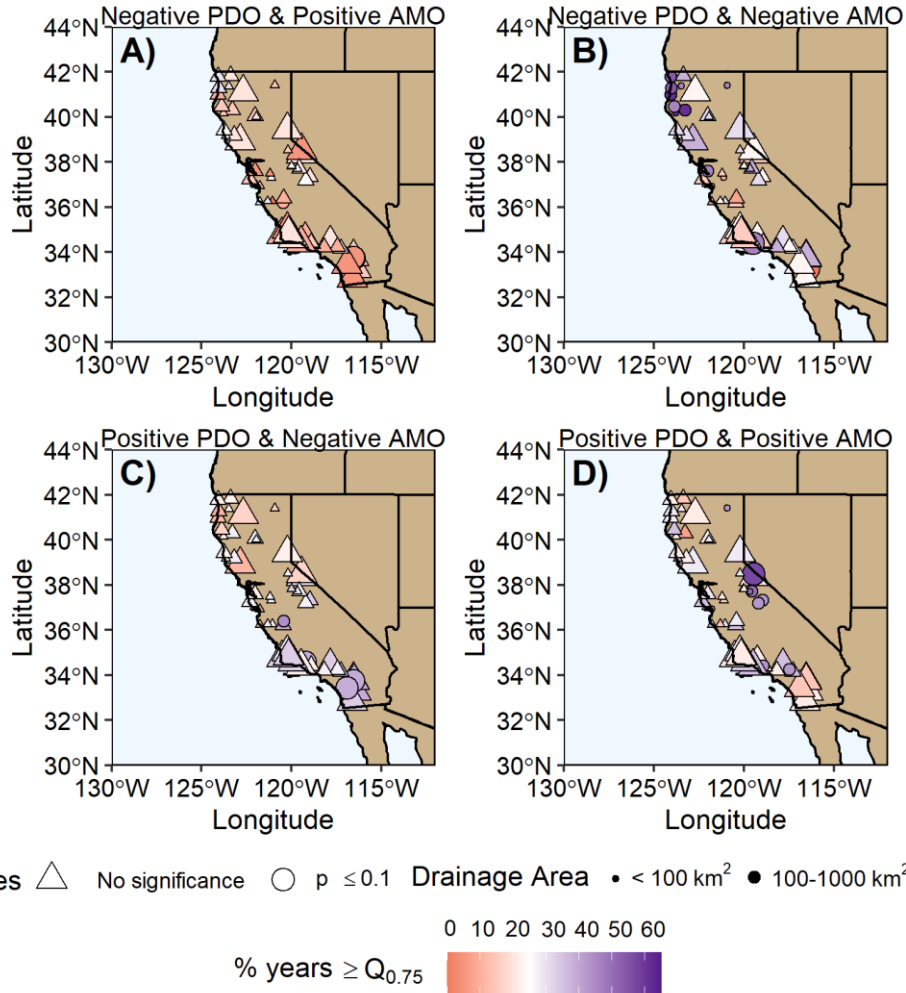


Figure S18. Percentages of upper quartile floods for the four PDO and AMO combinations for California: A) negative PDO and positive AMO, 1944-1963; B) negative PDO and negative AMO, 1964-1976; C) positive PDO and negative AMO, 1977-1994; and D) positive PDO and positive AMO, 1995-2008. Significance assessed by permutation tests (10,000 iterations, $p \leq 0.1$).

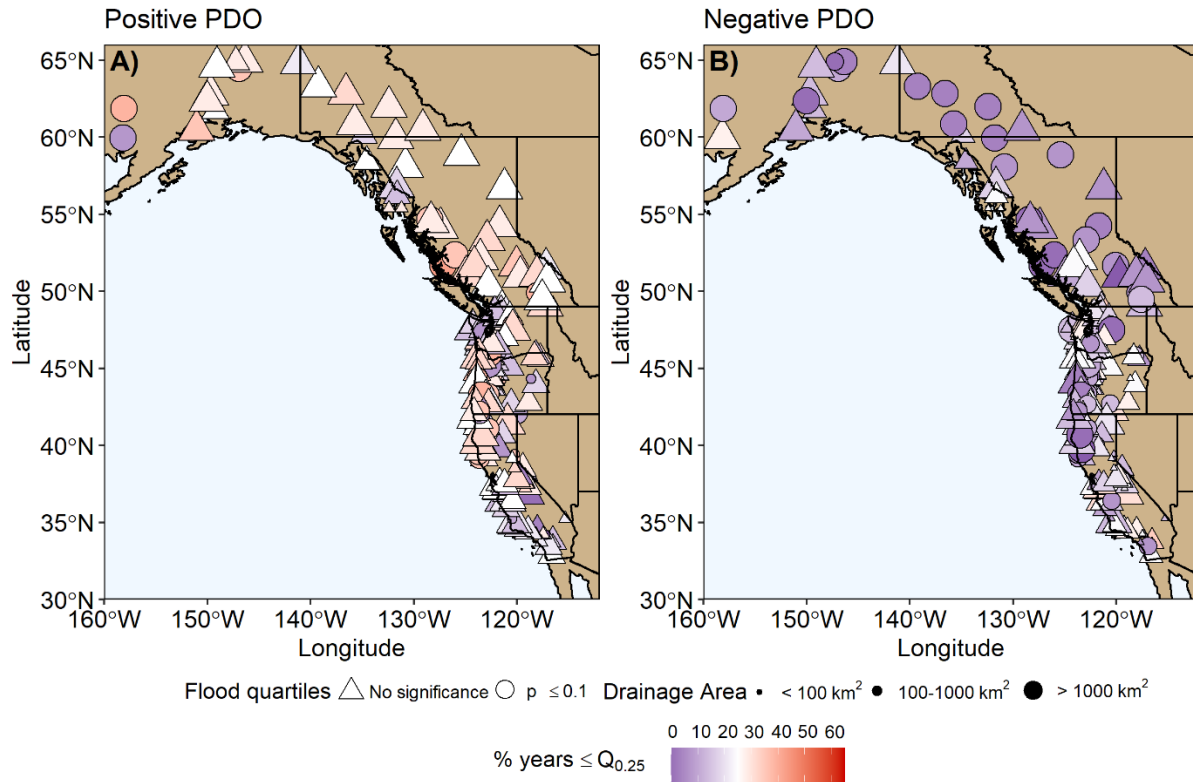


Figure S19. Percentages of lower quartile floods for the two PDO phases for the western North American margin: A) positive PDO, 1977-2008; B) negative PDO, 1944-1976. Significance assessed by permutation tests (10,000 iterations, $p \leq 0.1$).

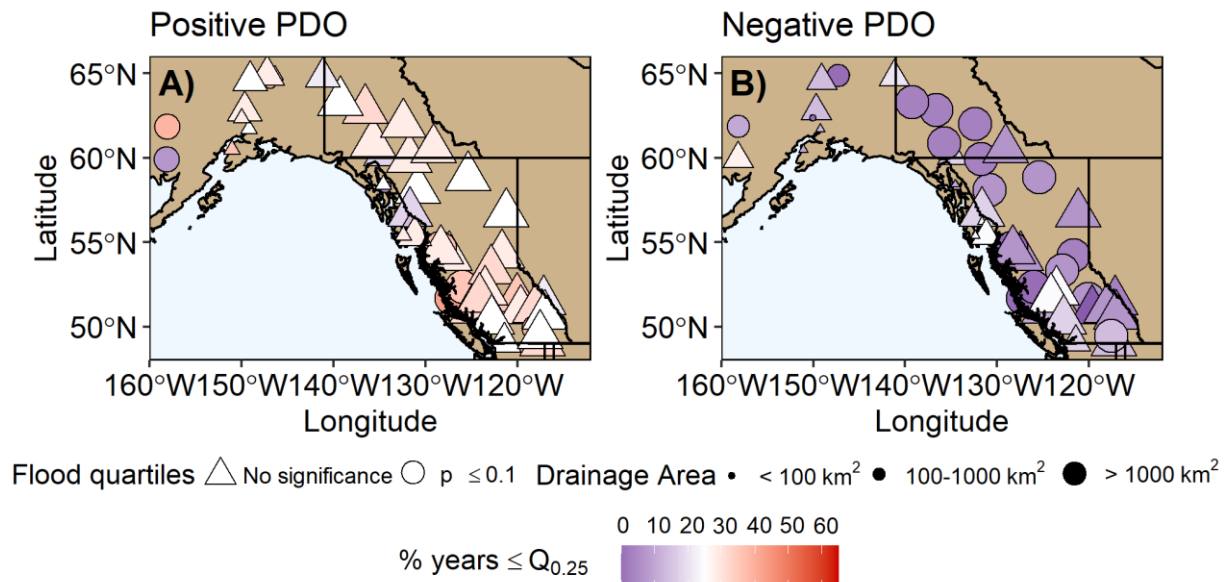


Figure S20. Percentages of lower quartile floods for the two PDO phases for the northern region: A) positive PDO, 1977-2008; B) negative PDO, 1944-1976. Significance assessed by permutation tests (10,000 iterations, $p \leq 0.1$).

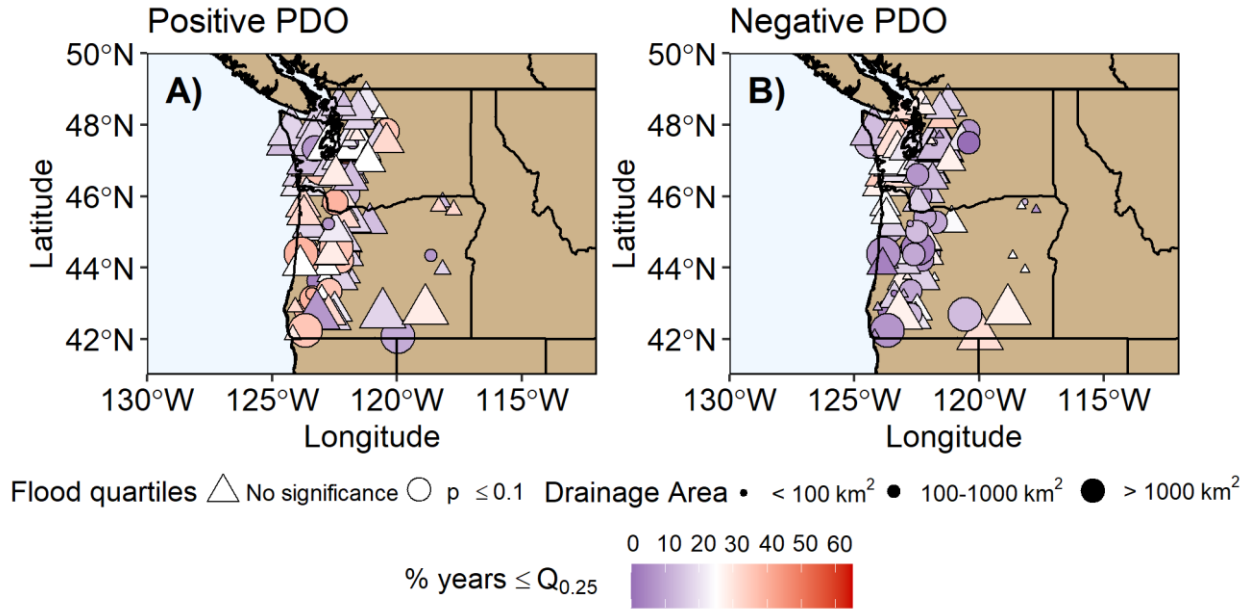


Figure S21. Percentages of lower quartile floods for the two PDO phases for the Pacific Northwest: A) positive PDO, 1977-2008; B) negative PDO, 1944-1976. Significance assessed by permutation tests (10,000 iterations, $p \leq 0.1$).

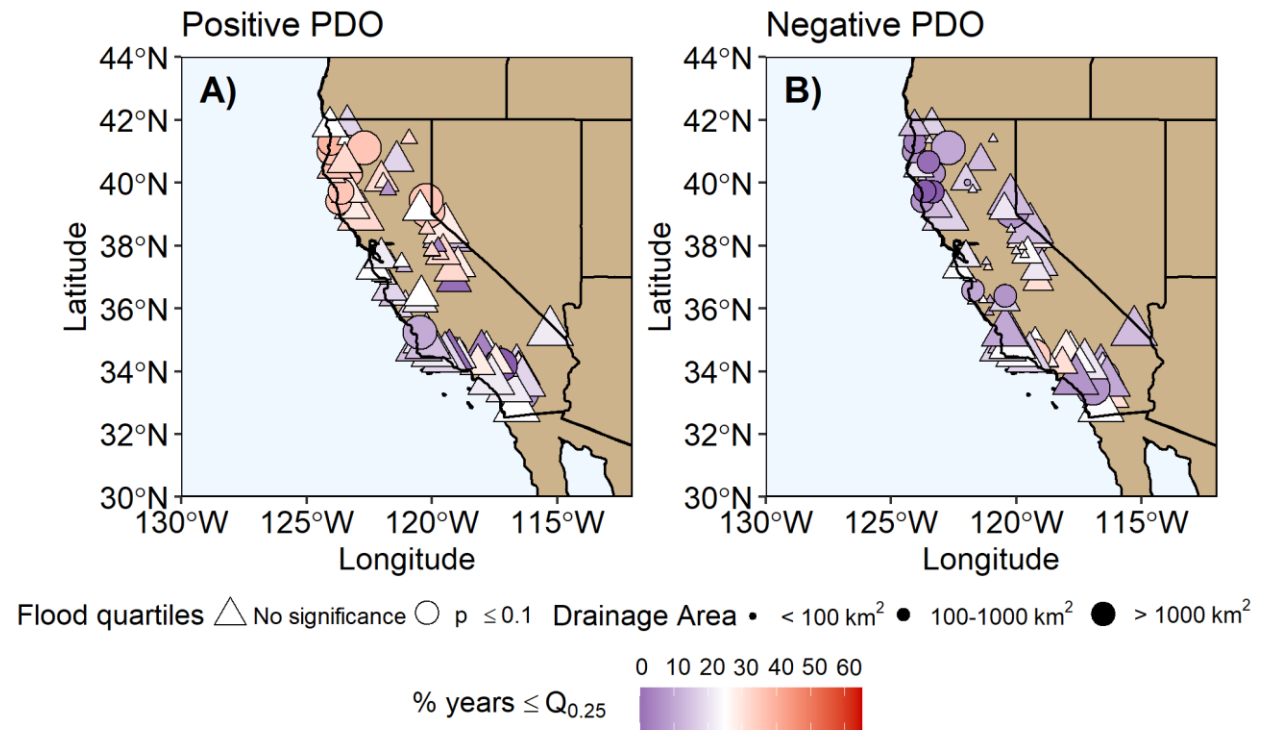


Figure S22. Percentages of lower quartile floods for the two PDO phases for California: A) positive PDO, 1977-2008; B) negative PDO, 1944-1976. Significance assessed by permutation tests (10,000 iterations, $p \leq 0.1$).

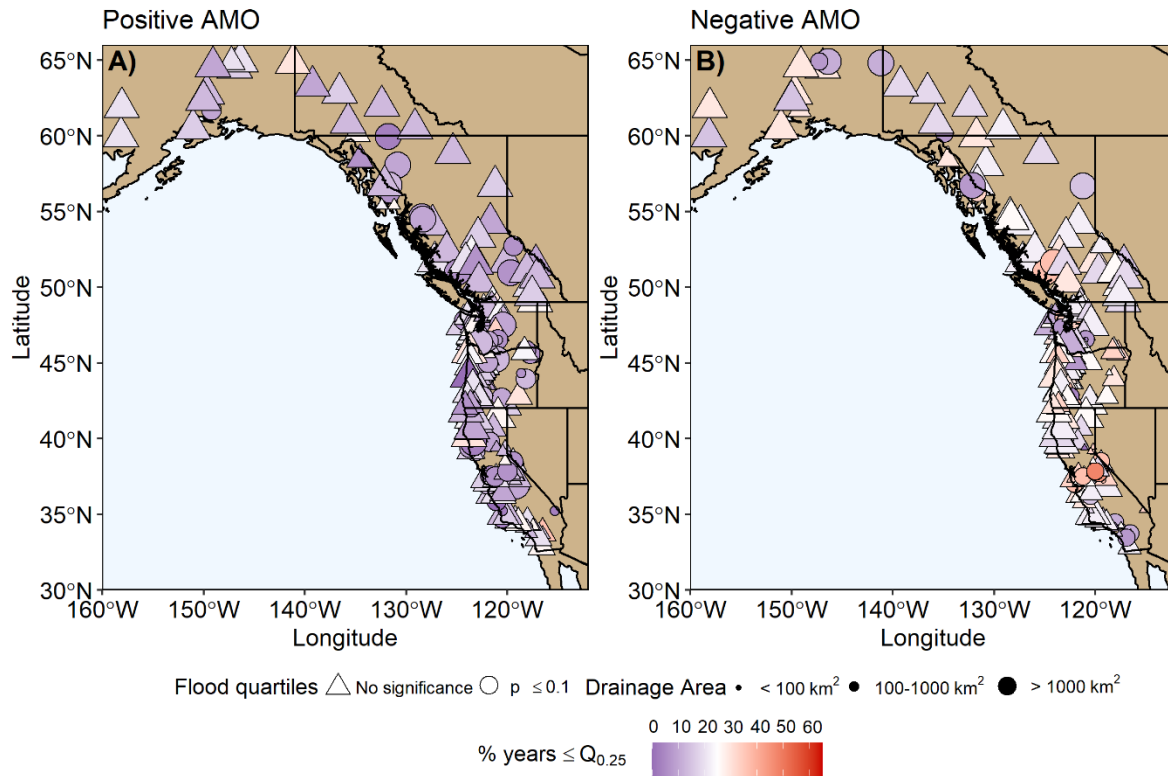


Figure S23. Percentages of lower quartile floods for the two AMO phases for the western North American margin: A) positive AMO, 1944-1963, 1995-2008; B) negative AMO, 1964-1994. Significance assessed by permutation tests (10,000 iterations, $p \leq 0.1$).

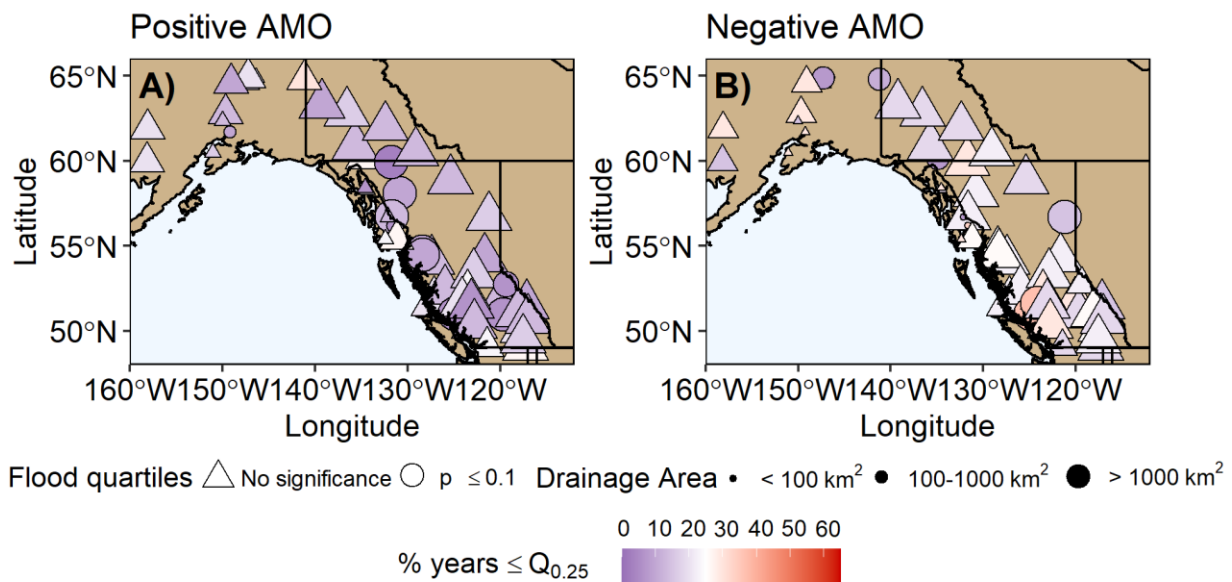
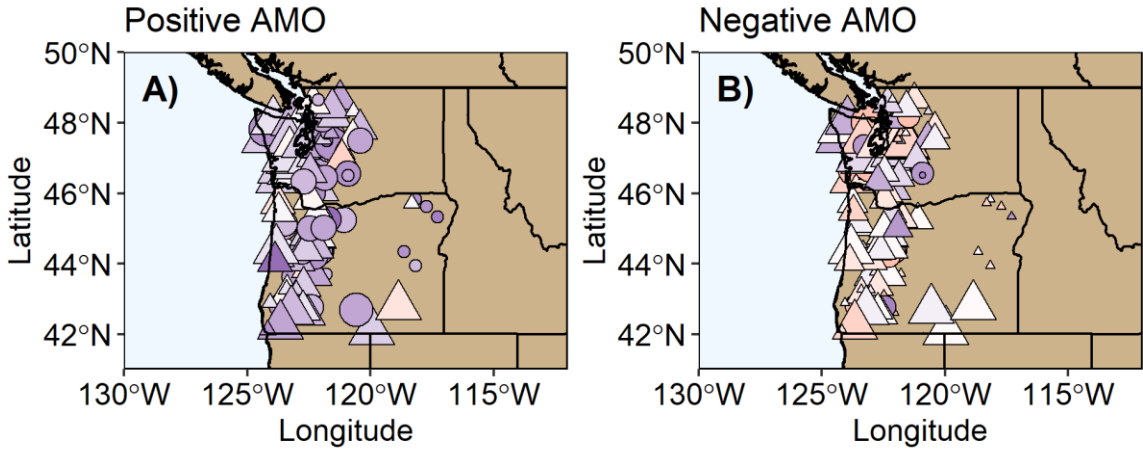


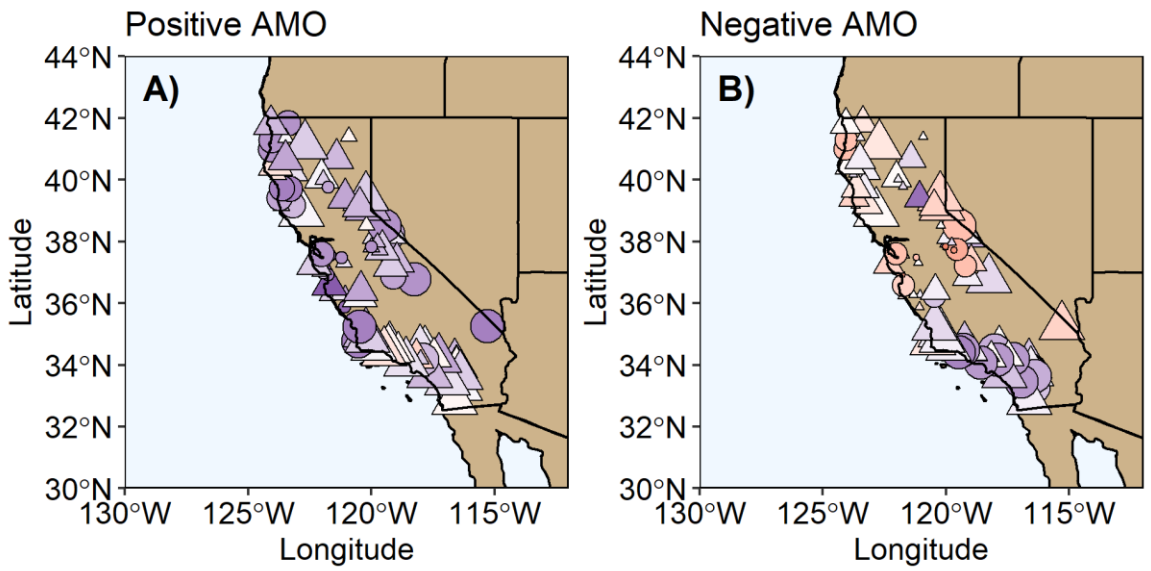
Figure S24. Percentages of lower quartile floods for the two AMO phases for the northern region: A) positive AMO, 1944-1963, 1995-2008; B) negative AMO, 1964-1994. Significance assessed by permutation tests (10,000 iterations, $p \leq 0.1$).



Flood quartiles \triangle No significance \circ $p \leq 0.1$ Drainage Area \bullet $< 100 \text{ km}^2$ \bullet $100\text{-}1000 \text{ km}^2$ \bullet $> 1000 \text{ km}^2$

0 10 20 30 40 50 60
% years $\leq Q_{0.25}$

Figure S25. Percentages of lower quartile floods for the two AMO phases for the Pacific Northwest: A) positive AMO, 1944-1963, 1995-2008; B) negative AMO, 1964-1994. Significance assessed by permutation tests (10,000 iterations, $p \leq 0.1$).



Flood quartiles \triangle No significance \circ $p \leq 0.1$ Drainage Area \bullet $< 100 \text{ km}^2$ \bullet $100\text{-}1000 \text{ km}^2$ \bullet $> 1000 \text{ km}^2$

0 10 20 30 40 50 60
% years $\leq Q_{0.25}$

Figure S26. Percentages of lower quartile floods for the two AMO phases for California: A) positive AMO, 1944-1963, 1995-2008; B) negative AMO, 1964-1994. Significance assessed by permutation tests (10,000 iterations, $p \leq 0.1$).

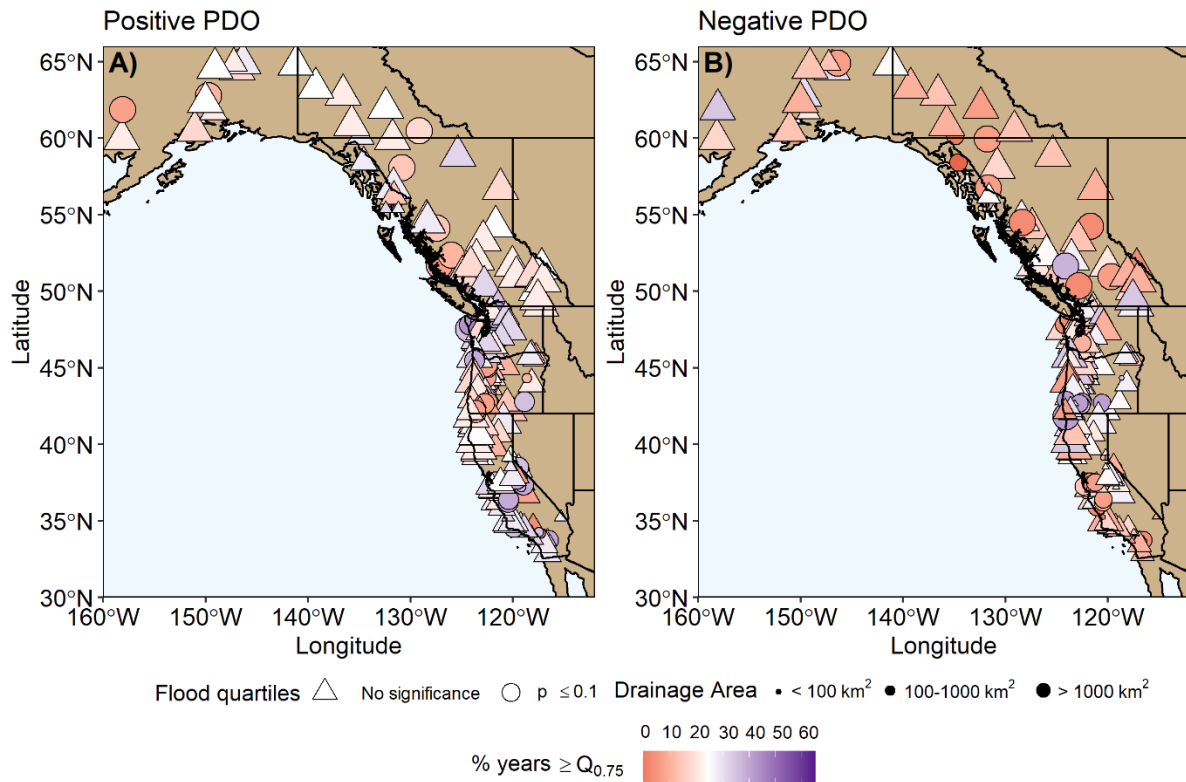


Figure S27. Percentages of upper quartile floods for the two PDO phases for the western North American margin: A) positive PDO, 1977-2008; B) negative PDO, 1944-1976. Significance assessed by permutation tests (10,000 iterations, $p \leq 0.1$).

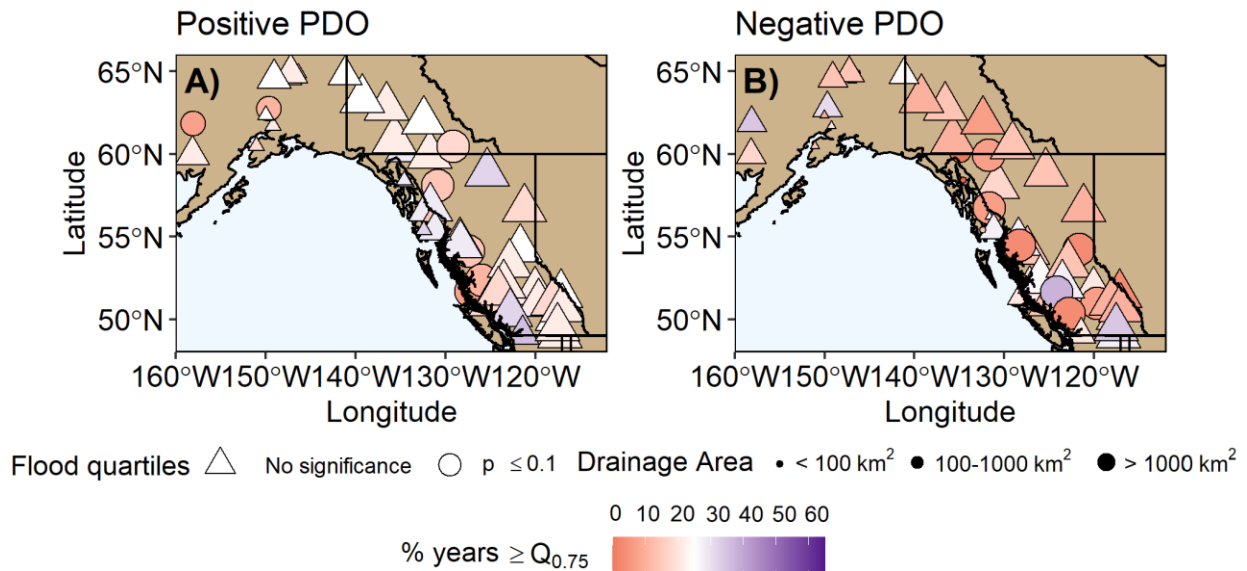


Figure S28. Percentages of upper quartile floods for the two PDO phases for the northern region: A) positive PDO, 1977-2008; B) negative PDO, 1944-1976. Significance assessed by permutation tests (10,000 iterations, $p \leq 0.1$).

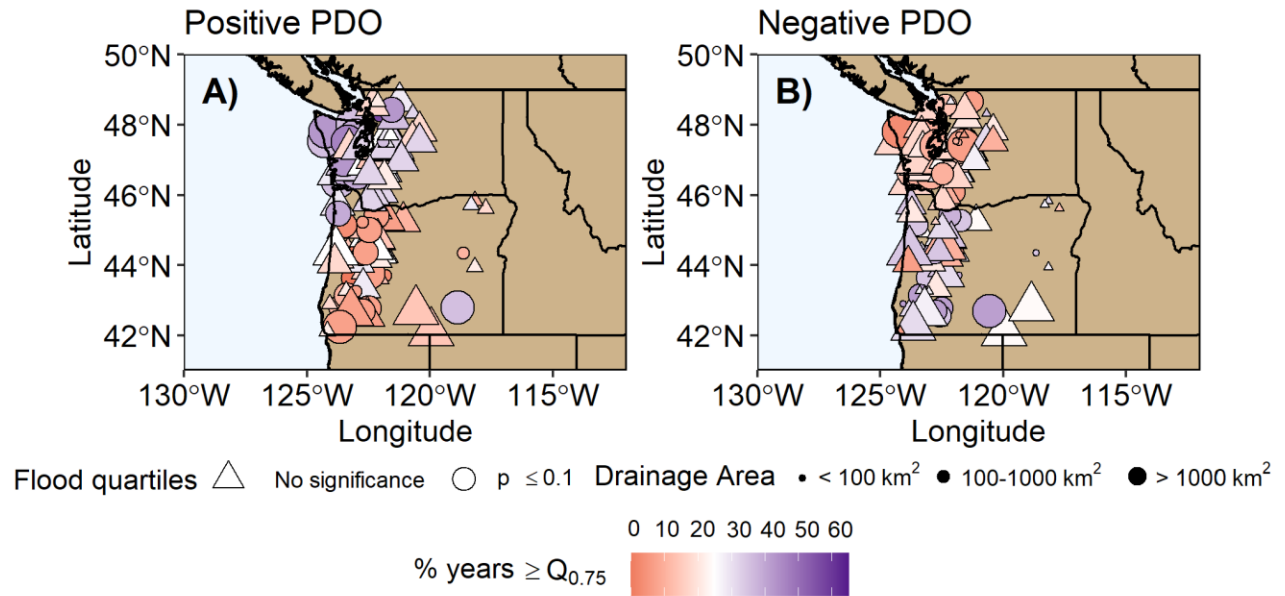


Figure S29. Percentages of upper quartile floods for the two PDO phases for the Pacific Northwest: A) positive PDO, 1977-2008; B) negative PDO, 1944-1976. Significance assessed by permutation tests (10,000 iterations, $p \leq 0.1$).

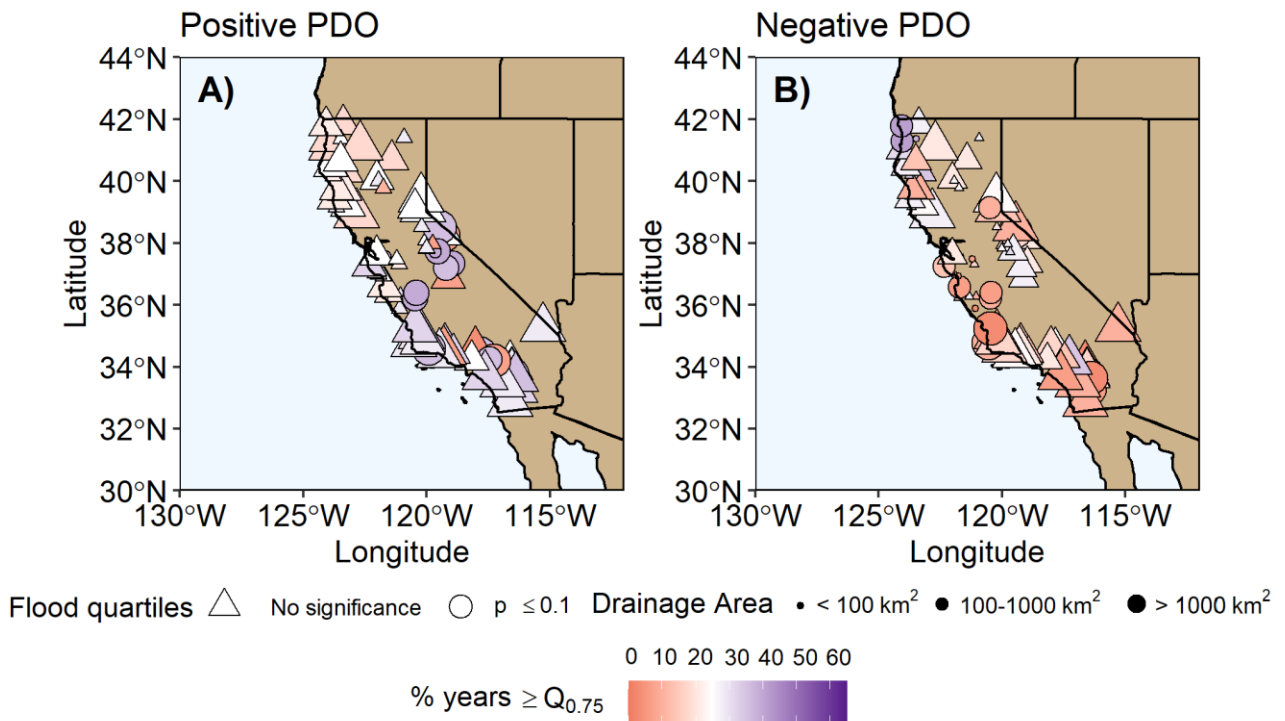


Figure S30. Percentages of upper quartile floods for the two PDO phases for California: A) positive PDO, 1977-2008; B) negative PDO, 1944-1976. Significance assessed by permutation tests (10,000 iterations, $p \leq 0.1$).

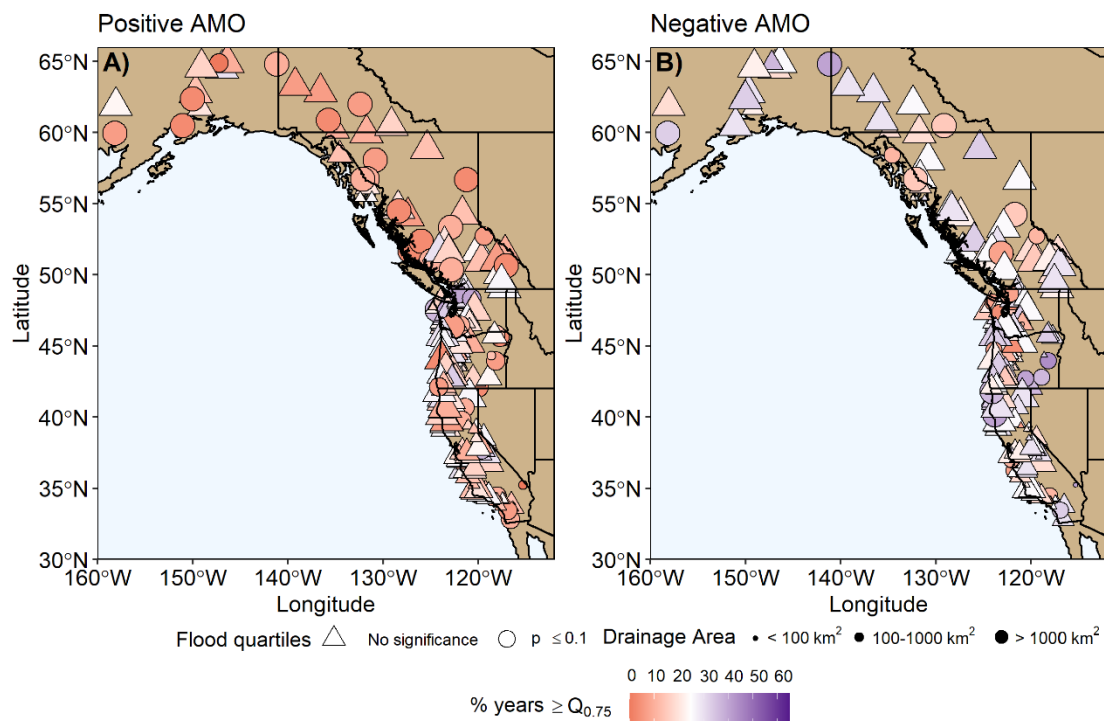


Figure S31. Percentages of upper quartile floods for the two AMO phases for the North American margin: A) positive AMO, 1944-1963, 1995-2008; B) negative AMO, 1964-1994. Significance assessed by permutation tests (10,000 iterations, $p \leq 0.1$).

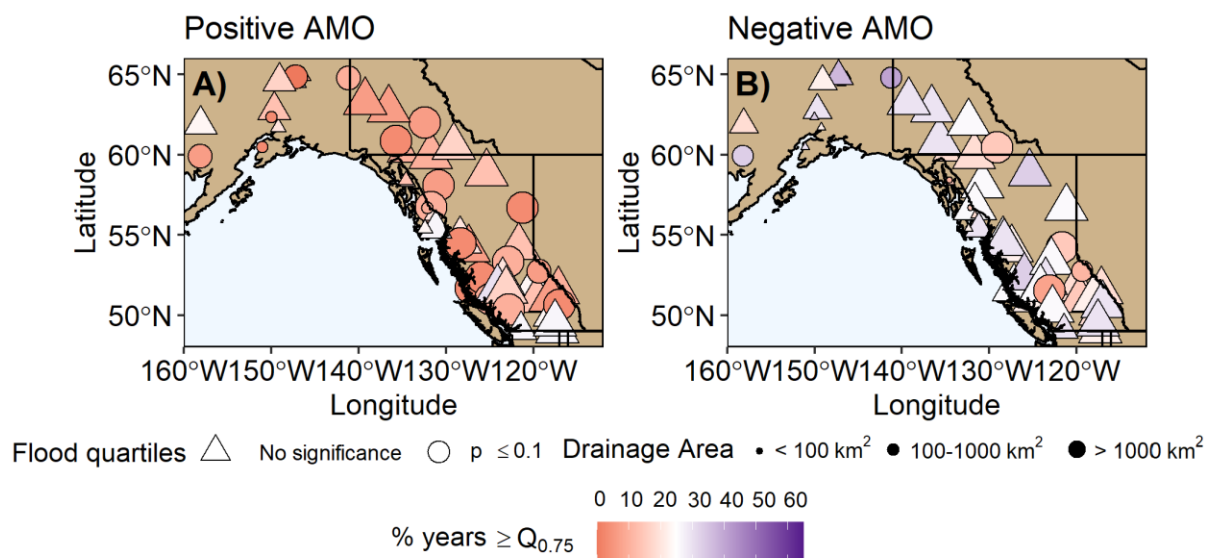


Figure S32. Percentages of upper quartile floods for the two AMO phases for the northern region: A) positive AMO, 1944-1963, 1995-2008; B) negative AMO, 1964-1994. Significance assessed by permutation tests (10,000 iterations, $p \leq 0.1$).

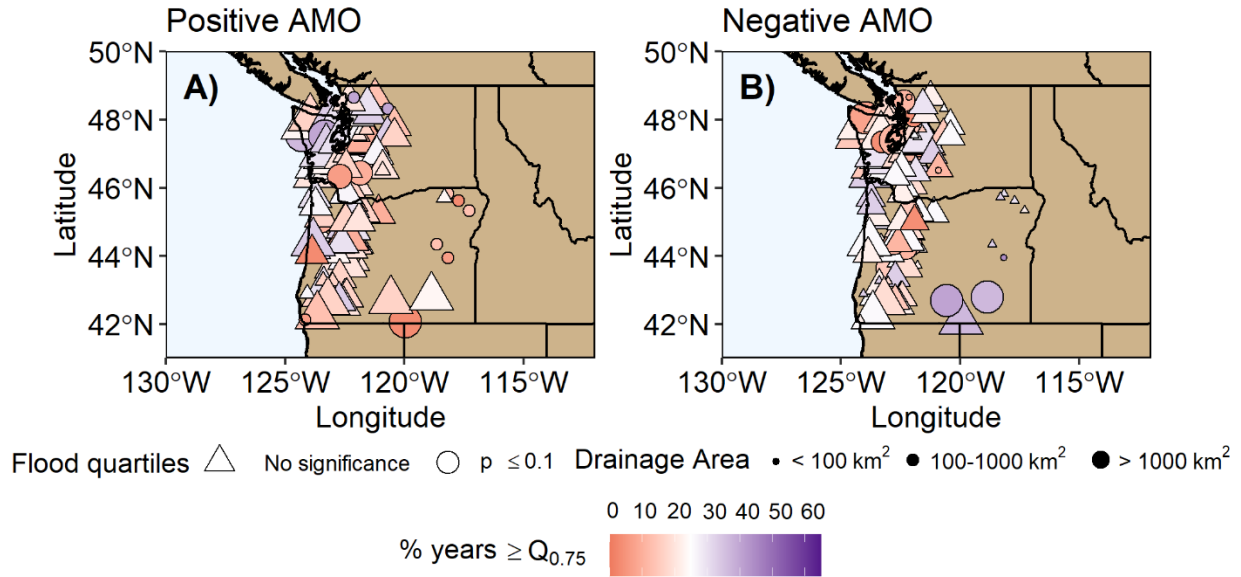


Figure S33. Percentages of upper quartile floods for the two AMO phases for the Pacific Northwest: A) positive AMO, 1944-1963, 1995-2008; B) negative AMO, 1964-1994. Significance assessed by permutation tests (10,000 iterations, $p \leq 0.1$).

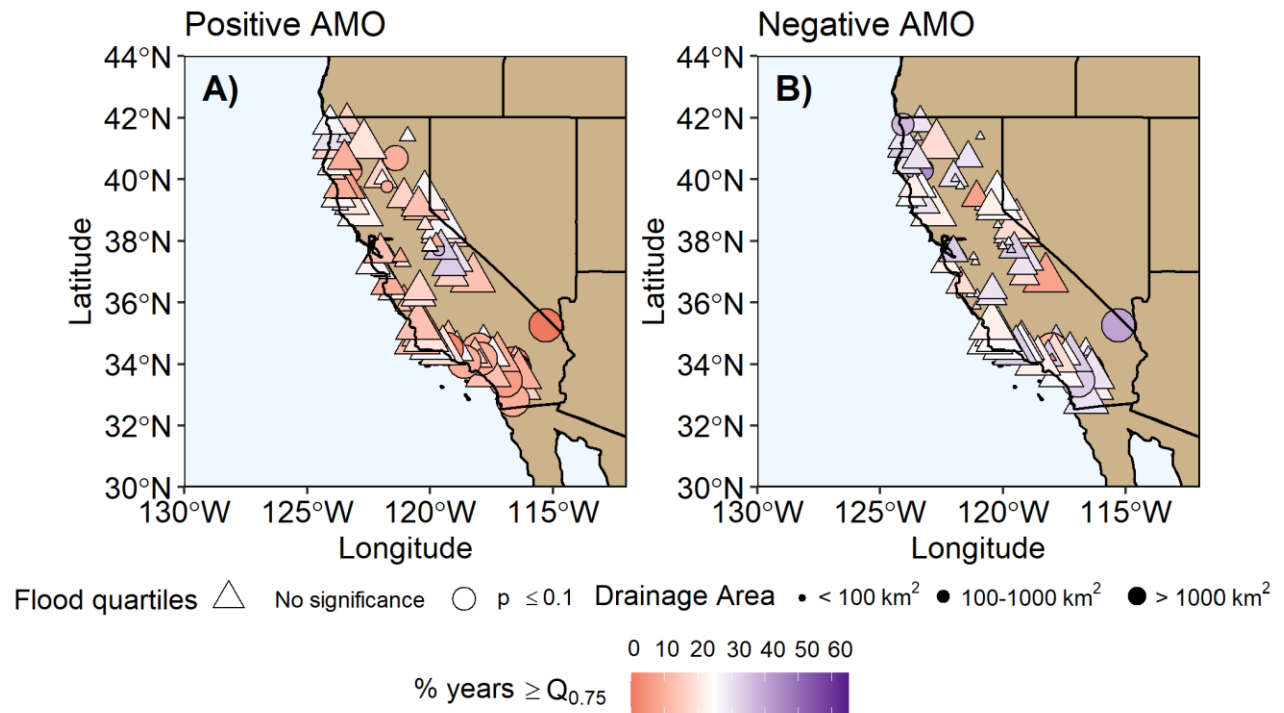


Figure S34. Percentages of upper quartile floods for the two AMO phases for California: A) positive AMO, 1944-1963, 1995-2008; B) negative AMO, 1964-1994. Significance assessed by permutation tests (10,000 iterations, $p \leq 0.1$).

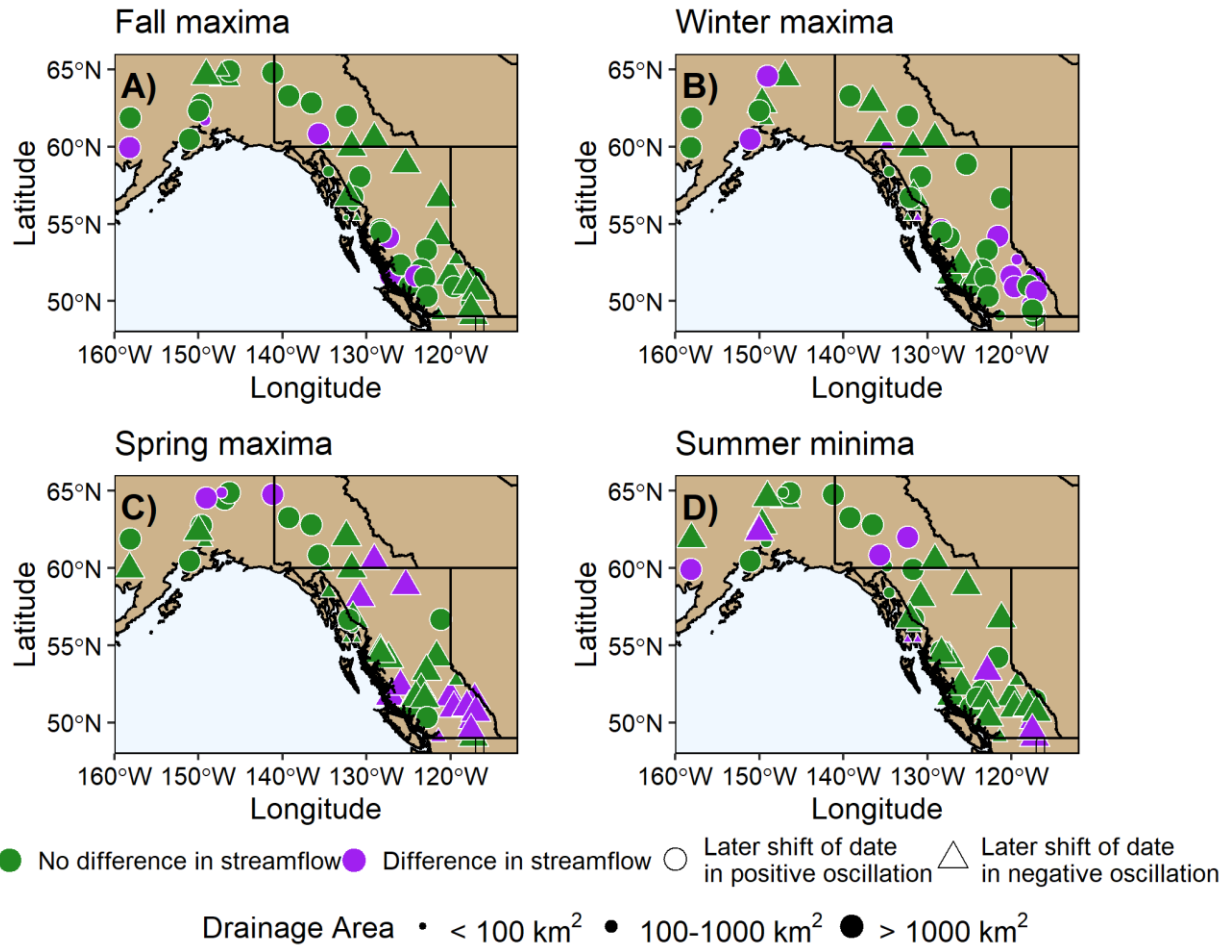


Figure S35. Differences in the Julian dates of the seasonal streamflow extremes according to the PDO phase in the northern region for: A) fall maxima, B) winter maxima, C) spring maxima, and D) summer minima ($p \leq 0.1$).

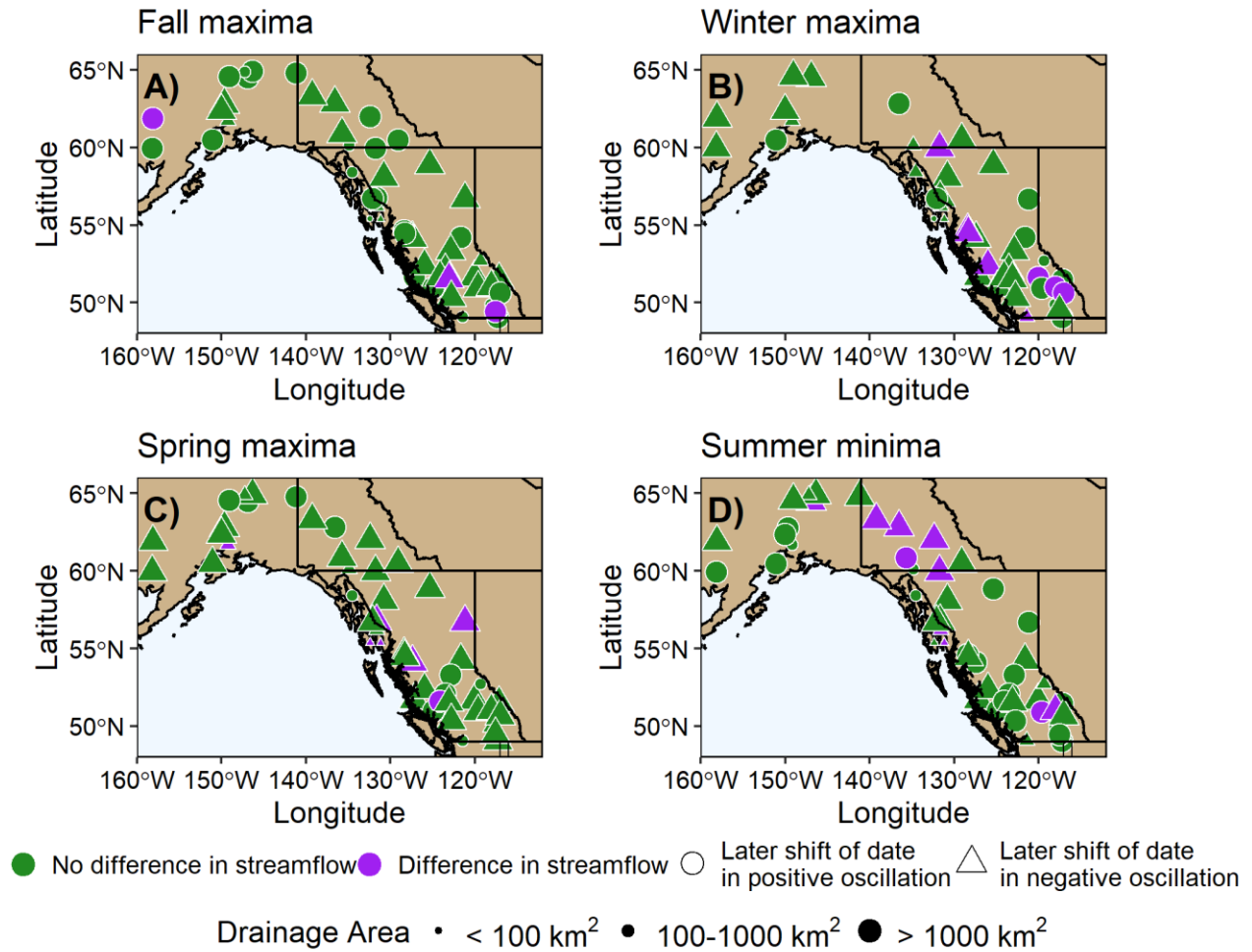


Figure S36. Differences in the Julian dates of the seasonal streamflow extremes according to AMO phase in the northern region for: A) fall maxima, B) winter maxima, C) spring maxima, and D) summer minima ($p \leq 0.1$).

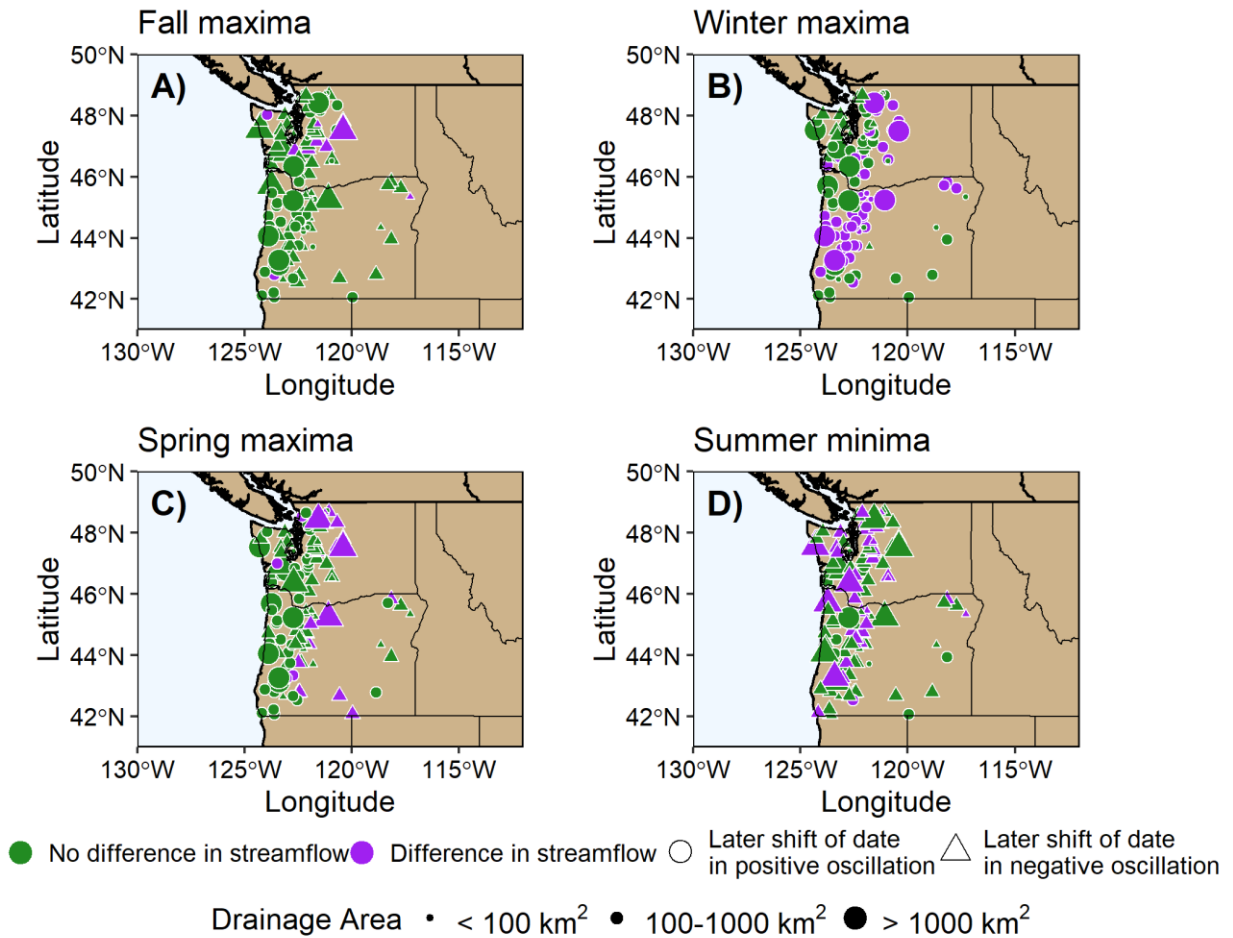


Figure S37. Differences in the dates of the seasonal streamflow extremes according to the PDO phase in the Pacific Northwest for: A) fall maxima, B) winter maxima, C) spring maxima, and D) summer minima ($p \leq 0.1$).

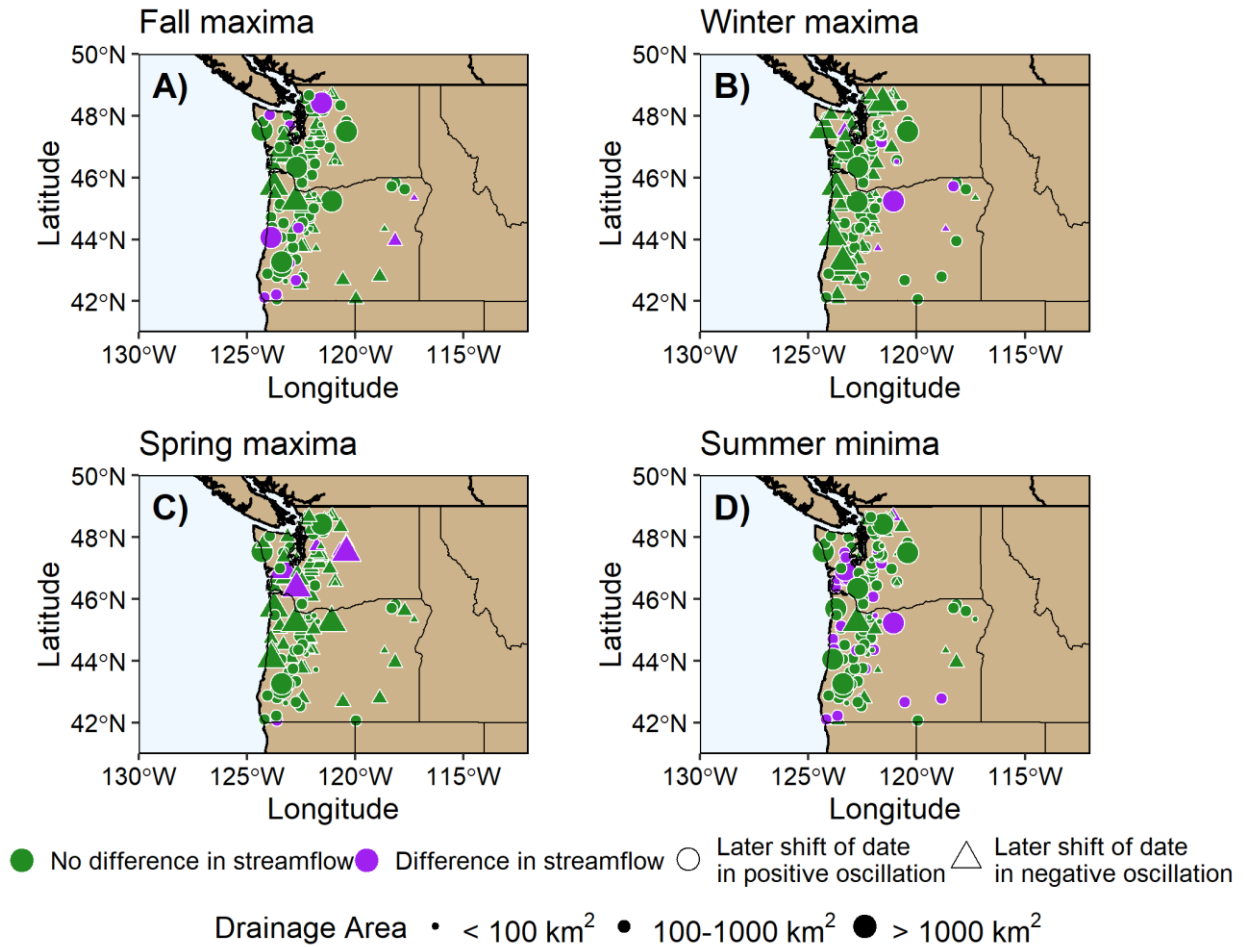
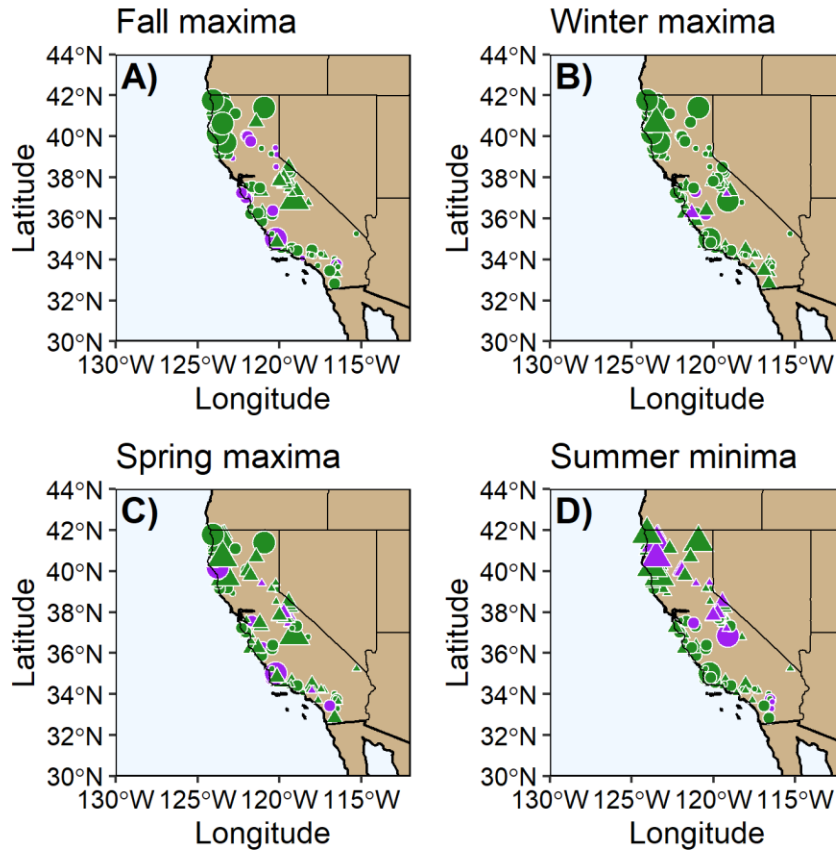


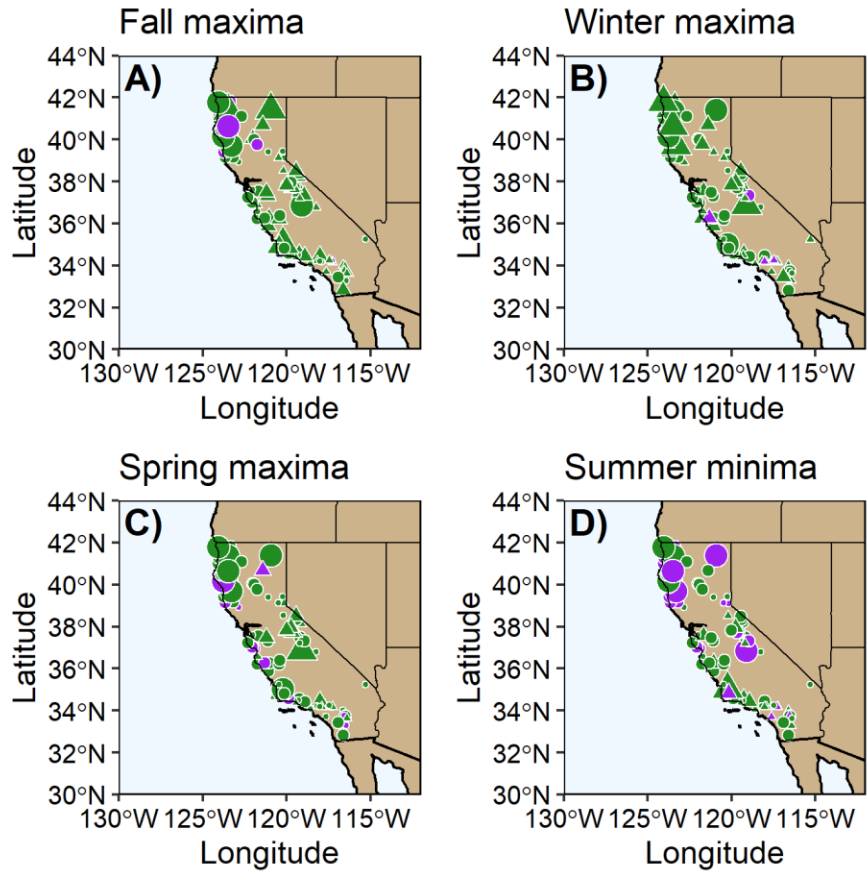
Figure S38. Differences in the dates of the seasonal streamflow extremes according to AMO phase in the Pacific Northwest for: A) fall maxima, B) winter maxima, C) spring maxima, and D) summer minima ($p \leq 0.1$).



● No difference in streamflow ● Difference in streamflow ○ Later shift of date in positive oscillation △ Later shift of date in negative oscillation

Drainage Area • <math>< 100 \text{ km}^2</math> • $100\text{-}1000 \text{ km}^2$ ● $> 1000 \text{ km}^2$

Figure S39. Differences in the dates of the seasonal streamflow extremes according to PDO phase in California for: A) fall maxima, B) winter maxima, C) spring maxima, and D) summer minima ($p \leq 0.1$).



● No difference in streamflow ● Difference in streamflow ○ Later shift of date in positive oscillation △ Later shift of date in negative oscillation
 Drainage Area • < 100 km² • 100-1000 km² ● > 1000 km²

Figure S40. Differences in the Julian dates of the seasonal streamflow extremes according to AMO phase in California for: A) fall maxima, B) winter maxima, C) spring maxima, and D) summer minima ($p \leq 0.1$).

SUPPLEMENTARY TABLES

Table S1. List of the 250 streamflow gauges from the U.S. Geological Survey and the Canadian Hydrometric Database (Water Survey of Canada) with their station number, location (AK = Alaska, BC = British Columbia, CA = California, OR = Oregon, WA = Washington, YT = Yukon), latitude (°N), longitude (°E), drainage area (km²), number of years in record, and elevation from the stream gauge (m). Station records compiled from 1900-2017, inclusively.

ID	Station Name	Location	Latitude	Longitude	Drainage Area	Number of years	Elevation
07FC003	Blueberry River below Aitken Creek	BC	56.68	-121.22	1770	47	1041
08CD001	Tuya River near Telegraph Creek	BC	58.07	-130.82	3550	52	716
08CG001	Iskut River below Johnson River	BC	56.74	-131.67	9500	55	412
08ED002	Morice River near Houston	BC	54.12	-127.42	1900	52	1179
08EF001	Skeena River at Usk	BC	54.63	-128.43	42300	64	505
08EF005	Zymoetz River above O.K. Creek	BC	54.48	-128.33	2850	52	937
08FA002	Wannock River at Outlet of Owikeno Lake	BC	51.68	-127.18	3900	55	453
08FB006	Atnarko River near the mouth	BC	52.36	-126.01	2550	46	623
08GD004	Homathko River at the mouth	BC	50.99	-124.92	5680	57	467
08KB003	McGregor River at Lower Canyon	BC	54.23	-121.67	4780	54	1046
08KG001	West Road River near Cinema	BC	53.31	-122.89	12400	56	1058
08LA001	Clearwater River near Clearwater Station	BC	51.65	-120.07	10300	62	854
08LD001	Adams River near Squilax	BC	50.94	-119.66	3210	44	853
08MA001	Chilko River near Redstone	BC	52.07	-123.54	6880	81	1204
08MA002	Chilko River at Outlet of Chilko Lake	BC	51.62	-124.14	2130	80	1619
08MB006	Big Creek above Groundhog Creek	BC	51.52	-123.12	1010	40	1755
08MG005	Lillooet River near Pemberton	BC	50.34	-122.80	2100	54	669
08MH016	Chilliwack River at Outlet of Chilliwack Lake	BC	49.08	-121.46	335	81	1093
08NB005	Columbia River at Donald	BC	51.48	-117.18	9700	48	1214
08NC004	Canoe River below Kimmel Creek	BC	52.73	-119.38	305	41	1395
08ND013	Illecillewaet River at Greely	BC	51.01	-118.08	1150	53	959
08NE074	Salmo River near Salmo	BC	49.05	-117.29	1240	66	1071
08NE077	Barnes Creek near Needles	BC	49.91	-118.13	204	62	1048
08NH016	Duck Creek near Wynndel	BC	49.20	-116.53	57	44	1199
08NH119	Duncan River below B.B. Creek	BC	50.64	-117.05	1310	54	1056
08NJ013	Slocan River near Crescent Valley	BC	49.46	-117.56	3330	83	963
09AA012	Wheaton River near Carcross	YT	60.13	-134.88	864	54	1010
09AC001	Takhini River near Whitehorse	YT	60.85	-135.74	7050	50	1001
09AE003	Swift River near Swift River	BC	59.93	-131.77	3390	50	1150
09BA001	Ross River at Ross River	YT	61.99	-132.41	7310	46	997
09BC001	Pelly River at Pelly Crossing	YT	62.83	-136.58	48900	53	1077
09DD003	Stewart River at the mouth	YT	63.28	-139.25	51000	50	643

ID	Station Name	Location	Latitude	Longitude	Drainage Area	Number of years	Elevation
10AB001	Frances River near Watson Lake	YT	60.47	-129.12	12800	52	1033
10BE004	Toad River above Nonda Creek	BC	58.86	-125.38	2540	55	1083
9423350	Caruthers Creek near Ivanpah	CA	35.25	-115.30	2	54	1719.1
10255810	Borrego Palm Creek near Borrego Springs	CA	33.28	-116.43	56	55	393.2
10257600	Mission Creek near Desert Hot Springs	CA	34.01	-116.63	91	50	577.3
10258000	Tahquitz Creek near Palm Springs	CA	33.81	-116.56	43	69	232.4
10258500	Palm Canyon Creek near Palm Springs	CA	33.75	-116.53	238	83	213.4
10259000	Andreas Creek near Palm Springs	CA	33.76	-116.55	22	69	243.8
10259200	Deep Creek near Palm Desert	CA	33.63	-116.39	78	56	438.9
10263500	Big Rock Creek near Valyermo	CA	34.42	-117.84	59	95	1234.4
10264000	Little Rock Creek above Little Rock Reservoir near Littlerock	CA	34.46	-118.02	125	51	1008.9
10281800	Independence Creek below Pinyon Creek near Independence	CA	36.78	-118.26	46	56	2186
10291500	Buckeye Creek near Bridgeport	CA	38.24	-119.33	113	46	47
10295500	Little Walker River near Bridgeport	CA	38.36	-119.44	162	55	2069.6
10296500	West Walker River near Coleville	CA	38.51	-119.45	640	92	1682.5
10336660	Blackwood Creek near Tahoe City	CA	39.11	-120.16	29	57	1900
10343500	Sagehen Creek near Truckee	CA	39.43	-120.24	27	64	1926.3
10366000	Twenty-mile Creek near Adel	CA	42.07	-119.96	497	61	1390.1
10384000	Chewaucan River near Paisley	CA	42.68	-120.57	704	77	1350.3
10396000	Donner Under Blitzen River near Frenchglen	CA	42.79	-118.87	512	91	1296.6
11015000	Sweetwater River near Descanso	CA	32.83	-116.62	116	83	996.5
11042400	Temecula Creek near Aguanga	CA	33.45	-116.92	335	60	484.6
11058500	East Twin Creek near Arrowhead Springs	CA	34.17	-117.26	23	93	484.6
11058600	Waterman Canyon Creek near Arrowhead Springs	CA	34.19	-117.27	12	78	560.8
11063500	Lone Pine Creek near Keenbrook	CA	34.25	-117.46	39	78	794.3
11075800	Santiago Creek at Modjeska	CA	33.70	-117.63	32	56	408.4
11084500	Fish Creek near Duarte	CA	34.17	-117.92	16	59	276.1
11098000	Arroyo Seco near Pasadena	CA	34.22	-118.18	41	103	426.1
11100000	Santa Anita Creek near Sierra Madre	CA	34.19	-118.02	25	54	449.7
11104000	Topanga Creek near Topanga Beach	CA	34.06	-118.59	46	49	81
11111500	Sespe Creek near Wheeler Springs	CA	34.57	-119.26	127	64	1085.1
11113000	Sespe Creek near Fillmore	CA	34.43	-118.93	645	79	172.2
11116000	North Fork Matilija Creek at Matilija Hot Springs	CA	34.49	-119.31	40	50	348.1
11119500	Carpinteria Creek near Carpinteria	CA	34.40	-119.49	34	76	39.6
11124500	Santa Cruz Creek near Santa Ynez	CA	34.58	-119.91	189	75	238.8

ID	Station Name	Location	Latitude	Longitude	Drainage Area	Number of years	Elevation
11136100	San Antonio Creek near Casmalia	CA	34.77	-120.53	346	50	37.5
11136800	Cuyama River below Buckhorn Canyon near Santa Maria	CA	35.02	-120.23	2268	60	868
11138500	Sisquoc River near Sisquoc	CA	34.83	-120.17	719	71	190.3
11141280	Lopez Creek near Arroyo Grande	CA	35.24	-120.47	54	51	176.8
11143000	Big Sur River near Big Sur	CA	36.23	-121.77	119	68	73.2
11149900	San Antonio River near Lockwood	CA	35.88	-121.09	556	52	242.3
11151300	San Lorenzo Creek below Bitterwater Creek near King City	CA	36.27	-121.07	596	59	131.5
11152000	Arroyo Seco near Soledad	CA	36.27	-121.32	625	112	103.4
11152540	El Toro Creek near Spreckels	CA	36.58	-121.71	82	40	64
11159200	Corralitos Creek at Freedom	CA	36.93	-121.77	71	62	27.3
11160000	Soquel Creek at Soquel	CA	36.98	-121.95	103	68	6.5
11160500	San Lorenzo River at Big Trees	CA	37.03	-122.07	271	81	69.2
11162500	Pescadero Creek near Pescadero	CA	37.25	-122.33	118	66	19
11176400	Arroyo Valle below Lang Canyon near Livermore	CA	37.56	-121.68	333	54	228.6
11180500	Dry Creek at Union City	CA	37.61	-122.02	24	62	25.9
11213500	Kings River above NF near Trimmer	CA	36.86	-119.12	2437	53	305.3
11224500	Los Gatos Creek above Nunez Canyon near Coalinga	CA	36.21	-120.47	245	72	324.7
11226500	San Joaquin River at Miller Crossing	CA	37.51	-119.20	637	44	1392.9
11228500	Granite Creek near Cattle Mountain	CA	37.53	-119.26	122	42	2675
11230500	Bear Creek near Lake Thomas A Edison	CA	37.34	-118.97	134	96	2245.4
11237500	Pitman Creek below Tamarack Creek	CA	37.20	-119.21	59	90	2139.7
11253310	Cantua Creek near Cantua Creek	CA	36.40	-120.43	119	60	207.3
11264500	Merced River at Happy Isles Bridge near Yosemite	CA	37.73	-119.56	463	102	1228.3
11265000	Tenaya Creek near Yosemite Village	CA	37.74	-119.56	120	46	1219.2
11266500	Merced River at Pohono Bridge near Yosemite	CA	37.72	-119.67	822	101	1177
11274500	Orestimba Creek near Newman	CA	37.32	-121.12	343	86	65.8
11274630	Del Puerto Creek near Patterson	CA	37.49	-121.21	186	59	659
11275000	Falls Creek near Hetch Hetchy	CA	37.97	-119.76	118	68	1630.7
11281000	San Francisco Tuolumne River near Oakland Recreation Camp	CA	37.82	-120.01	223	80	853.4
11282000	Middle Tuolumne River at Oakland Recreation Camp	CA	37.83	-120.01	188	86	853.4
11315000	Cole Creek near Salt Springs Dam	CA	38.52	-120.21	54	89	1804.4
11348500	Pit River near Canby	CA	41.41	-120.93	3663	88	1300.2
11355500	Hat Creek near Hat Creek	CA	40.69	-121.42	415	71	1307.6
11381500	Mill Creek near Los Molinos	CA	40.05	-122.02	335	89	117.3

ID	Station Name	Location	Latitude	Longitude	Drainage Area	Number of years	Elevation
11383500	Deer Creek near Vina	CA	40.01	-121.95	532	101	146.1
11384000	Big Chico Creek near Chico	CA	39.78	-121.75	185	57	91.4
11409500	Oregon Creek near North San Juan	CA	39.40	-121.08	88	56	481.6
11427700	Duncan Canyon Creek near French Meadows	CA	39.14	-120.48	25	57	1606.3
11449500	Kelsey Creek near Kelseyville	CA	38.93	-122.84	94	71	449.7
11461000	Russian River near Ukiah	CA	39.18	-123.19	256	67	182.6
11468000	Navarro River near Navarro	CA	39.17	-123.67	776	67	1.5
11468500	Noyo River near Fort Bragg	CA	39.42	-123.74	271	66	3.6
11469000	Mattole River near Petrolia	CA	40.30	-123.28	627	69	15.1
11473900	Middle Fork Eel River near Dos Rios	CA	39.71	-123.32	1907	52	274.8
11475560	Elder Creek near Branscomb	CA	39.73	-123.64	17	51	424
11476500	San Francisco Eel River near Miranda	CA	40.17	-123.78	1375	77	66.3
11476600	Bull Creek near Weott	CA	40.35	-124.00	72	57	82.1
11478500	Van Duzen River near Bridgeville	CA	40.47	-123.89	568	78	109.2
11481200	Little River near Trinidad	CA	41.00	-124.08	104	63	5.4
11482500	Redwood Creek at Orick	CA	41.28	-124.05	709	67	1.6
11521500	Indian Creek near Happy Camp	CA	41.83	-123.38	307	66	365.3
11522500	Salmon River at Somes Bar	CA	41.37	-123.48	1923	94	147.2
11523200	Trinity River above Coffee Creek near Trinity Center	CA	41.11	-122.70	381	61	773.3
11528700	South Fork Trinity River below Hyampom	CA	40.65	-123.49	1956	53	369.2
11532500	Smith River near Crescent City	CA	41.78	-124.08	1572	86	24.2
12010000	Naselle River near Naselle	WA	46.38	-123.74	140	88	7.3
12013500	Willapa River near Willapa	WA	46.66	-123.65	333	66	1.1
12020000	Chehalis River near Doty	WA	46.62	-123.28	289	78	0
12025000	Newaukum River near Chehalis	WA	46.63	-122.94	397	77	0
12025700	Skookumchuck River near Vail	WA	46.77	-122.59	102	50	0
12027500	Chehalis River near Grand Mound	WA	46.78	-123.03	2291	89	0
12031000	Chehalis River at Porter	WA	46.94	-123.31	3313	70	0
12035000	Satsop River near Satsop	WA	47.00	-123.49	765	88	0
12040500	Queets River near Clearwater	WA	47.54	-124.31	1139	80	4.4
12041200	HOH River at US Highway 101 near Forks	WA	47.81	-124.25	648	57	49.9
12041500	Soleduck River near Fairholm	WA	48.04	-123.96	215	51	323.1
12048000	Dungeness River near Sequim	WA	48.01	-123.13	399	87	173.5
12054000	Duckabush River near Brinnon	WA	47.68	-123.01	170	79	73.6
12056500	North Fork Skokomish River below Staircase near Hoodsport	WA	47.51	-123.33	146	93	232.3
12060500	South Fork Skokomish River near Union	WA	47.34	-123.28	195	75	31.5
12073500	Huge Creek near Wauna	WA	47.39	-122.70	17	62	34.4

ID	Station Name	Location	Latitude	Longitude	Drainage Area	Number of years	Elevation
12079000	Deschutes River near Rainier	WA	46.85	-122.67	230	62	106.3
12082500	Nisqually River near National	WA	46.75	-122.08	340	75	442
12083000	Mineral Creek near Mineral	WA	46.74	-122.14	193	75	408.4
12092000	Puyallup River near Electron	WA	46.90	-122.03	238	80	497.6
12094000	Carbon River near Fairfax	WA	47.03	-122.03	202	76	366.3
12095000	South Prairie Creek at South Prairie	WA	47.14	-122.09	204	60	121.9
12097500	Greenwater River at Greenwater	WA	47.15	-121.63	188	75	526.4
12108500	Newaukum Creek near Black Diamond	WA	47.28	-122.06	70	72	94.5
12114500	Cedar River below Bear Creek near Cedar Falls	WA	47.34	-121.55	65	60	573
12115000	Cedar River near Cedar Falls	WA	47.37	-121.62	104	72	475.5
12115500	Rex River near Cedar Falls	WA	47.35	-121.66	34	71	518.2
12117000	Taylor Creek near Selleck	WA	47.39	-121.85	44	61	286.5
12141300	Middle Fork Snoqualmie River near Tanner	WA	47.49	-121.65	394	57	237.7
12142000	North Fork Snoqualmie River near Snoqualmie Falls	WA	47.62	-121.71	164	86	344.4
12143400	South Fork Snoqualmie River above Alice Creek near Garcia	WA	47.42	-121.59	106	57	438.2
12144000	South Fork Snoqualmie River at North Bend	WA	47.49	-121.79	209	80	128.9
12145500	Raging River near Fall City	WA	47.54	-121.91	78	71	76.2
12147500	North Fork Tolt River near Carnation	WA	47.71	-121.79	102	62	182.9
12147600	South Fork Tolt River near Index	WA	47.71	-121.60	14	54	563.9
12161000	South Fork Stillaguamish River near Granite Falls	WA	48.10	-121.94	305	52	94.5
12167000	North Fork Stillaguamish River near Arlington	WA	48.26	-122.05	671	89	27.2
12175500	Thunder Creek near Hewhalem	WA	48.67	-121.07	269	87	371.9
12177500	Stetattle Creek near Newhalem	WA	48.72	-121.15	56	50	276.3
12178100	Newhalem Creek near Newhalem	WA	48.66	-121.25	69	57	304.8
12182500	Cascade River at Marblemount	WA	48.53	-121.41	440	62	100.6
12186000	Sauk River above Whitechuck River near Darrington	WA	48.17	-121.47	389	94	283.5
12189500	Sauk River near Sauk	WA	48.42	-121.57	1828	90	81.1
12201500	Samish River near Burlington	WA	48.55	-122.34	225	61	13.7
12209000	South Fork Nooksack River near Wickersham	WA	48.66	-122.13	264	63	117.3
12451000	Stehekin River at Stehekin	WA	48.33	-120.69	822	96	334.8
12452800	Entiat River near Ardenvoir	WA	47.82	-120.42	520	60	475.8
12458000	Icicle Creek above Snow Creek near Leavenworth	WA	47.54	-120.72	494	70	442
12462500	Wematchee River at Monitor	WA	47.50	-120.42	3331	55	207.3
12488500	American River near Nile	WA	46.98	-121.17	202	79	823

ID	Station Name	Location	Latitude	Longitude	Drainage Area	Number of years	Elevation
12500500	North Fork Ahtanum Creek near Tampico	WA	46.56	-120.92	176	61	746.8
12501000	South Fork Ahtanum Creek at Conrad Ranch near Tampico	WA	46.51	-120.92	63	58	731.5
13216500	North Fork Malheur River above Beulah Reservoir near Beulah	OR	43.95	-118.17	909	58	1020.9
13329500	Hurricane Creek near Joseph	OR	45.34	-117.29	76	56	1371.6
13331500	Minam River near Minam	OR	45.62	-117.73	614	53	774.3
14010000	South Fork Walla Walla River near Milton	OR	45.83	-118.17	161	69	624.8
14020000	Umatilla River above Meacham Creek, near Gibbon	OR	45.72	-118.32	335	85	565.3
14037500	Strawberry Creek above Slide Creek near Prairie City	OR	44.34	-118.66	18	61	1496.4
14054500	Brown Creek near La Pine	OR	43.71	-121.80	54	56	1332
14101500	White River below Tygh Valley	OR	45.24	-121.09	1068	73	265.2
14134000	Salmon River near Government Camp	OR	45.27	-121.72	20	67	1050.2
14137000	Sandy River near Marmot	OR	45.40	-122.14	676	106	0
14138800	Blazed Alder Creek near Rhododendron	OR	45.46	-121.89	21	54	774.2
14141500	Little Sandy River near Bull Run	OR	45.41	-122.17	59	99	219.5
14146500	Salmon Creek near Oakridge	OR	43.75	-122.37	300	67	445.7
14147500	North Fork of Middle Fork Willamette River, near Oakridge	OR	43.76	-122.50	630	64	313.8
14152500	Coast Fork Willamette at London	OR	43.64	-123.08	185	55	251.6
14154500	Row River above Pitcher Creek, near Dorena	OR	43.75	-122.87	540	82	261
14158500	McKenzie River at Outlet of Clear Lake	OR	44.36	-121.99	237	73	919.1
14158790	Smith River above Smith River Reservoir, near Belknap Springs	OR	44.34	-122.05	40	57	795.5
14161500	Lookout Creek near Blue River	OR	44.21	-122.26	62	60	419.9
14165000	Mohawk River near Springfield	OR	44.09	-122.96	453	71	134.9
14166500	Long Tom River near Noti	OR	44.06	-123.43	229	82	118.6
14171000	Mary's River near Philomath	OR	44.53	-123.33	407	62	68.3
14172000	Calapooia River at Holley	OR	44.35	-122.79	269	55	160.8
14178000	North Santiam River below Boulder Creek, near Detroit	OR	44.71	-122.10	553	92	484.7
14179000	Breitenbush River above French Creek near Detroit	OR	44.76	-122.13	276	74	479.7
14182500	Little North Santiam River near Mehama	OR	44.80	-122.58	287	86	199.8
14185000	South Santiam River below Cascadia	OR	44.39	-122.50	445	82	236.2
14185900	Quartzville Creek near Cascadia	OR	44.54	-122.43	254	54	320
14187000	Willey Creek near Foster	OR	44.37	-122.62	133	55	219.5
14192500	South Yamhill River near Willamina	OR	45.05	-123.50	340	59	71.8

ID	Station Name	Location	Latitude	Longitude	Drainage Area	Number of years	Elevation
14193000	Willamina Creek near Willamina	OR	45.14	-123.49	166	58	96
14198500	Molalla River above PC near Wilhoit	OR	45.01	-122.48	248	58	241.2
14202000	Pudding River at Aurora	OR	45.23	-122.75	1226	57	22
14208000	Clackamas River at Big Bottom	OR	45.02	-121.92	348	50	621.8
14216500	Muddy Creek below Clear Creek near Cougar	WA	46.08	-122.00	346	60	314.8
14219800	Speel Yai Creek near Cougar	WA	46.00	-122.34	32	58	152.4
14222500	East Fork Lewis River near Heisson	WA	45.84	-122.47	320	88	108.8
14232500	Cispus River near Randle	WA	46.45	-121.86	822	68	372.3
14236200	Tilton River above Bear Canyon Creek near Cinebar	WA	46.60	-122.46	361	61	128.9
14242500	Toutle River near Silver Lake	WA	46.34	-122.72	1213	57	124.1
14301000	Nehalem River near Foss	OR	45.70	-123.75	1708	78	9.9
14301500	Wilson River near Tillamook	OR	45.48	-123.72	412	87	12.8
14305500	Siletz River at Siletz	OR	44.72	-123.89	517	100	31.2
14306500	Alsea River near Tidewater	OR	44.39	-123.83	855	78	14.7
14307620	Siuslaw River near Mapleton	OR	44.06	-123.88	1505	44	12.5
14309500	West Fork Cow Creek near Glendale	OR	42.80	-123.61	222	62	310.4
14312000	South Umpqua River near Brockway	OR	43.13	-123.40	4275	87	141
14316700	Steamboat Creek near Glide	OR	43.35	-122.73	581	62	344
14318000	Little River at Peel	OR	43.25	-123.03	453	53	252.5
14319500	North Umpqua River at Winchester	OR	43.27	-123.41	3441	75	113.7
14325000	South Fork Coquille River at Powers	OR	42.89	-124.07	433	99	60.2
14328000	Rogue River above Prospect	OR	42.78	-122.50	799	80	798.6
14333500	Red Blanket Creek near Prospect	OR	42.78	-122.43	116	55	847.3
14335500	South Fork Big Butte Creek near Butte Falls	OR	42.54	-122.55	353	72	719.3
14338000	Elk Creek near Trail	OR	42.68	-122.74	330	72	455.3
14371500	Grave Creek at Pease Bridge	OR	42.64	-123.21	57	48	717.6
14372500	East Fork Illinois River near Takilma	OR	42.07	-123.63	108	54	542.5
14377100	Illinois River near Kerby	OR	42.23	-123.66	973	58	365.2
14400000	Chetco River near Brookings	OR	42.12	-124.19	694	49	15
15022000	Harding River near Wrangell	AK	56.20	-131.64	173	52	6.1
15024800	Stikine River near Wrangell	AK	56.71	-132.13	50253	41	7.6
15050000	Gold Creek at Juneau	AK	58.31	-134.40	25	51	76.2
15052500	Mendenhall River near Auke Bay	AK	58.42	-134.57	217	52	18.3
15072000	Fish Creek near Ketchikan	AK	55.39	-131.19	89	98	6.1
15085100	Old Tom Creek near Kasaan	AK	55.39	-132.41	16	68	3
15266300	Kenai River at Soldotna	AK	60.48	-151.08	5171	53	12.3

ID	Station Name	Location	Latitude	Longitude	Drainage Area	Number of years	Elevation
15290000	Little Susitna River near Palmer	AK	61.71	-149.23	159	69	280.7
15292000	Susitna River at Gold Creek	AK	62.77	-149.69	15693	64	207.9
15292700	Talkeetna River near Talkeetna	AK	62.35	-150.02	5146	54	121.9
15302000	Nuyakuk River near Dillingham	AK	59.94	-158.19	3866	55	99.1
15304000	Kuskokwim River at Crooked Creek	AK	61.87	-158.11	79616	65	45.7
15356000	Yukon River at Eagle	AK	64.79	-141.20	2856960	70	259.1
15484000	Salcha River near Salchaket	AK	64.47	-146.93	5632	67	194.2
15493000	Chena River near Two Rivers	AK	64.90	-146.36	2391	51	221.3
15511000	Little Chena River near Fairbanks	AK	64.89	-147.25	952	51	141.5
15515500	Tanana River at Nenana	AK	64.56	-149.09	65434	57	104.8

Table S2. List of the significant streamflow gauges assessed by permutation tests on quantile-quantile (Q-Q) plots stratified according to the winter-averaged (November-March) PDO index with their station number, station name, location (AK = Alaska, BC = British Columbia, CA = California, OR = Oregon, WA = Washington, YT = Yukon), p -values ($p \leq 0.1$) and peak streamflow phase (negative and positive).

ID	Station Name	Location	p -value	Peak Phase
08CD001	Tuya River near Telegraph Creek	BC	0.063	Negative
08ED002	Morice River near Houston	BC	0.057	Negative
08EF001	Skeena River at Usk	BC	0.067	Negative
08FA002	Wannock River at Outlet of Owikeno Lake	BC	0.001	Negative
08FB006	Atnarko River near the mouth	BC	0.001	Negative
08KG001	West Road River near Cinema	BC	0.026	Negative
08LD001	Adams River near Squilax	BC	0.020	Negative
08MA002	Chilko River at Outlet of Chilko Lake	BC	0.014	Negative
08NJ013	Slocan River near Crescent Valley	BC	0.012	Negative
09AE003	Swift River near Swift River	BC	0.100	Negative
09BC001	Pelly River at Pelly Crossing	YT	0.036	Negative
10AB001	Frances River near Watson Lake	YT	0.100	Negative
09423350	Caruthers Creek near Ivanpah	CA	0.090	Positive
10255810	Borrego Palm Creek near Borrego Springs	CA	0.004	Positive
10258500	Palm Canyon Creek near Palm Springs	CA	0.004	Positive
10263500	Big Rock Creek near Valyermo	CA	0.036	Positive
11111500	Sespe Creek near Wheeler Springs	CA	0.098	Positive
11113000	Sespe Creek near Fillmore	CA	0.017	Positive
11116000	North Fork Matilija Creek at Matilija Hot Springs	CA	0.096	Positive
11136800	Cuyama River below Buckhorn Canyon near Santa Maria	CA	0.036	Positive
11274630	Del Puerto Creek near Patterson	CA	0.089	Positive
11468500	Noyo River near Fort Bragg	CA	0.081	Negative
11469000	Mattole River near Petrolia	CA	0.012	Negative
11475560	Elder Creek near Branscomb	CA	0.014	Negative
11476500	San Francisco Eel River near Miranda	CA	0.074	Negative
11476600	Bull Creek near Weott	CA	0.054	Negative
11478500	Van Duzen River near Bridgeville	CA	0.040	Negative
11481200	Little River near Trinidad	CA	0.024	Negative
11482500	Redwood Creek at Orick	CA	0.002	Negative
11522500	Salmon River at Somes Bar	CA	0.023	Negative
11528700	South Fork Trinity River below Hyampom	CA	0.074	Negative
11532500	Smith River near Crescent City	CA	0.001	Negative
12041200	HOH River at US Highway 101 near Forks	WA	0.062	Positive
12108500	Newaukum Creek near Black Diamond	WA	0.074	Negative
12175500	Thunder Creek near Hewhalem	WA	0.100	Positive
12178100	Newhalem Creek near Newhalem	WA	0.086	Positive
12458000	Icicle Creek above Snow Creek near Leavenworth	WA	0.088	Negative
12500500	North Fork Ahtanum Creek near Tampico	WA	0.003	Negative
12501000	South Fork Ahtanum Creek at Conrad Ranch near Tampico	WA	0.040	Negative
13329500	Hurricane Creek near Joseph	OR	0.006	Negative
13331500	Minam River near Minam	OR	0.013	Negative
14037500	Strawberry Creek above Slide Creek near Prairie City	OR	0.093	Negative
14054500	Brown Creek near La Pine	OR	0.001	Negative
14141500	Little Sandy River near Bull Run	OR	0.002	Negative
14166500	Long Tom River near Noti	OR	0.045	Negative
14171000	Mary's River near Philomath	OR	0.071	Negative
14172000	Calapooia River at Holley	OR	0.085	Negative

ID	Station Name	Location	<i>p</i> -value	Peak Phase
14185000	South Santiam River below Cascadia	OR	0.046	Negative
14187000	Willey Creek near Foster	OR	0.036	Negative
14192500	South Yamhill River near Willamina	OR	0.018	Negative
14193000	Willamina Creek near Willamina	OR	0.031	Negative
14198500	Molalla River above PC near Wilhoit	OR	0.038	Negative
14202000	Pudding River at Aurora	OR	0.069	Negative
14306500	Alsea River near Tidewater	OR	0.005	Negative
14309500	West Fork Cow Creek near Glendale	OR	0.015	Negative
14312000	South Umpqua River near Brockway	OR	0.041	Negative
14319500	North Umpqua River at Winchester	OR	0.027	Negative
14333500	Red Blanket Creek near Prospect	OR	0.061	Negative
14335500	South Fork Big Butte Creek near Butte Falls	OR	0.029	Negative
14338000	Elk Creek near Trail	OR	0.086	Negative
14371500	Grave Creek at Pease Bridge	OR	0.087	Negative
14372500	East Fork Illinois River near Takilma	OR	0.087	Negative
14377100	Illinois River near Kerby	OR	0.027	Negative
15050000	Gold Creek at Juneau	AK	0.014	Positive
15292000	Susitna River at Gold Creek	AK	0.007	Negative
15304000	Kuskokwim River at Crooked Creek	AK	0.001	Negative

Table S3. List of the significant streamflow gauges assessed by permutation tests on quantile-quantile (Q-Q) plots stratified according to the annually-averaged (January-December) AMO index with their station number, station name, location (AK = Alaska, BC = British Columbia, CA = California, OR = Oregon, WA = Washington, YT = Yukon), p -values ($p \leq 0.1$) and peak streamflow phase (negative and positive).

ID	Station Name	Location	p -value	Peak Phase
08EF005	Blueberry River below Aitken Creek	BC	0.096	Negative
08GD004	Homathko River at the mouth	BC	0.076	Positive
08LA001	Clearwater River near Clearwater Station	BC	0.061	Positive
09BC001	Pelly River at Pelly Crossing	YT	0.045	Negative
10BE004	Toad River above Nonda Creek	BC	0.041	Negative
10259000	Andreas Creek near Palm Springs	CA	0.082	Negative
11015000	Sweetwater River near Descanso	CA	0.062	Negative
11042400	Temecula Creek near Aguanga	CA	0.020	Negative
11058600	East Twin Creek near Arrowhead Springs	CA	0.052	Negative
11075800	Santiago Creek at Modjeska	CA	0.091	Negative
11119500	Carpinteria Creek near Carpinteria	CA	0.014	Negative
11138500	Sisquoc River near Sisquoc	CA	0.077	Negative
11152540	El Toro Creek near Spreckels	CA	0.006	Positive
11159200	Corralitos Creek at Freedom	CA	0.067	Positive
11160000	Soquel Creek at Soquel	CA	0.063	Positive
11176400	Arroyo Valle below Lang Canyon near Livermore	CA	0.052	Positive
11224500	Los Gatos Creek above Nunez Canyon near Coalinga	CA	0.094	Negative
11274630	Del Puerto Creek near Patterson	CA	0.031	Positive
12025700	Skookumchuck River near Vail	WA	0.080	Positive
12054000	Duckabush River near Brinnon	WA	0.027	Positive
12115000	Cedar River near Cedar Falls	WA	0.060	Positive
14158500	McKenzie River at Outlet of Clear Lake	OR	0.054	Positive
14158790	Smith River above Smith River Reservoir, near Belknap Springs	OR	0.093	Positive
14161500	Lookout Creek near Blue River	OR	0.054	Positive
15052500	Mendenhall River near Auke Bay	AK	0.035	Positive
15072000	Fish Creek near Ketchikan	AK	0.022	Negative
15085100	Old Tom Creek near Kasaan	AK	0.082	Positive
15292700	Talkeetna River near Talkeetna	AK	0.041	Negative
15356000	Yukon River at Eagle	AK	0.073	Negative
15511000	Little Chena River near Fairbanks	AK	0.072	Negative

Table S4. Significant streamflow gauges assessed by Spearman’s rank correlation ρ stratified according to the winter-averaged (November-March) PDO index with their station number, station name, location (AK = Alaska, BC = British Columbia, CA = California, OR = Oregon, WA = Washington, YT = Yukon), ρ value and p -values ($p \leq 0.1$).

ID	Station Name	Location	ρ	p -value
08CD001	Tuya River near Telegraph Creek	BC	-0.302	0.027
08ED002	Morice River near Houston	BC	-0.368	0.007
08EF001	Skeena River at Usk	BC	-0.342	0.006
08FB006	Atnarko River near the mouth	BC	-0.475	0.001
08KG001	West Road River near Cinema	BC	-0.516	0.000
08LA001	Clearwater River near Clearwater Station	BC	-0.224	0.080
08LD001	Adams River near Squilax	BC	-0.301	0.047
08MA002	Chilko River at Outlet of Chilko Lake	BC	-0.187	0.096
08MH016	Chilliwack River at Outlet of Chilliwack Lake	BC	-0.264	0.017
08NB005	Columbia River at Donald	BC	-0.387	0.007
08NJ013	Slocan River near Crescent Valley	BC	-0.234	0.034
09AE003	Swift River near Swift River	BC	-0.276	0.053
10AB001	Frances River near Watson Lake	YT	-0.269	0.052
10255810	Borrego Palm Creek near Borrego Springs	CA	0.377	0.005
11275000	Falls Creek near Hetch Hetchy	CA	-0.207	0.091
11482500	Redwood Creek at Orick	CA	-0.312	0.008
11532500	Smith River near Crescent City	CA	-0.348	0.001
12020000	Chehalis River near Doty	WA	-0.205	0.072
12025700	Skookumchuck River near Vail	WA	-0.436	0.002
12027500	Chehalis River near Grand Mound	WA	-0.247	0.020
12031000	Chehalis River at Porter	WA	-0.319	0.007
12054000	Duckabush River near Brinnon	WA	0.215	0.058
12079000	Deschutes River near Rainier	WA	-0.262	0.040
12083000	Mineral Creek near Mineral	WA	-0.236	0.042
12097500	Greenwater River at Greenwater	WA	-0.307	0.007
12108500	Newaukum Creek near Black Diamond	WA	-0.322	0.006
12451000	Stehekin River at Stehekin	WA	-0.171	0.096
12458000	Icicle Creek above Snow Creek near Leavenworth	WA	-0.312	0.009
12500500	North Fork Ahtanum Creek near Tampico	WA	-0.409	0.001
12501000	South Fork Ahtanum Creek at Conrad Ranch near Tampico	WA	-0.338	0.009
13329500	Hurricane Creek near Joseph	OR	-0.348	0.009
14010000	South Fork Walla Walla River near Milton	OR	-0.211	0.082
14020000	Umatilla River above Meacham Creek, near Gibbon	OR	-0.181	0.097
14054500	Brown Creek near La Pine	OR	-0.303	0.023
14137000	Sandy River near Marmot	OR	-0.259	0.007
14138800	Blazed Alder Creek near Rhododendron	OR	-0.380	0.005
14141500	Little Sandy River near Bull Run	OR	-0.327	0.001
14146500	Salmon Creek near Oakridge	OR	-0.384	0.001
14147500	North Fork of Middle Fork Willamette River, near Oakridge	OR	-0.410	0.001
14152500	Coast Fork Willamette at London	OR	-0.323	0.016
14154500	Row River above Pitcher Creek, near Dorena	OR	-0.347	0.001
14161500	Lookout Creek near Blue River	OR	-0.284	0.028
14165000	Mohawk River near Springfield	OR	-0.322	0.006
14166500	Long Tom River near Noti	OR	-0.232	0.036
14171000	Mary’s River near Philomath	OR	-0.236	0.065
14172000	Calapooia River at Holley	OR	-0.434	0.001
14178000	North Santiam River below Boulder Creek, near Detroit	OR	-0.273	0.009
14179000	Breitenbush River above French Creek near Detroit	OR	-0.336	0.003
14182500	Little North Santiam River near Mehama	OR	-0.347	0.001

ID	Station Name	Location	ρ	p -value
14185000	South Santiam River below Cascadia	OR	-0.390	0.000
14185900	Quartzville Creek near Cascadia	OR	-0.338	0.013
14187000	Willey Creek near Foster	OR	-0.349	0.009
14192500	South Yamhill River near Willamina	OR	-0.279	0.032
14193000	Willamina Creek near Willamina	OR	-0.339	0.009
14198500	Molalla River above PC near Wilhoit	OR	-0.219	0.098
14202000	Pudding River at Aurora	OR	-0.264	0.047
14222500	East Fork Lewis River near Heisson	WA	-0.185	0.086
14301000	Nehalem River near Foss	OR	-0.330	0.003
14301500	Wilson River near Tillamook	OR	-0.276	0.010
14305500	Siletz River at Siletz	OR	-0.287	0.004
14306500	Alsea River near Tidewater	OR	-0.283	0.012
14312000	South Umpqua River near Brockway	OR	-0.237	0.027
14316700	Steamboat Creek near Glide	OR	-0.298	0.019
14318000	Little River at Peel	OR	-0.302	0.028
14319500	North Umpqua River at Winchester	OR	-0.326	0.005
14325000	South Fork Coquille River at Powers	OR	-0.187	0.065
14328000	Rogue River above Prospect	OR	-0.267	0.017
14333500	Red Blanket Creek near Prospect	OR	-0.424	0.001
14335500	South Fork Big Butte Creek near Butte Falls	OR	-0.347	0.003
14372500	East Fork Illinois River near Takilma	OR	-0.266	0.052
15024800	Stikine River near Wrangell	AK	-0.334	0.033
15304000	Kuskokwim River at Crooked Creek	AK	-0.449	0.000
15484000	Salcha River near Salchaket	AK	-0.322	0.008

Table S5. Significant streamflow gauges assessed by Spearman’s rank correlation ρ stratified according to the annually-averaged (January-December) AMO index with their station number, station name, location (AK = Alaska, BC = British Columbia, CA = California, OR = Oregon, WA = Washington, YT = Yukon), ρ value and p -values ($p \leq 0.1$).

ID	Station Name	Location	ρ	p -value
07FC003	Blueberry River below Aitken Creek	BC	-0.293	0.046
09BC001	Pelly River at Pelly Crossing	YT	-0.271	0.047
10257600	Mission Creek near Desert Hot Springs	CA	0.264	0.070
10281800	Independence Creek below Pinyon Creek near Independence	CA	0.266	0.048
11136100	San Antonio Creek near Casmalia	CA	0.241	0.092
11143000	Big Sur River near Big Sur	CA	0.267	0.028
11152000	Arroyo Seco near Soledad	CA	0.206	0.029
11152540	El Toro Creek near Spreckels	CA	0.306	0.054
11159200	Corralitos Creek at Freedom	CA	0.342	0.006
11160000	Soquel Creek at Soquel	CA	0.310	0.010
11160500	San Lorenzo River at Big Trees	CA	0.246	0.027
11176400	Arroyo Valle below Lang Canyon near Livermore	CA	0.284	0.037
11274500	Orestimba Creek near Newman	CA	0.219	0.063
11274630	Del Puerto Creek near Patterson	CA	0.281	0.031
11427700	Duncan Canyon Creek near French Meadows	CA	0.311	0.019
11469000	Mattole River near Petrolia	CA	-0.213	0.079
12488500	American River near Nile	WA	-0.190	0.094
12500500	North Fork Ahtanum Creek near Tampico	WA	-0.294	0.021
12501000	South Fork Ahtanum Creek at Conrad Ranch near Tampico	WA	-0.253	0.056
13216500	North Fork Malheur River above Beulah Reservoir near Beulah	OR	-0.244	0.065
13329500	Hurricane Creek near Joseph	OR	-0.238	0.078
14020000	Umatilla River above Meacham Creek, near Gibbon	OR	-0.248	0.022
14101500	White River below Tygh Valley	OR	-0.282	0.016
14137000	Sandy River near Marmot	OR	-0.282	0.003
14138800	Blazed Alder Creek near Rhododendron	OR	-0.239	0.082
14141500	Little Sandy River near Bull Run	OR	-0.376	0.000
14179000	Breitenbush River above French Creek near Detroit	OR	-0.313	0.007
14185000	South Santiam River below Cascadia	OR	-0.186	0.095
14185900	Quartzville Creek near Cascadia	OR	-0.230	0.095
14232500	Cispus River near Randle	WA	-0.220	0.072
14242500	Toutle River near Silver Lake	WA	-0.322	0.015
15052500	Mendenhall River near Auke Bay	AK	0.329	0.017
15356000	Yukon River at Eagle	AK	-0.283	0.018
15511000	Little Chena River near Fairbanks	AK	-0.322	0.021